siRNA screen identifies QPCT as a druggable target for Huntington's disease

Maria Jimenez-Sanchez[1], Wun Lam[1,2], Michael Hannus[3,§], Birte Sönnichsen[3,§], Sara Imarisio[1,2,§,] Angeleen Fleming[1,4,§], Alessia Tarditi[6,#], Fiona Menzies[1], Teresa Ed Dami[1,4,5], Catherine Xu[1,4], Eduardo Gonzalez-Couto[6,€], Giulia Lazzeroni[6], Freddy Heitz[6,£], Daniela Diamanti[6], Luisa Massai[6], Venkata P. Satagopam[7,8], Guido Marconi[6,$], Chiara Caramelli[6,&], Arianna Nencini[6], Matteo Andreini[6], Gian Luca Sardone[6], Nicola P. Caradonna[6], Valentina Porcari[6], Carla Scali[6], Reinhard Schneider[7,8], Giuseppe Pollio[6], Cahir J. O'Kane[2], Andrea Caricasole[6,^,*] and David C. Rubinsztein[1,*]

[1]Department of Medical Genetics, University of Cambridge, Cambridge Institute for Medical Research, Addenbrooke's Hospital, Hills Road, Cambridge CB2 0XY, UK

[2] Department of Genetics, University of Cambridge, Cambridge CB2 3EH, UK

[3]Cenix BioScience GmbH, Tatzberg 47, 01307 Dresden, Germany

[4]Department of Physiology, Development and Neuroscience, University of Cambridge, Downing Street, Cambridge, UK, CB2 3EG.

[5] Department of Neuroscience, Psychology, Drug Research and Child Health, Division of Pharmacology and Toxicology, University of Florence, Florence, Italy

[6]Siena Biotech. Strada del Petriccio e Belriguardo, 35 53100 Siena, Italy

[7]Structural and Computational Biology, EMBL, Meyerhofstr.1, 69117, Heidelberg, Germany

[8]Luxembourg Centre for Systems Biomedicine (LCSB), University of Luxembourg, Campus Belval, House of Biomedicine, 7 avenue des Hauts-Fourneaux, L-4362 Esch-sur-Alzette, Luxembourg

[#]Current address: TPV GmbH, Messerschmittstr. 1+3 , D-80992 München, Germany

[£]Current address: GenKyoTex S.A.,16 Chemin des Aulx, CH-1228,Geneva, Switzerland

[€]Current address: Integromics S.L., Santiago Grisolía, 2 E-28760 Tres Cantos (Madrid)

[$]Current address: Autifony S.r.l., Via Fleming, 437135 Verona (VR), Italy

[&]Current address: Novartis Vaccines and Diagnostics srl CQ Bioprocess support unit 53018 Rosia (SI), Italy

^Current address: IRBM Promidis, Via Pontina Km 30.600, 00040 Pomezia (Rome, Italy)

[§] Authors contributed equally to this work

*Address correspondence to: David C. Rubinsztein – Tel: +44 (0)1223 762608,

Fax: +44 (0)1223 331206, E-mail: dcr1000@hermes.cam.ac.uk or to Andrea Caricasole E-mail A.Caricasole@irbm.it

Huntington's disease (HD) is a currently incurable neurodegenerative condition caused by an abnormally expanded polyglutamine tract in huntingtin (HTT). We identified novel modifiers of mutant HTT toxicity by performing a large-scale "druggable genome" siRNA screen in human cultured cells, followed by hit validation in *Drosophila.* We focused on glutaminyl cyclase (QPCT), which had one of the strongest effects on mutant HTT-induced toxicity and aggregation in the cell-based siRNA screen, and which also rescued these phenotypes in *Drosophila*. We found that QPCT inhibition induced the levels of the molecular chaperone alpha B-crystallin and reduced the aggregation of diverse proteins. We generated novel QPCT inhibitors using *in silico* methods followed by *in vitro* screens, which rescued the HD-related phenotypes in cell, *Drosophila* and zebrafish HD models. Our data reveal a novel HD druggable target affecting mutant huntingtin aggregation, and provide proof-of-principle for a discovery pipeline from druggable genome screen to drug development.

Introduction

Huntington's disease (HD) is a fatal, currently incurable, late-onset neurodegenerative disorder. The disease signs include involuntary and repetitive choreic movements, psychological dysfunction and cognitive impairment, which result from progressive degeneration of cortical and striatal neurons [1 2].

HD is caused by the expansion of a CAG repeat tract in exon 1 of the gene encoding huntingtin (HTT), which results in an abnormally long polyglutamine stretch in the N-terminus of the protein [3]. Although the mechanisms are not fully understood, it is believed that the disease arises from a toxic-gain-of function of the mutant protein [4 5]. A hallmark of HD is the presence of intracellular aggregates, which is also a characteristic of the other ten polyglutamine-expansion disorders, as well as other neurodegenerative conditions such as Parkinson's or Alzheimer's disease [6]. The role of these aggregates in the disease is not clear, although an increasing importance of the oligomeric forms in toxicity is emerging [7 8] and reducing mutant HTT aggregation with strategies such as pharmacological upregulation of chaperone function has been pursued as a therapeutic strategy in HD [9]. Mutant HTT toxicity is believed to be accentuated, or possibly induced, after cleavage events resulting in the formation of short N-terminal polyglutamine containing fragments, which can also be produced by aberrant splicing [10]. Hence, exon 1 models have been frequently used for disease modeling.

Here, we combined two approaches to identify modifiers of mutant HTT toxicity by first performing a cell-based screen to identify genes that when knocked down could suppress mutant HTT-induced toxicity, using a library of 5,623 siRNAs selected according to the potential druggability of their targets with small molecules [11]. We performed this screen in two different HD models. Initially, we screened the effects of siRNAs in a mammalian cell line inducibly expressing HTT with an abnormal polyglutamine expansion. In a secondary analysis, we validated primary hits in a *Drosophila* model of HD.

One of the strongest suppressors of mutant HTT toxicity in both mammalian cells and *Drosophila* was an enzyme responsible for the modification of N-terminal residues of glutamine or glutamate into an N-terminal 5-oxoproline or pyroglutamate (pE), named glutaminyl cyclase (QPCT).. QPCT not only suppressed mutant HTT induced toxicity but also greatly reduced the number of aggregates. This effect is not HTT-specific, since QPCT exerted a general effect on aggregation of different aggregate-prone proteins, including other proteins containing an expanded polyglutamine or polyalanine tract, which could be attributed to increased levels of the chaperone alpha B-crystallin upon QPCT inhibition. Furthermore, we designed small molecule modulators of QPCT activity, which effectively suppressed mutant HTT aggregation and toxicity in cells, neurons, fly and zebrafish models of the disease.

Results

Primary cell screen for suppressors of mutant Htt toxicity

We performed the primary screen using a stable HEK293/T Rex cell line expressing full-length human HTT bearing 138 polyglutamines (Q138) under the control of a tetracycline-inducible promoter. We confirmed the expression of HTT(Q138) after inducing the cells with doxycycline using antibodies recognizing the N-terminus of human HTT (Supplementary Results, Supplementary Fig. 1a and Supplementary Note 1), and quantitative RT-PCR using primers spanning different areas of the human *HTT* cDNA (Supplementary Fig. 1b). This cell line had reduced cell viability after expression of mutant HTT, which was reverted by treatment with a known reference compound (Y27632) [12] (Supplementary Fig. 1c), suggesting that this model could be used to identify potential modulators of mutant HTT cellular toxicity in a large-scale screen.

For our high-throughput screen, we utilised a strategy consisting of an iterative siRNA screen where positive genes were selected after three consecutive rounds to compensate for the variability of the assay. We eliminated non-positive siRNAs and added

new siRNAs targeting the selected genes in consecutive passes. We assessed rescue of cellular toxicity by each siRNA by fluorescence microscopy and automated image analysis using three independent readouts: 1) number of cell nuclei (#nuclei), 2) apoptotic index and 3) aberrant nuclei index, and used rescue indices to express the effect of each individual siRNA for each parameter analysed. In an initial screen, we tested 3 independent siRNAs for each of the 5,623 genes (a total of 16,869 siRNAs), from which we selected 670 primary genes (see Supplementary Note 1 for screen assay and criteria selection). As shown in supplementary figure 2a, the three readouts were partially redundant, as more than 50% of the 1,000 top scoring siRNAs of one rescue index also ranked amongst the top 1,000 siRNAs of at least one of the other rescue indices. In supplementary figure 1b, a representation of rescue indices obtained in pass 1 shows the relatively large variability of the assay, with non-targeting negative control siRNAs, negQ and negF, showing a #nuclei rescue indices of 14% and 3% respectively, while using siRNA targeting HTT as a positive control rendered a mean #nuclei rescue index of 81%.

After 3 consecutive rounds of screening, we selected and 257 genes and ranked these based on all three rescue indices, using #nuclei rescue index as a primary criterion (Supplementary Data Set 1).

Secondary RNAi screening in a *Drosophila* model of HD

To validate the hits obtained in mammalian cells and to focus on targets with potential relevance *in vivo*, we performed a secondary screen in a *Drosophila* model that expressed a construct containing 48 polyglutamines, Q48, that causes eye degeneration when expressed using a *GMR-GAL4* driver [13]. For most genes selected, we studied two UAS-RNAi constructs from the Vienna *Drosophila* RNAi Center (VDRC): a *P*-element (GD) and a *phiC31* (KK) construct, the latter of which carries more GAL4-binding sites and should therefore express the RNAi more strongly [14]. Of the 257 mammalian genes previously selected, we detected 133 that had one or more gene orthologs in flies (Supplementary Data

Set 1 and 2). Of these 133 mammalian genes with fly orthologs, 74 *Drosophila* genes (corresponding to 66 mammalian genes) rescued the Q48-induced eye degeneration with at least one RNAi line, while the others showed no obvious or significant effect (Supplementary Fig. 3a and 3b and Supplementary Data Sets 1 and 2). We crossed suppressor RNAi lines to transgenic flies that expressed EGFP, also driven by the same *GMR-GAL4* driver. We used EGFP to test whether modifiers affected transgene protein synthesis, since Q48 levels can be modified by aggregation or autophagic degradation, which do not impact EGFP levels. Two of these fly RNAi lines, targeting orthologs to human CTSF and to human ADAM8, ADAM11 and ADAM33, reduced EGFP levels on western blots (Supplementary Data Set 2), suggesting a general effect of these genes in protein expression, while suppression exerted by the other RNAi lines seemed to be polyglutamine-specific.

Functional categorization of mutant HTT modifiers

To gain further insight into the biological relevance of the data generated, we categorized the different sets of HD toxicity modulators according to their molecular function. Suppressors were enriched for certain classes of proteins such as GPCRs or transporters compared to the initial library, while the number of positive kinases in the screen was reduced and no cytokines, growth factors or translational regulators were represented. We observed similar functional categorizations after selection from the cell and *Drosophila* screen (Supplementary Fig. 4a). An Ingenuity Pathway Analysis (IPA) of the hits obtained in the primary screen in cells (Supplementary Table 1a) revealed that the majority of these proteins participate in general processes such as GPCR- or cAMP-mediated signalling, but also in canonical pathways related to neurodegeneration, such as apoptosis, mitochondrial dysfunction, amyloid processing or protein ubiquitination. Importantly, 10 of these proteins have been previously related to HD signalling, including subunits of the succinate dehydrogenase complex and huntingtin-associated protein 1 (HAP1) (Supplementary Table 1a). Many of the genes validated in *Drosophila* (Supplementary Fig. 4b and Supplementary Table 1b) are also involved in processes related to neurodegeneration but were enriched in

mitochondrial metabolic pathways, especially those associated with fatty acid biosynthesis and metabolism.

Validation of QPCT in *Drosophila*

We focused our attention on a gene that had one of the strongest and most consistent effects in rescuing mutant HTT-induced toxicity in the cell-based siRNA screen. The gene product has glutaminyl cyclase activity and is named QPCT. Two orthologs have been reported in fly [15], *Glutaminyl cyclase* (*QC*) and *iso Glutaminyl cyclase (isoQC*), which show about 39% amino acid identity; a third fly ortholog, CG6168, shows expression restricted to male accessory glands (www.flyatlas.org) and is not considered further here. RNAi lines targeting either *QC* or *isoQC* partially rescued eye depigmentation and mediated a significant decrease in the number of black spots in flies expressing Q48 (Fig. 1a, 1b and Supplementary Fig. 5a) (Data are shown for GD- and KK-RNAi lines in the case of *QC*, but only a KK line was available for *isoQC*). These effects are likely independent of transcription/translation of the Q48, since no change in EGFP protein levels were seen when we crossed transgenic flies expressing EGFP driven by the same *GMR-GAL4* driver as Q48 with *QC* or *isoQC* RNAi lines (Supplementary Fig. 5b). Thus, QPCT represents an interesting candidate for studying in HD.

To further evaluate the benefits of downregulating QPCT on HD, we took advantage of an additional *Drosophila* model of neurodegeneration, HD flies that express exon 1 of HTT with 120 polyglutamines, *GMR-HTT.Q120* in eye photoreceptors [16]. *Drosophila melanogaste*r has a compound eye consisting of many ommatidia, each of which is composed of 8 photoreceptors, seven of which can be visualized by light microscopy using the pseudopupil technique [17]. Neurodegeneration results in the loss of visible rhabdomeres of each photoreceptor and can be rescued or enhanced by genetic or chemical approaches [18]. Consistent with our data using the Q48 flies, the loss of visible photoreceptors in transgenic flies expressing *GMR-HTT.Q120* was partially rescued when

they were crossed with RNAi lines for either of the two QPCT fly orthologues, *QC* and *isoQC* (Fig. 1c). We observed no effect on the number of rhabdomeres in QPCT RNAi lines in the absence of *GMR-HTT.Q120*. The effects of QPCT knockdown on toxicity correlated with a reduction in HTT aggregation, which we assessed in flies expressing GFP-tagged expanded huntingtin exon 1, *HTTEx1-Q46-eGFP* in the eye [19] (Fig. 1d).

QPCT modulates mutant HTT aggregation

To further validate QPCT, we first confirmed the protective effect of its knockdown against toxicity and aggregation in HEK293 cells expressing the exon 1 of *HTT* (from residue 8) with a 74 polyglutamine expansion fused at its N-terminal to EGFP (*EGFP-HTT(Q74*)) [20] (Fig. 2a, Supplementary fig. 6a and 6b). The QPCT siRNAs used in these experiments as well as in the screen do not target QPCT-like, which encodes a paralogous protein that catalyzes a similar reaction and shows 51% of sequence identity to QPCT (Supplementary Fig. 6b and 6c). We also validated the effect of QPCT knockdown on aggregation in HeLa cells (Supplementary Fig. 6d) which, like HEK293 cells, express QPCT [21]. We also confirmed a decrease in protein aggregation of a construct which expresses full-length HTT carrying 138 polyglutamines (similar to the one used in the initial screen) (Supplementary Fig. 6e). QPCT siRNA did not have a general anti-apoptotic effect as it did not affect caspase 3 activity in response to staurosporine treatment (Supplementary Fig. 6f). Consistent with these data, QPCT shRNA reduced EGFP-Q80 (80 glutamines fused to EGFP) aggregation in primary cortical neurons (Fig. 2b and Supplementary fig. 6g). We could not assess the effect of QPCT knockdown on polyglutamine-mediated toxicity in these neurons, where the levels of cell death obtained in this assay were very low, as can be appreciated in fig. 2b. While knocking down QPCT was protective, overexpression of QPCT in HeLa and HEK293 cells increased the numbers of apoptotic nuclei and also led to a large accumulation of HTT(Q74) aggregates (Fig. 2c and Supplementary Fig. 7a), while QPCT did not increase caspase activity upon staurosporine treatment (Supplementary Fig. 7b). The effects of QPCT were activity-dependent, since the catalytically inactive E201Q mutant did

not increase the percentage of cells with HTT(Q74) aggregates (Fig. 2d and Supplementary Fig. 7c and 7d).

We measured mRNA levels of QPCT in HD mice and found that its expression was reduced when compared to their wild-type littermates, suggesting that QPCT expression may be downregulated as a compensatory mechanism (Supplementary Fig. 8) and that raised QPCT activity may not be a prerequisite for aggregation.

QPCT catalyzes the modification of N-terminal glutamines or glutamates into a pyroglutamate (pE) residue. Although the presence of an extended polyglutamine tract makes HTT a potential substrate for QPCT, this enzyme only modifies N-terminal residues, suggesting that any modification on mutant HTT would require an N-terminal cleavage to reveal a glutamine at the N-terminal that could be cyclated. The formation of a pE residue may then affect its stability and propensity to aggregate, a hypothesis that was previously suggested [22]. This cleavage model in either the polyglutamine tract or HTT exon 1 or GFP is unlikely, as QPCT modulated the aggregation of constructs consisting only of isolated polyglutamine expansions (Q57 and Q81) fused C-terminal to EGFP (Fig. 2e and 2f), or HTT exon 1 with 74 glutamines fused to HA [23] (Supplementary Fig. 9a and 9b), and QPCT siRNA also reduced the aggregation of an expansion of 37 alanines [24] (Fig. 2f). QPCT appeared to modulate the early stages of mutant HTT oligomerisation, since QPCT overexpression increased the amounts of Flag-tagged monomeric mutant HTT that were co-immunoprecipitated by GFP-tagged mutant HTT (Fig. 2g) [25]. Since QPCT did not interact with HTT directly by immunoprecipitation (e.g. Fig. 2g), its effect on HTT oligomer formation is likely mediated via intermediaries.

Design and characterization of compounds that inhibit QPCT

To target QPCT pharmacologically, we tested a previously described QPCT inhibitor [26], which did not rescue the HD phenotype in mammalian cells (Supplementary Fig. 10a and 10b). While this compound has been effective in Alzheimer disease (AD) models by reducing

the formation of extracellular pE-Aβ, this may be due to extracellular QPCT inhibition [21] [27]. Thus, we reasoned that the failure of this compound was likely due to poor cell permeability. In order to generate novel QPCT inhibitors, we employed existing data on its structure and known inhibitors to generate three 3D pharmacophore models, two ligand-based and one structure-based (using the human QPCT X-Ray structure (PDB id: 2AFW)). We used these models, along with stringently applied CNS filters and a solubility model developed in-house, to select 10,000 compounds from both commercially available screening compounds and the SienaBiotech compound library. We screened these molecules in a functional assay assessing the conversion of the H-Glu-AMC fluorogenic substrate into pyroGlu-AMC, as previously described [28], and selected hits associated with predicted robust binding for the hit-to-lead phase. The optimization strategy was based on physicochemical properties and ensemble docking model-driven approaches. The ensemble docking methodology [29] [30] was chosen to take into account the flexibility of human QPCT catalytic site and was constructed using both X-Ray structures and protein conformations coming from a 100 ns molecular dynamic study of the human QPCT 2AFW X-Ray structure. The ensemble docking model was evolved during the project development. Initially, only 4 X-Ray structures were used (PDB ID: 2AFW, 2AFX, 2AFZ[31]), then a set of 16 protein conformations, selected by clustering of molecular dynamic simulations, were added to improve model accuracy. Recently, two more X-Ray structures were added to the model (3PBB[32] an 3SI0[33]). All the docking calculations were performed using CCDC Gold (versions 4 and 5)[34] [35] [36] along with an ad-hoc developed program to rank and select the best scored ligand docking pose from the pool of QPCT conformations. Along with the biochemical readouts used during this optimization, we included a range of *in vitro* ADME assays, including solubility measurements, a CNS membrane permeability assay (PAMPA-BBB) [37] and stability in the presence of human CYP3A4, a member of the cytochrome P450 mixed-function oxidase system, and a key enzyme involved in the metabolism of xenobiotics in humans.

We selected a series of compounds on the basis of these properties and validated their effects on mutant HTT aggregation and toxicity in cells expressing HTT(Q74)GFP, which led to the selection of three of them, SEN177 (1), SEN817 (2) and SEN180 (3) (Supplementary note 2, Fig. 3a, Supplementary Fig. 11a). Non-toxic concentrations of these compounds caused a dose-dependent reduction in the percentage of cells with aggregates, which correlated with a suppression of mutant HTT-induced apoptosis (Fig. 3b, 3c, 3d, 3d and Supplementary Fig. 11b). As seen with genetic knockdown experiments, pharmacologic inhibition of QPCT using these compounds also reduced aggregation of polyalanines (Fig. 3d) and did not affect protein levels, as assessed by measuring GFP levels by western blotting (Supplementary Fig. 11c) or by metabolic labeling of wild type HTT followed by detection of newly synthesized protein in the presence of SEN177 (Supplementary Fig. 11d). Importantly, the effect of these compounds was blocked when QPCT expression was suppressed by shRNA, confirming that they protect by a mechanism that requires QPCT inhibition (Fig 3e, Supplementary Fig. 11e and 11f). Thus, even though these compounds also inhibited QPCT-like (Supplementary Fig. 11a) and we cannot exclude the possibility that at least some of the effects observed may be mediated by this QPCT isoenzyme, their effects on aggregation were QPCT-dependent, as the shRNA used did not target QPCT-like. Consistent with these data, SEN177 greatly reduced the early stages of mutant HTT oligomerisation, as it decreased the amounts of GFP-tagged monomeric HTT that were co-immunoprecipitated by Flag-tagged HTT (Fig. 3f). The protective effect of these compounds was also confirmed in primary cortical neurons (Fig. 3g), with SEN177 and SEN817 significantly reducing the percentage of neurons with Q80 aggregates.

QPCT modulates the levels of alpha B-crystallin

The effects of QPCT inhibition on HTT aggregation appeared to be independent of effects on protein clearance pathways targeting mutant huntingtin (autophagy and the ubiquitin-proteasome system) (Supplementary Fig. 12), changes in mRNA or protein levels (Supplementary Fig. 13a and 13b), or secretion of the enzyme into the medium

(Supplementary Fig. 13c). QPCT is localized in the ER and secretory pathway and its knockdown, overexpression or inhibition seemed to have inconsistent and rather modest effects on different readouts of the ER stress response, measured by GRP78/BIP levels or phosphorylation of eIF2α, which did not correlate with its effect on aggregation (Supplementary Fig. 14). Our data also suggested that CREB (c-AMP response element binding protein) or ERK (extracellular signal-regulated kinase) signaling, recently reported to be activated upon QPCT inhibition [38] (Supplementary Fig. 15a and 15b), or JNK signaling (Supplementary Fig. 15c) were unlikely contributors to the effects we have observed.

QPCT overexpression or knockdown did not modulate levels of HSP70, the main inducible stress response chaperone (Supplementary Fig. 15d). We performed transcriptional profiling to assess changes in alternative molecular chaperones induced by SEN177 in the presence of mutant HTT, and observed upregulation of several small heat shock proteins (sHSPs) (HSPB6 with 1.6 fold-change; HSPB3 with 1.5 fold-change; HSPB7 with 1.5 fold-change; and notably, alpha B-crystallin which had >2.5 fold increase in transcript levels) (Supplementary Fig. 16a and Supplementary Data Set 3). We confirmed this induction at the protein level as well as with other QPCT inhibitors (Fig. 4a). Genetic inhibition of QPCT dramatically increased alpha B-crystallin protein and mRNA levels in the presence of HTT(Q74) (Fig. 4b and 4c and Supplementary Fig. 16b), while QPCT overexpression, which increased mutant HTT aggregation and toxicity (Fig. 2c and Supplementary Fig. 7a), reduced alpha B-crystallin levels (Supplementary Fig. 16c). QPCT also modestly modulated alpha B-crystallin levels in the absence of mutant HTT or in the presence of the non-pathogenic Q23 (Supplementary Fig. 16b and 16c).

As a sHSP, alpha B-crystallin acts as a molecular chaperone and is a suppressor of polyglutamine toxicity in cells and in *Drosophila* [39] [40] [41]. As expected, overexpression of alpha B-crystallin lowered the number of HTT(Q74) aggregates, while QPCT inhibitors failed to reduce aggregation further (Fig. 4d and Supplementary Fig. 16d), suggesting that this

increment in alpha B-crystallin was a major contributor to the protection afforded by QPCT inhibition.

QPCT inhibition protects fly and zebrafish HD models

We tested QPCT inhibitors in flies expressing Httex1Q46 in the eye and found a reduction in the number of aggregates (Fig. 5a). The compound with a greatest effect, SEN177, was able to also rescue the number of visible rhabdomeres and prevent neurodegeneration (Fig. 5b).

A transgenic zebrafish expressing Htt exon 1 with 71Q fused to EGFP in the rod photoreceptors using the rhodopsin promoter has been established and validated as a model to study mutant huntingtin aggregation in vivo [42] . Zebrafish have two homologs with putative glutaminyl-peptide cyclotransferase activity, QPCT and QPCTLA with 51% and 47% protein identity with QPCT and QPCT-like respectively. In order to test the effect of pharmacologic inhibition of QPCT in this model, we first determined the maximum tolerated concentration for each of the three compounds tested in mammalian cells and subsequently treated HD larvae. SEN817 and SEN180 reduced total number of EGFP-aggregates in the retina (Fig. 6a), which correlated with a marked decrease in toxicity similar to the positive control, clonidine [42], assessed by a rescue in the total area of eye photoreceptors (Fig. 6b).

Although the three compounds were protective, their effectiveness varied between these models, which might be due to intrinsic properties of each system, SEN180 only mildly reduced aggregation in neurons and the effect of SEN817 was not significant in *Drosophila*. Although SEN177 had the highest *in vitro* activity and was able to efficiently reduce aggregates in mammalian cells, primary neurons and *Drosophila*, we found that this compound was tolerated at much higher concentrations than its analogs in zebrafish and therefore the bioavailability in this model is much lower, which could explain the lack of effect in this system. All together, we have identified a number of small molecules that through QPCT inhibition have beneficial effects on the treatment of HD in a variety of *in vivo* models.

Discussion

Our approach using a two-step screen, starting with an initial large-scale analysis in human cell models followed by a validation in *Drosophila,* has yielded a number of potentially druggable targets which may be suitable for HD. A variety of HT-RNAi screens have identified genetic suppressors of phenotypes mediated by mutant HTT N-terminal fragments in *Drosophila*, *C. elegans* and mammalian (mouse and human) cells [44] [45] [46] [47]. In most cases, aggregation was the primary readout, often measured with C-terminal GFP fusions. Differences in the nature of the previous screens (species, cellular context, huntingtin fragment length, length of the polyglutamine expansion, primary readout and differences in siRNA/shRNA sequences) complicates cross-screen comparisons. Also, virtually no screens in this area have examined their false negative rates due to inefficient knockdown. Additionally, the screen presented here was biased towards the druggable component of the human genome, and a further selection was made in the course of triaging towards specific protein target classes. This likely contributes to the relatively poor overlap of hits in the present and previous screens. A comparison with a screen performed in HEK293T cells to identify genetic suppressors of inducibly expressed mutant HTT exon 1 toxicity [46] revealed an overlap of only 4 genes (CPA1, GRIN2A, NR3C2 and USP21) when considering the top 257 hits (Supplementary Data Set 1). However, matrix metalloproteases, identified in HEK293T cells as modulators of fragmentation and toxicity of N-terminal portions of mutant HTT [45] were also identified in our dataset, as well as PAK1, which we previously identified as a kinase promoting mutant HTT self-association and toxicity [25], thus validating the effectiveness of the screen.

Based on the reproducible and clear rescue that QPCT inhibition exerts on mutant HTT toxicity in cells and in *Drosophila*, we focused on this target. A catalytically inactive QPCT was not able to increase the number of aggregates, suggesting that pE modifications modulate the levels of aggregates in HD models. Although one obvious mechanism would

involve cleavage of the polyglutamine tract followed by cyclation of an N-terminal pE residue that may change properties such as stability or hydrophobicity, which would account for its change in aggregation [22], our data suggest that the effect of QPCT on HTT may be indirect. We found that modulation of aggregation by QPCT was not restricted to mutant HTT but it also affected aggregation of other aggregate-prone proteins and that QPCT influences the formation of mutant HTT oligomeric species. We observed an induction in several sHSPs, mostly alpha B-crystallin, suggesting that QPCT inhibition caused a stress response distinct from classical Hsp70 induction, which might be mediated by indirect substrates for pE modification. This molecular chaperone reduces aggregation of polyglutamine containing proteins [39 41], alpha-synuclein [48 41]or amyloid-*β* peptide [49 50] , underscoring QPCT inhibition as an effective target for misfolded protein disorders. Since alpha B-crystallin is regulated at the transcriptional level while QPCT resides in the secretory pathway, inhibition of QPCT may activate a signalling response that enhance alpha B-crystallin transcription. Our data suggest that this is likely independent of an ER stress response or the involvement of ERK and CREB, which have been recently found phosphorylated upon QPCT inhibition [38], as well as other stress signalling pathways such as JNK. Further work will need to clarify the QPCT substrate mediating this effect. It is important to stress that the benefits of QPCT downregulation may not be restricted to alpha B-crystallin as an effector, as the upregulation of other related sHSPs may also contribute beneficially.

We identified and characterised a series of compounds that efficiently reduce mutant HTT aggregation in mammalian cell lines and also in primary mouse neurons, fly eye and in zebrafish. While the levels of rescue and significance obtained varied between compounds depending on the model used, this may be as a result of differences in absorption routes and bioavailability. Nevertheless, our data showed that pharmacologic inhibition of QPCT using this compound series can rescue HD phenotypes and provides proof-of-principle for QPCT as a potential therapeutic target for HD and possibly other related intracellular proteinopathies by modulating the formation of oligomeric forms, which have been proposed

as the most toxic species in these diseases [7] [8]. Clearly, further work is required before considering that this will be clinically relevant, including likely additional drug development. Nevertheless, in a broader perspective, our data suggest that a discovery pipeline from druggable genome screen to drug development may be tractable for neurodegenerative diseases.

Acknowledgements

We are grateful for funding from the MRC (COEN Grant MR/J006904/1 to DCR and CJO'K), the Wellcome Trust (Principal Fellowship to DCR; 095317/Z/11/Z), NIHR Biomedical Research Unit in Dementia at Addenbrooke's Hospital, the TAMAHUD project (European community's FP6 grant n.03472 under the Thematic Call LSH-2005-2.1.3-8 "Early markers and new targets for neurodegenerative diseases") and the NEUROMICS project (European community's Seventh Framework Programme under grant agreement No. 2012-305121). We thank J. L. Marsh, N. Perrimon, and the Vienna *Drosophila* RNAi Center for fly stocks, M. Renna and S. Luo for helpful comments, M Lichtenberg for help with flow cytometry assays, F. Siddiqi and M. Garcia-Arencibia for help with primary cultures, W. Fecke for advice and assistance and Stefano Gotta for help in HR-MS analysis of compounds.

Author Contributions

M.J.S. performed most post-screen cell biology experiments. W.L. and S.I. performed the Drosophila experiments. M.H. and B.S. performed the cell-based screen. A.F., T.E.D. and C.X performed the zebrafish experiments and A.F. supervised these. A.T., E.C.G. V.P.S. and R.S. performed the bioinformatics analyses. F.M. performed the chaperone transcription array experiments and non-radioactive pulse-chase. E.G.C. and F.H. participated in experimental design of the screen. F.H., G.L., D.D., L.M. and G.P. generated and validated the stable cell lines for the screen. G.M., C.C., A.N. synthesized and analyzed the compounds. M.A. performed the selection of compound for HTS and supported the hit to lead optimization by in-silico drug design methodologies. V.P. optimized glutaminyl cyclase

enzymatic assays for compound screening. G.L.S. and N.P.C. performed in vitro ADME experiments. C.S. provided support for experiments at Siena Biotech. C.O.K. supervised Drosophila experiments. G.P. also supervised molecular biology activities at Siena Biotech. A.C. supervised primary screen and chemical biology. D.C.R. supervised cell biology, Drosophila and zebrafish experiments. D.C.R and A.C. conceived the project and co-ordinated work between sites with assistance from G.P. M.J.S., D.C.R. and A.C drafted the manuscript which was commented on by all authors.

Conflict of interest

The authors declare competing financial interests: Alessia Tarditi, Eduardo Gonzalez-Couto, Giulia Lazzeroni, Freddy Heitz, Daniela Diamanti, Luisa Massai, Giuseppe Pollio, Guido Marconi, Chiara Caramelli, Arianna Nencini, Matteo Andreini, Gian Luca Sardone, Nicola P. Caradonna, Valentina Porcari, Carla Scali and Andrea Caricasole were employed by Siena Biotech; Michael Hannus and Birte Sönnichsen were employed by Cenix BioScience GmbH.

Figure legends

Figure 1. Downregulation of QPCT in flies rescues HD toxicity.

a. The eye phenotype of flies that express Q48 crossed to w^{1118} (VDRC stock number 60000) is rescued upon downregulation of *Drosophila Glutaminyl cyclase* ($QC^{GD38277}$, VDRC GD-RNAi line 38277). Representative images of eye pigmentation rescue are shown. F=female; M=male.

b. Downregulation of QPCT fly orthologs *QC* and *isoQC* using KK-RNAi lines (lines $QC^{KK106341}$ and $isoQC^{KK101533}$) reduced the number of black necrotic-like spots on Q48 flies (see Supplementary Fig.5a for quantification). Fisher's exact test was applied for statistical

comparison between control and test genotypes. Females: *isoQC*^{KK101533} *p*=2.42 E-14; *QC*^{KK106341} *p*= 3.05 E-12; males: *isoQC*^{KK101533} *p*=3.53 E-0.8; *QC*^{KK106341} *p*= 1.72 E-0.9

c. Loss of rhabdomeres due to expression of expanded huntingtin exon1 (*elav-Gal4; GMR-HTT.Q120*) in the eye was significantly rescued upon downregulation of QPCT fly orthologues *QC* or *isoQC* (GD- or KK-RNAi lines as indicated). Graph shows the mean ± SEM of the average number of rhabdomeres per eye from 4 independent experiments; one-tailed paired t-test was used to test significance.

d. The number of aggregates in the eyes of flies expressing expanded huntingtin HTTex1-Q46-eGFP using GMR-GAL4 was reduced by downregulating QPCT fly orthologs *QC* and *isoQC (*RNAi lines *isoQC*^{KK101533}*, QC*^{KK10634}*, QC*^{GD38277}). Graph shows mean ± SEM of the number of aggregates from 4 independent crosses for each genotype with control levels set at 100%. One-tailed paired t-test was used for comparison between control and test genotypes (n = 4).

In all panels, * $p<0.05$, ** $p<0.01$ and *** $p<0.001$. Scale bars represent 200 µm.

Figure 2. QPCT modulates HTT toxicity and aggregation in mammalian cell lines and primary neurons

a. The percentage of cells with apoptotic nuclei or HTT(Q74) aggregates is reduced in HEK293 cells transiently expressing EGFP-HTT(Q74) and treated with QPCT siRNA. Representative images are shown in supplementary figure 6a.

b. QPCT shRNA significantly reduced the number of aggregates in mouse primary cortical neurons expressing Q80-EGFP. Scale bar represents 10 µm. The mean of 3 independent experiments in triplicate is represented in the graph. Significance was analysed by two-tailed paired Student's t-test.

c,d. Overexpression of QPCT (*pCMV6-QPCT*) together with EGFP-HTT(Q74) in HeLa cells for 48h increased the percentage of cells with apoptotic nuclear morphology and aggregates (**c**), this effect is not observed with a catalytically inactive QPCT (QPCT(E201Q)-Flag) (**d**).

e. The percentage of HeLa cells expressing EGFP-HTT(Q74), EGFP-Q57 or EGFP-Q81 with aggregates is enhanced upon QPCT-Flag overexpression for 48 h.

f. QPCT siRNA reduces the percentage EGFP-Q81 or EGFP-A37 with aggregates in HEK293.

g. Overexpression of QPCT enhanced the amount of mutant HTT(1-548)-Flag co-immunoprecipitating with HTT(1-588)-GFP. Levels of Flag-HTT(1-588) co-immunoprecipitated relative to total lysates from 5 independent experiments are represented in the graph. Data were analyzed by two-tailed paired Student's t-test (n= 5 experiments). Full blot images are shown in Supplementary Fig. 17a.

In all panels, unless indicated, graphs show mean values with control conditions set to 100 and error bars represent standard deviation from a triplicate experiment representative of at least three independent experiments. Statistical analyses were performed by two-tailed unpaired Student's t-test: ***p<0.001, **p<0.01; *p<0.05; NS, not significant

Figure 3. Design of QPCT inhibitors that reduce mutant HTT aggregation

a. Chemical structure of compounds designed to inhibit QPCT activity. Table indicating the activity and in vitro ADME properties of the compounds is shown in supplementary fig. 11a.

b,c. Treatment of HeLa cells expressing EGFP-HTT(Q74) with SEN177, 817 and 180 (50 µM) for 24h reduced the percentage of cells with aggregates (**b**) and apoptotic nuclei (**c**).

d. SEN177 reduces the percentage of HEK293 cells with EGFP-HTT(Q74) or EGFP-A37 aggregates in a concentration-dependent manner.

e. SEN177 does not further reduce the percentage of EGFP-HTT(Q74) aggregates in QPCT shRNA transfected cells.

f. SEN177 reduces the amount of HTT(1-588)-GFP co-immunoprecipitating with HTT(1-548)-Flag in HeLa cells (25 µM SEN177). The amount of GFP-HTT(1-548) immunoprecipitated relative to total lysates was quantifiedand the average of 5 independent experiments is shown in the graph. Data were analyzed by two-tailed paired Student's t-test (n= 5 experiments). Full blot images are shown in Supplementary information 17b.

g. Primary neurons expressing EGFP-Q80 for 3 days were treated with 50 µM of indicated compounds for further 24h.

In all panels, unless indicated, graphs show mean values with control conditions set to 100 and error bars represent standard deviation from a triplicate experiment representative of at least three independent experiments. Statistical analyses were performed by two-tailed unpaired Student's t-test: ***p<0.001, **p<0.01; *p<0.05; NS, not significant.

Figure 4. QPCT inhibition induces alpha B-crystallin levels

a. Alpha B-crystallin (Cryab) protein levels were increased in cells transfected with HTT(Q74)GFP and treated with the indicated compounds at 25 µM for 24 h. Full blot images are shown in Supplementary information 17c.

b,**c**. Knockdown of QPCT for 24 h followed by transfection with HTT(Q74)GFP for another 24h increased protein (**b**) and mRNA (**c**) levels of alpha B-crystallin. Fold change in mRNA of QPCT or alpha B-crystallin is represented in the graph with error bars representing standard deviation. The mean of three independent experiments in triplicate was normalized to 1 and significance was calculated by one sample t-test. Full blot images are shown in Supplementary information 17d.

d. Overexpression of alpha B-crystallin (CRYAB-Flag) reduced the percentage of cells with HTT(Q74)GFP aggregates. SEN817 decreased aggregation when added at 25 µM for 24h in

control but not CRYAB-expressing cells. In all panels, unless indicated, graphs show mean values with control conditions set to 100 or 1, and error bars represent standard deviation from a triplicate experiment representative of at least three independent experiments. Statistical analyses were performed by two-tailed unpaired Student's t-test: $^{**}p<0.01$; $^{*}p<0.05$; NS, not significant.

Figure 5. Pharmacologic inhibition of QPCT in fly

a. Flies that expressed HTTex1-Q46-eGFP in the eye have fewer aggregates after treatment with 50 µM of indicated compounds . Graph represents mean ± SEM from 4 independent crosses for each compound. Statistical analyses were performed by one-tailed unpaired Student's t-test. Scale bars represent 200 µm.

b. Flies expressing HTTEx1-Q120 (*GMR-HTT.Q120*) show more rhabdomeres after treatment with SEN177 (50 µM). Graph represents the average number of rhabdomeres per eye ±SEM from 3 independent experiments with females and males counted separately, each based on approximately 10 individuals per datapoint, scoring 15 ommatidia from each individual. Statistical analysis was performed using one-tailed paired Student's t-test.

Figure 6. Pharmacologic inhibition of QPCT in zebrafish

a. Representative sections through the central retina of transgenic HD zebrafish at 7 d.p.f. treated with DMSO, SEN177 (1 mM), SEN817 (100 µM) or SEN180 (100 µM) showing aggregates (arrow) within the rod photoreceptors. Scale bar represents 10 µm. Treatment with QPCT inhibitors resulted in reduction in aggregates (Student's t-test) for SEN187 and SEN810.

b. Representative sections through the central retina of transgenic HD zebrafish at 9 d.p.f. treated with DMSO, SEN177 (1 mM), SEN817 (100 µM) or SEN180 (100 µM). To demonstrate that loss of GFP corresponds to loss of photoreceptors, sections were stained

with anti-rhodopsin (1D1) antibody (red). GFP labels the whole rod photoreceptor, whereas rhodopsin is present in the rod outer segment. Merged images show co-localisation of GFP the rhodopsin (red). Photoreceptor degeneration is ameliorated by SEN817 and SEN180. Scale bars, 10 µm.

In all panels, $**p<0.01$; $*p<0.05$; NS, not significant.

Online Methods

Assays for validation polyglutamine toxicity modifiers in *Drosophila*

***Drosophila* fly stocks**: As a model of polyglutamine toxicity, flies that expressed a protein with 48 glutamines encoded by *P{UAS-Q48.myc/flag}31* [13] in eyes under control of the GMR-Gal4 driver *P{GAL4-ninaE.GMR}12* [51] (Q48) were used. Fly orthologs to the genes identified in the cell screen were selected by performing reciprocal BLASTP and cross checking with databases including http://www.ncbi.nlm.nih.gov/homologene, http://www.genecards.org/, http://www.ensembl.org/index.html. The RNAi lines corresponding to the identified genes were obtained from Vienna *Drosophila* RNAi Center (VDRC, http://stockcenter.vdrc.at/control/main).

The following stocks were generous gifts: *UAS-Q48.myc/flag* from J.L. Marsh [13], *UAS-Httex1-Q46-eGFP* from N. Perrimon [19]. Fly lines that are not referenced here are documented in FlyBase (www.flybase.org).

All fly crosses and experiments were performed at 25°C.

***Drosophila* RNAi screen**: Five virgins of genotype *w; GMR-GAL4; UAS-Q48.myc/flag* (Q48) were crossed to males carrying each *UAS-RNAi* (GD- and KK-RNAi collections, VDRC, http://stockcenter.vdrc.at/control/main). Genetic background was controlled by crossing *w; GMR-GAL4; UAS-Q48.myc/flag* females to w^{1118} males that share the same genetic background (VDRC stock number 60000 for the GD-RNAi lines and 60100 for the KK-RNAi lines). For

Glutaminyl cyclase (CG32412) the GD-RNAi line 38277 and the KK-RNAi line 106341 were used. For *isoGlutaminyl cyclase* (CG5976), the KK-RNAi line 101533 was used. For GD-RNAi lines, degeneration was determined by scoring the eye depigmentation in the progeny of the above crosses 4 days after eclosion, assessing modification of polyglutamine loss-of-pigmentation and black necrotic-like spots. For KK-RNAi lines, as their background leads to dark eye pigmentation (http://www.vdrc.at/rnai-library/rnai-protocols), toxicity was assessed by scoring the presence or abscence of black necrotic-like spots in the eyes of 10-day old flies. Fisher's exact test was performed to compare the numbers of necrotic-spot-containing flies in the KK-RNAi crosses with controls using an arbitrary $p<0.005$ as a statistical cut-off for significance. Eyes were imaged using a Nikon CoolPix 990 digital camera attached to a dissecting microscope.

EGFP expression levels assessed in Drosophila RNAi lines: Western blot analysis was performed using progeny of crosses between virgins of the genotype *w; GMR-GAL4; UAS-EGFP* and males of each VDRC-RNAi line used or background control (VDRC stock number 60100). Fly heads were homogenized in Laemmli sample buffer. Rabbit polyclonal anti-GFP at 1:1000 (AbCam, Ab6556) and monoclonal anti-beta tubulin at 1:10000 (Developmental Studies Hybridoma Bank) were used. Blots were scanned using Odyssey Fc Imaging System (LI-COR Biosciences). This validation was initially performed once on each suppressor, and subsequently RNAi lines showing an apparent reduction in EGFP levels were re-tested using the progeny of three independent crosses. Statistical analysis was performed by two-tailed paired t-test between the RNAi lines and the control line.

Pseudopupil assay: Analysis was performed as previously described [17]. Virgins of genotype *elav-GAL4^{C155}*; *{GMR-HD.Q120}4.62/TM3* (elav-Gal4; GMR-HTT.Q120) [16] were crossed with males carrying the RNAi construct for *Glutaminyl cyclase* (lines *QC^{GD38277}* or *QC^{KK106341})* or *isoGlutaminyl cyclase* (line *isoQC^{KK101533})* and compared to background control line.

To evaluate the effect of QPCT inhibitors, virgins of genotype *yw*; {*GMR-HD.Q120}2.4* (GMR-HTT.Q120) were allowed to mate with w^{1118} control males for 48 hours on standard cornmeal food and then transferred on fly food containing the compounds.

The number of rhabdomeres per ommatidium was scored in progeny of the above crosses at 3 (GMR-Q120) or 4 (elav-Gal4; GMR-HTT.Q120) days post-eclosion. Statistical analysis was performed using one-tailed t-test on data from 3 or 4 independent experiments, each based on approximately 10 individuals for each genotype, scoring 15 ommatidia per eye. When compounds were tested, the analysis was done on females and males of each treatment separately.

Aggregate counting: Virgins of genotype *w; GMR-GAL4; UAS-Httex1-Q46-eGFP* [19] were crossed with males of QPCT *UAS-RNAi* lines or from the background KK-RNAi control line, since all the background controls show similar aggregate scoring. Eye pictures of 18-day old progeny were taken using a Leica MZ16F microscope connected to a Leica DFC340FX digital camera. For each genotype, GFP punctae indicating aggregate formation was counted using ImageJ "Cell Counter" plugin in the eyes of 20 males, a pool of 5 males from four independent crosses. For compound testing, virgins of genotype *w; GMR-GAL4; UAS-Httex1-Q46-eGFP* were crossed with w^{1118} control males, and females of the progeny scored 15 days post-eclosion. The experiment was repeated at least three times and for each experiment at least 4 female eyes were scored. An unpaired one-tailed t-test was used to determine statistical significance for single comparisons between two groups using GraphPad Prism.

Compound treatment*:* Flies were reared on food (Instant Fly Food, Philip Harris, Ashby de la Zouch, UK) containing either QPCT inhibitor (50 µM) dissolved in DMSO or DMSO alone. The progeny were flipped every 2 days on fresh food containing the specific inhibitor or DMSO.

Bioinformatics Analysis

Ingenuity Pathways Analysis (Ingenuity® Systems, www.ingenuity.com) was used to analyze the distribution of siRNAs tested among the different protein classes as well as to determine the canonical pathways associated to the confirmed primary actives.

Assays for validation of polyglutamine toxicity and aggregation modifiers in human cell lines

Cell culture: HEK293 (Human Embryonic Kidney), HeLa (Human cervical carcinoma) cells and Atg5-deficient (Atg5-/-) mouse embryonic fibrolasts (MEFs) (gift from N. Mizushima) were grown in Dulbecco's modified eagle medium supplemented with 10% FBS, 100 U/ml penicillin/streptomycin and 2 mM l-glutamine at 37ºC in 5% CO_2. UbG76V-GFP-expressing stable HeLa cell line (kind gift from N.P. Dantuma) was maintained in medium containing 0.5 mg/ml G418.

Isolation and culture of mouse primary cortical neurons: Primary cortical neurons were isolated from C57BL/6 mice (Jackson Laboratories) embryos at E16.5. Briefly, brains were harvested and placed in ice-cold PBS/glucose where the meninges were removed and the cerebral cortices were dissected. After mechanical dissociation using sterile micropipette tips, dissociated neurons were resuspended in PBS/glucose and collected by centrifugation. Viable cells were seeded on poly-ornithine-coated 12-multiwell plates. Cells were cultured in Neurobasal medium supplemented with 2 mM glutamine, 200 mM B27 supplement, and 1% Penicillin-Streptomycin at 37°C in a humidified incubator with 5% CO_2. One half of the culture medium was changed every two days until treatment. After 5 days of culturing *in vitro*, differentiated cortical neurons were infected with lentiviral particles bearing EGFP-Q80 and scramble or QPCT-directed shRNAs. Compounds were added 3 days after EGFP-Q80 viral infection and left for another 24h. When EGFP-Q80 was

expressed together with shRNA, 5-6 days were needed before cultures were fixed in a 2% PFA-7.5% glucose solution.

DNA constructs: Human QPCT (NM_012413) plasmid was purchased from Origene (*pCMV6-XL5-QPCT*). A C-terminal Flag-tagged QPCT construct was generated by PCR amplification of *QPCT* cDNA from *pCMV6-XL5-QPCT* using primers overhanging HindIII and BglII sites and insertion into the pCMV5-FLAG in HindIII and BamHI restriction sites, using standard restriction enzyme digestion and ligation procedures. *QPCT(E201Q)-Flag* was generated using QuickChange II Agilent Site-Directed mutagenesis kit with the following primers Fw 5'-CTTCTTTGATGGTCAAGAGGCTTTTCTTCACTGG-3' and Rev 5'-CCAGTGAAGAAAA GCCTCTTGACCATCAAAGAAG-3'. *pcDNA* or *pCMV5-Flag* empty vectors were used as mock controls for *pCMV6-XL5-QPCT* or *QPCT-Flag* respectively.

Constructs expressing the first exon of the Htt gene carrying 74 polyglutamines expressed from *pEGFP-C1* (Clontech) (*EGFP-HTTQ74*) or pHM6 (Roche Diagnostics) (*HA-HTTQ74*), or with only 23 polyglutamines (*EGFP-HTTQ23*), were described previously [52]. *pEGFP-N1-Q57* and *pEGFP-N1-Q81* [23] and *pEGFP-C1-A37* [24] have been previously described. Mutant *HTT(1-588)-Flag* was provided by MR Hayden and mutant *HTT(1-548)GFP* generated by S. Luo [25]. 3xFlag-CRYAB construct has been previously described [53]. The pGL3-BIP/GRP78-luciferase construct was kindly provided by M. Renna [54]

Reagents: Chemical compounds used in cell culture were the autophagy inhibitors Bafilomycin A1 (400nM, DMSO; 4 hours; Millipore) and 3MA (10 mM, 16 hours; SIGMA), staurosporine (3 μM) and the proteasome inhibitor MG132 (10 μM). PBD150 was synthesized as described in [26].

Transfection: Cells were transfected in 6-well plates with 0.5-1.5 μg of DNA and 5 μl of Lipofectamine (Invitrogen) or TransIT-2020 (Mirus) per well for 4 hours in Optimem (GIBCO-BRL) and then incubated in full media for 48 hours. Gene knockdown experiments were performed using ON-TARGETplus SMARTpool siRNA (Dharmacon) for human QPCT, consisting on 4 siRNAs with the following sequences: CUAUGGGUCUCGACACUUA;

GUACCGGUCUUUCUCAAAU; CCUUAAAGACUGUUUCAGA; GGAACUUGCUCGUGCCUUA, and which do not target the QPCT like sequence. For siRNA treatment, a single transfection protocol using 50nM siRNA for 48 h or a double transfection protocol which consisted on a first 50 nM siRNA transfection followed by a second 50 nM siRNA transfection after 48 hours.

Western blotting: Cells were washed once in PBS and harvested on lysis buffer (20 mM Tris-HCl pH 6.8, 137nM NaCl, 1 mM EGTA, 1% Triton X-100, 10% glycerol, 1x Roche complete mini protease inhibitor). Equal loading was obtained by protein concentration determination using a Bio-Rad assay followed by resuspension and boiling in Laemli buffer. Samples were subjected to 12% SDS-PAGE and transferred to PVDF membrane (Immobilion-P, GE Healthcare). Blots were proved with primary antibody: anti-LC3 (1:2000; Novus Biologicals, NB100-2220), anti-Hsp70 (1:1000; Enzo SPA810), anti-CRYAB (1:1000; Cell signalling 8851), anti-actin (1:2000; Sigma, A2066), anti-α-tubulin (1:4000; T9026, Sigma), anti-Flag epitope (1:2000; SIGMA, F7425), anti-GFP (1:1000; Clontech, Living colours, polyclonal), eIF2α (1:1000, Abcam 5369) and phospho-S51-eIF2α_(1:1000, Abcam 32157), GRP78 (1:1000, Abcam 21685), anti-phospho-ERK (1:1000, Cell signalling, 9101), anti-ERK (1:1000, Cell signalling, 9102), anti-phospho-CREB (S133) (1:1000, Cell signalling 9191), anti-CREB 86B10 (1:1000, Cell signalling, 9104), anti-phospho-JNK (1:1000, Cell signalling, 9255), anti-JNK (1:1000, Cell signalling, 9252). The appropriate anti-mouse or anti-rabbit secondary antibodies were used and visualized using an ECL detection kit (Amersham) or LI-COR Biosciences infrared imager (Odyssey).

Caspase 3/7 activity assay. Cells were seeded in a 96-well plate 24h prior to the assay and 1 μM staurosporine or DMSO was added for the last 8h. Caspase 3/7 activity was measured by using a luminogenic caspase 3/7 substrate (Caspase 3/7-Glo Assay, Promega) following manufacturer protocols in a Glomax luminometer (Promega). Protein concentration was determined in each cell lysate and caspase 3/7 activity was normalized to protein levels.

Co-inmunoprecipitation assays: Assays were performed as previously described [25], where HTT(1-588)Flag(Q138) and HTT(1-548)GFP(Q138) were expressed in HeLa cells together with QPCT plasmid for 48h, or treated with 25 µM SEN177 for 24h. Cells were lysed in buffer B containing 10 mM Tris pH 7.4, 150 mM NaCl, 1 mM EDTA pH8, 1% triton and 1x Roche complete mini protease inhibitor for 20 min on ice, followed by centrifugation at 13000 rpm for 10 min. Five hundred micrograms total protein were incubated with primary anti-Flag M2 (Sigma) or anti-GFP (Clontech, Living colours, polyclonal) at 5 µg/ml overnight at 4°C. Protein G Dynabeads (LifeTechnologies) were added and incubated for further 2 h. Beads were washed 3 times with buffer B and eluted using 0.1 M glycine pH 2.5M followed by boiling in laemli buffer. Samples were subjected to western blot and visualized using LICOR. A fraction of the total lysates was run simultaneously.

Reverse-transcriptase PCR analysis: Total RNA was isolated from cell pellets using Trizol Reagent (Invitrogen), treated with DNase I, and cDNA synthesis was performed by SuperScript III First-Strand Synthesis System (Invitrogen). Standard conditions were used for cDNA amplification and PCR products were analyzed by agarose gel electrophoresis and ethidium bromide staining or quantitated with real-time PCR. For real-time PCR analysis, the reaction mixture containing cDNA template, primers, and SYBR Green PCR Master Mix (Invitrogen) was run in a 7900 Fast Real-time PCR System (Applied Bio-systems, Carlsbad, CA). Fold changes on mRNA levels were determined by standard curve and after normalization to internal control β-actin RNA levels. Primer sequences used in this study are: QPCT, 5'-CATGGCATGGATTTATTGG-3' and 5'- GACGGTATCAGATCAAAC-3'; QPCT-like, 5'- CAGCGTCTCTGGAGCACTTA-3' and 5'- GCCTCCAGGAACTTTCTGACT -3; GFP 5'- ACGTAAACGGCCACAAGTTC-3' and 5'- TTCAGGGTCAGCTTGCCGTA-3'; actin, 5'-AGAAAATCTGGCCCACACC-3' and 5'-GGGGTGTTGAAGGTCTCAAA-3'; CRYAB, 5'- TCTTGAGCTCAGTGAGTACTGG-3' and 5'-AGCTCACCAGCAGTTCATGG-3'; and mouse QPCT, 5'-CGACTTGAGCCAATTGCTGA-3' and 5'-CTTCCGGGTTAAGAGTGCTG-3'.

mRNA isolation from mouse brain: All mouse experiments were performed under appropriate UK Home Office licences and following institutional procedures. We analyzed samples from N171 mutant HD mice and wild-type littermate controls at 20 week. mRNA was extracted from brains homogenized in Trizol (Invitrogen) using an Ultra torax homogenizer.

Lentivirus infection: shRNA containing pLKO.1 vectors targeting both mouse and human QPCT (TRCN032432) were obtained from The RNAi Consortium (TRC) and scramble shRNA vector was generated in D. Sabatinit's laboratory (Addgene, plasmid 1864). Lentiviral plasmids to express Q80-GFP were kindly provided by J. Uney [55]. Lentiviral particles were produced and transduced following The RNAi Consortium protocols.

***Cell toxicity and aggregation assays*:** Cells were fixed for 7 minutes in 4% paraformaldehyde (PFA). For EGFP-tagged constructs, slides were mounted in Citifluor (Citifluor, Ltd.) containing 4',6-diamidino-2-phenylindole (DAPI; 3 µg/ml; Sigma) and visualized using an Eclipse E600 fluorescence microscope (plan-apo 60x/1.4 oil immersion lens) (Nikon). For detection of HA-tagged constructs, inmunofluorescence with an anti-HA (Covance laboratories 1:500) and anti-mouse Alexa488 secondary antibody (Invitrogen, 1:1000) was performed followed by mounting in Citiflour-DAPI. We assessed the percentage of transfected cells (EGFP- or HA-positive cells) with at least one aggregate per cell. Apoptotic cell death was determined by assessing the nuclear morphology (nuclei fragmented or condensed) in transfected cells. Slides were blinded and at least 200 transfected cells per slide were scored; each individual experiment was performed in triplicate.

Detection of nascent protein synthesis: Protein synthesis was assessed by metabolic incorporation of AHA (L-azidohomoalanine) into cells transfected with EGFP-HTT(Q23). Briefly, 12 hours after HeLa cells transfection, media was washed and replaced with L-methionine/L-cysteine free medium and treated with DMSO or SEN177 (50 uM) for 1h prior to addition of AHA (L-azidohomoalanine) to the media and collection of cells every 2

hours. Labelled protein was detected by western blot after performing Click-IT protein detection assay (Life Technologies) using biotin, following manufacturer protocols.

***Luciferase reporter assay*:** Cells were transfected with 1 µg of GRP78-luciferase (*firefly*) reporter construct and 50 ng of *renilla*-luciferase (pRL-TK) as an internal transfection efficiency control. Cells were collected in Passive lysis buffer and luciferase activity was measured using the Dual-luciferase Reporter Assay System (Promega) following manufacturer's protocol in a Glomax Luminometer (Promega). GRP78-luciferase relative activity was calculated relative to the *renilla*-luciferase transfection efficiency control activity for each sample; experiments were performed in triplicate.

Statistical analysis: Quantification of immunoblots was performed by densitometric analysis using the Image J software or the LI-COR Biosciences infrared imager software and normalized to loading control (actin or tubulin, as indicated). The *p*-values were determined by two-tailed Student's t-test.

Aggregates were counted in at least 200 cells per slide (with the observer blinded to their identity), and percentage was calculated relative to control conditions. *p*-values were determined by unpaired two-tailed Student's t-test.

All experiments were done at least three times in triplicate and a representative blot or graph from a triplicate experiment is shown unless indicated.

Heat shock proteins and chaperones PCR array. The Human Heat Shock Proteins and Chaperones RT2 Profiler PCR Array (SABiosciences, Frederick, MD) was used to study the expression profile of 84 heat shock proteins according to the manufacturer's procedure. Briefly, total RNA was extracted from cells transfected with HTT(Q74)GFP treated with DMSO or 25 uM of SEN177 inhibitor for 24h, using Trizol (Invitrogen) and further purified using RNeasy mini kit with oncolumn DNAse digest (Qiagen), cDNA was then synthesized using an RT2 First strand kit (SABiosciences) and real-time PCR was

performed using 7900HT fast real time PCR system (Applied iosciences). Data were analysed with RT2 profiler PCR array data analysis software version 3.5.

Assays for validation of polyglutamine aggregation modifiers in zebrafish

Maintenance of zebrafish stocks and collection of embryos: All zebrafish husbandry and experiments were performed in accordance with UK legislation under a licence granted by the Home Office and with local ethical approval. Zebrafish were reared under standard conditions (Westerfield et al, 2005) on a 14 h light/10 h dark cycle. Embryos were collected from natural spawnings, staged according to the established criteria [56] and reared in embryo medium (5 mM NaCl, 0.17 mM KCl, 0.33 mM $CaCl_2$, 0.33 mM Mg_2SO_4, 5 mM HEPES).

***Determination of the maximum-tolerated concentration of compounds in larval zebrafish*:** Compound exposure experiments were performed on wild-type larvae (TL strain) from 2 to 3 days post-fertilization (d.p.f.). Concentration response assays were performed over log intervals, from 100 nM to 1 mM, to determine the maximum non-toxic concentration (MTC) for subsequent aggregate analysis assays (n=10 larvae per concentration). Compound exposure experiments were performed in the dark at 28.5 ^{o}C.

Measuring aggregate number and rhodopsin protein levels in transgenic HD zebrafish: Aggregate counting and analysis of rod photoreceptor degeneration (photoreceptor number) was performed using heterozygous larvae from Tg (rho:EGFP-HTT71Q)^{cu5} zebrafish [42] (hereafter referred to as transgenic HD zebrafish). Embryos from outcrossed transgenic HD zebrafish were raised in 0.2 mM 1-phenyl-2-thiourea (PTU) from 1 to 3 d.p.f. to inhibit pigment formation, screened for transgene expression using EGFP fluorescence, and then washed twice in the embryo medium to remove PTU. From 3 to 9 d.p.f., transgenic HD zebrafish larvae were dark-reared in embryo medium alone or embryo medium contain containing either DMSO, 1mM SEN177, 100 µM SEN180 or 100 µM SEN817. Embryo medium and compounds were replenished daily. Larvae were

anaesthetized by immersion in 0.2 mg/ml 3-amino benzoic acid ethyl ester (MS222), then fixed for aggregate counting at 7 d.p.f. or for photoreceptor analysis at 9 d.p.f. Anaesthetised larvae were fixed using 4% paraformaldehyde (PFA) in PBS at 4 ^{o}C. Larvae were washed briefly in PBS, allowed to equilibrate in 30% sucrose in PBS then embedded in OCT medium (Tissue-Tek) and frozen on dry ice for subsequent cryosectioning. Sections were cut at 10 µm thickness using a cryostat (Bright Instruments). For aggregate counting, sections were mounted in 50% glycerol in PBS and the total number of GFP-positive aggregates were counted over 100 µm of the central retina, either side of the optic nerve head and mean values were calculated (n = 5 fish (10 eyes)) for each treatment group. For quantification of photoreceptor number, the GFP-positive area of the central retina was quantified using image thresholding and area analysis in ImageJ (n ≥ 5 fish (10 eyes) for each treatment group). To demonstrate that loss of GFP corresponds to loss of photoreceptors, sections were stained with anti-rhodopsin (1D1) antibody (a kind gift from Paul Linser, University of Florida, FL [57] and mounted using VectaShield hard set mounting medium (Vector Laboratories). Sections were viewed and representative images acquired using a GX Optical LED fluorescent microscope, GXCAM3.3 digital camera and GX Capture software.

References

1. Imarisio, S. *et al*. Huntington's disease: from pathology and genetics to potential therapies. *Biochem. J.* **412,** 191–209 (2008).
2. Zuccato, C., Valenza, M. & Cattaneo, E. Molecular mechanisms and potential therapeutical targets in Huntington's disease. *Physiol. Rev.* **90,** 905–981 (2010).
3. A novel gene containing a trinucleotide repeat that is expanded and unstable on Huntington's disease chromosomes. The Huntington's Disease Collaborative Research Group. *Cell* **72,** 971–983 (1993).

4. Mangiarini, L. *et al.* Exon 1 of the HD gene with an expanded CAG repeat is sufficient to cause a progressive neurological phenotype in transgenic mice. *Cell* **87,** 493–506 (1996).
5. Hodgson, J. G. *et al.* A YAC mouse model for Huntington's disease with full-length mutant huntingtin, cytoplasmic toxicity, and selective striatal neurodegeneration. *Neuron* **23,** 181–192 (1999).
6. Soto, C. & Estrada, L. D. Protein misfolding and neurodegeneration. *Arch. Neurol.* **65,** 184–189 (2008).
7. Takahashi, T. *et al.* Soluble polyglutamine oligomers formed prior to inclusion body formation are cytotoxic. *Hum. Mol. Genet.* **17,** 345–356 (2008).
8. Lajoie, P. & Snapp, E. L. Formation and toxicity of soluble polyglutamine oligomers in living cells. *PloS One* **5,** e15245 (2010).
9. Hartl, F. U., Bracher, A. & Hayer-Hartl, M. Molecular chaperones in protein folding and proteostasis. *Nature* **475,** 324–332 (2011).
10. Sathasivam, K. *et al.* Aberrant splicing of HTT generates the pathogenic exon 1 protein in Huntington disease. *Proc. Natl. Acad. Sci. U. S. A.* **110,** 2366–2370 (2013).
11. Bleicher, K. H., Böhm, H.-J., Müller, K. & Alanine, A. I. Hit and lead generation: beyond high-throughput screening. *Nat. Rev. Drug Discov.* **2,** 369–378 (2003).
12. Li, M., Huang, Y., Ma, A. A. K., Lin, E. & Diamond, M. I. Y-27632 improves rotarod performance and reduces huntingtin levels in R6/2 mice. *Neurobiol. Dis.* **36,** 413–420 (2009).
13. Marsh, J. L. *et al.* Expanded polyglutamine peptides alone are intrinsically cytotoxic and cause neurodegeneration in Drosophila. *Hum. Mol. Genet.* **9,** 13–25 (2000).
14. Dietzl, G. *et al.* A genome-wide transgenic RNAi library for conditional gene inactivation in Drosophila. *Nature* **448,** 151–156 (2007).

15. Schilling, S. *et al.* Isolation and characterization of glutaminyl cyclases from Drosophila: evidence for enzyme forms with different subcellular localization. *Biochemistry* **46,** 10921–10930 (2007).
16. Jackson, G. R. *et al.* Polyglutamine-expanded human huntingtin transgenes induce degeneration of Drosophila photoreceptor neurons. *Neuron* **21,** 633–642 (1998).
17. Franceschini, N. & Kirschfeld, K. [Pseudopupil phenomena in the compound eye of drosophila]. *Kybernetik* **9,** 159–182 (1971).
18. Ravikumar, B. *et al.* Dynein mutations impair autophagic clearance of aggregate-prone proteins. *Nat. Genet.* **37,** 771–776 (2005).
19. Zhang, S., Binari, R., Zhou, R. & Perrimon, N. A genomewide RNA interference screen for modifiers of aggregates formation by mutant Huntingtin in Drosophila. *Genetics* **184,** 1165–1179 (2010).
20. Wyttenbach, A. *et al.* Effects of heat shock, heat shock protein 40 (HDJ-2), and proteasome inhibition on protein aggregation in cellular models of Huntington's disease. *Proc. Natl. Acad. Sci. U. S. A.* **97,** 2898–2903 (2000).
21. Cynis, H. *et al.* Inhibition of glutaminyl cyclase alters pyroglutamate formation in mammalian cells. *Biochim. Biophys. Acta* **1764,** 1618–1625 (2006).
22. Saido, T. C. Involvement of polyglutamine endolysis followed by pyroglutamate formation in the pathogenesis of triplet repeat/polyglutamine-expansion diseases. *Med. Hypotheses* **54,** 427–429 (2000).
23. Onodera, O. *et al.* Oligomerization of expanded-polyglutamine domain fluorescent fusion proteins in cultured mammalian cells. *Biochem. Biophys. Res. Commun.* **238,** 599–605 (1997).

24. Rankin, J., Wyttenbach, A. & Rubinsztein, D. C. Intracellular green fluorescent protein-polyalanine aggregates are associated with cell death. *Biochem. J.* **348 Pt 1,** 15–19 (2000).

25. Luo, S., Mizuta, H. & Rubinsztein, D. C. p21-activated kinase 1 promotes soluble mutant huntingtin self-interaction and enhances toxicity. *Hum. Mol. Genet.* **17,** 895–905 (2008).

26. Buchholz, M. *et al.* The first potent inhibitors for human glutaminyl cyclase: synthesis and structure-activity relationship. *J. Med. Chem.* **49,** 664–677 (2006).

27. Schilling, S. *et al.* Glutaminyl cyclase inhibition attenuates pyroglutamate Abeta and Alzheimer's disease-like pathology. *Nat. Med.* **14,** 1106–1111 (2008).

28. Schilling, S. *et al.* Continuous spectrometric assays for glutaminyl cyclase activity. *Anal. Biochem.* **303,** 49–56 (2002).

29. Yoon, S. & Welsh, W. J. Identification of a minimal subset of receptor conformations for improved multiple conformation docking and two-step scoring. *J. Chem. Inf. Comput. Sci.* **44,** 88–96 (2004).

30. Polgár, T. & Keserü, G. M. Ensemble docking into flexible active sites. Critical evaluation of FlexE against JNK-3 and beta-secretase. *J. Chem. Inf. Model.* **46,** 1795–1805 (2006).

31. Huang, K.-F., Liu, Y.-L., Cheng, W.-J., Ko, T.-P. & Wang, A. H.-J. Crystal structures of human glutaminyl cyclase, an enzyme responsible for protein N-terminal pyroglutamate formation. *Proc. Natl. Acad. Sci. U. S. A.* **102,** 13117–13122 (2005).

32. Huang, K.-F. *et al.* Structures of human Golgi-resident glutaminyl cyclase and its complexes with inhibitors reveal a large loop movement upon inhibitor binding. *J. Biol. Chem.* **286,** 12439–12449 (2011).

33. Ruiz-Carrillo, D. *et al.* Structures of glycosylated mammalian glutaminyl cyclases reveal conformational variability near the active center. *Biochemistry (Mosc.)* **50,** 6280–6288 (2011).
34. Jones, G., Willett, P. & Glen, R. C. Molecular recognition of receptor sites using a genetic algorithm with a description of desolvation. *J. Mol. Biol.* **245,** 43–53 (1995).
35. Jones, G., Willett, P., Glen, R. C., Leach, A. R. & Taylor, R. Development and validation of a genetic algorithm for flexible docking. *J. Mol. Biol.* **267,** 727–748 (1997).
36. Verdonk, M. L., Cole, J. C., Hartshorn, M. J., Murray, C. W. & Taylor, R. D. Improved protein-ligand docking using GOLD. *Proteins* **52,** 609–623 (2003).
37. Palm, K., Luthman, K., Ros, J., Grasjo, J. & Artursson, P. Effect of molecular charge on intestinal epithelial drug transport: pH-dependent transport of cationic drugs. *J. Pharmacol. Exp. Ther.* **291,** 435–443 (1999).
38. Song, H. *et al.* Inhibition of Glutaminyl Cyclase Ameliorates Amyloid Pathology in an Animal Model of Alzheimer's Disease via the Modulation of γ-Secretase Activity. *J. Alzheimers Dis. JAD* (2014). doi:10.3233/JAD-141356
39. Robertson, A. L. *et al.* Small heat-shock proteins interact with a flanking domain to suppress polyglutamine aggregation. *Proc. Natl. Acad. Sci. U. S. A.* **107,** 10424–10429 (2010).
40. Bilen, J. & Bonini, N. M. Drosophila as a model for human neurodegenerative disease. *Annu. Rev. Genet.* **39,** 153–171 (2005).
41. Tue, N. T., Shimaji, K., Tanaka, N. & Yamaguchi, M. Effect of αB-crystallin on protein aggregation in Drosophila. *J. Biomed. Biotechnol.* **2012,** 252049 (2012).
42. Williams, A. *et al.* Novel targets for Huntington's disease in an mTOR-independent autophagy pathway. *Nat. Chem. Biol.* **4,** 295–305 (2008).

44. Lejeune, F.-X. *et al.* Large-scale functional RNAi screen in C. elegans identifies genes that regulate the dysfunction of mutant polyglutamine neurons. *BMC Genomics* **13,** 91 (2012).

45. Miller, J. P. *et al.* Matrix metalloproteinases are modifiers of huntingtin proteolysis and toxicity in Huntington's disease. *Neuron* **67,** 199–212 (2010).

46. Miller, J. P. *et al.* A genome-scale RNA-interference screen identifies RRAS signaling as a pathologic feature of Huntington's disease. *PLoS Genet.* **8,** e1003042 (2012).

47. Yamanaka, T. *et al.* Large-scale RNA interference screening in mammalian cells identifies novel regulators of mutant huntingtin aggregation. *PloS One* **9,** e93891 (2014).

48. Waudby, C. A. *et al.* The interaction of alphaB-crystallin with mature alpha-synuclein amyloid fibrils inhibits their elongation. *Biophys. J.* **98,** 843–851 (2010).

49. Raman, B. *et al.* AlphaB-crystallin, a small heat-shock protein, prevents the amyloid fibril growth of an amyloid beta-peptide and beta2-microglobulin. *Biochem. J.* **392,** 573–581 (2005).

50. Hochberg, G. K. A. *et al.* The structured core domain of αB-crystallin can prevent amyloid fibrillation and associated toxicity. *Proc. Natl. Acad. Sci. U. S. A.* **111,** E1562–1570 (2014).

51. Freeman, M. Reiterative use of the EGF receptor triggers differentiation of all cell types in the Drosophila eye. *Cell* **87,** 651–660 (1996).

52. Narain, Y., Wyttenbach, A., Rankin, J., Furlong, R. A. & Rubinsztein, D. C. A molecular investigation of true dominance in Huntington's disease. *J. Med. Genet.* **36,** 739–746 (1999).

53. D'Agostino, M. *et al.* The cytosolic chaperone α-crystallin B rescues folding and compartmentalization of misfolded multispan transmembrane proteins. *J. Cell Sci.* **126,** 4160–4172 (2013).

54. Renna, M., Caporaso, M. G., Bonatti, S., Kaufman, R. J. & Remondelli, P. Regulation of ERGIC-53 gene transcription in response to endoplasmic reticulum stress. *J. Biol. Chem.* **282,** 22499–22512 (2007).

55. Howarth, J. L. *et al.* Hsp40 molecules that target to the ubiquitin-proteasome system decrease inclusion formation in models of polyglutamine disease. *Mol. Ther. J. Am. Soc. Gene Ther.* **15,** 1100–1105 (2007).

56. Kimmel, C. B., Ballard, W. W., Kimmel, S. R., Ullmann, B. & Schilling, T. F. Stages of embryonic development of the zebrafish. *Dev. Dyn. Off. Publ. Am. Assoc. Anat.* **203,** 253–310 (1995).

57. Hyatt, G. A., Schmitt, E. A., Fadool, J. M. & Dowling, J. E. Retinoic acid alters photoreceptor development in vivo. *Proc. Natl. Acad. Sci. U. S. A.* **93,** 13298–13303 (1996).

Figure 1

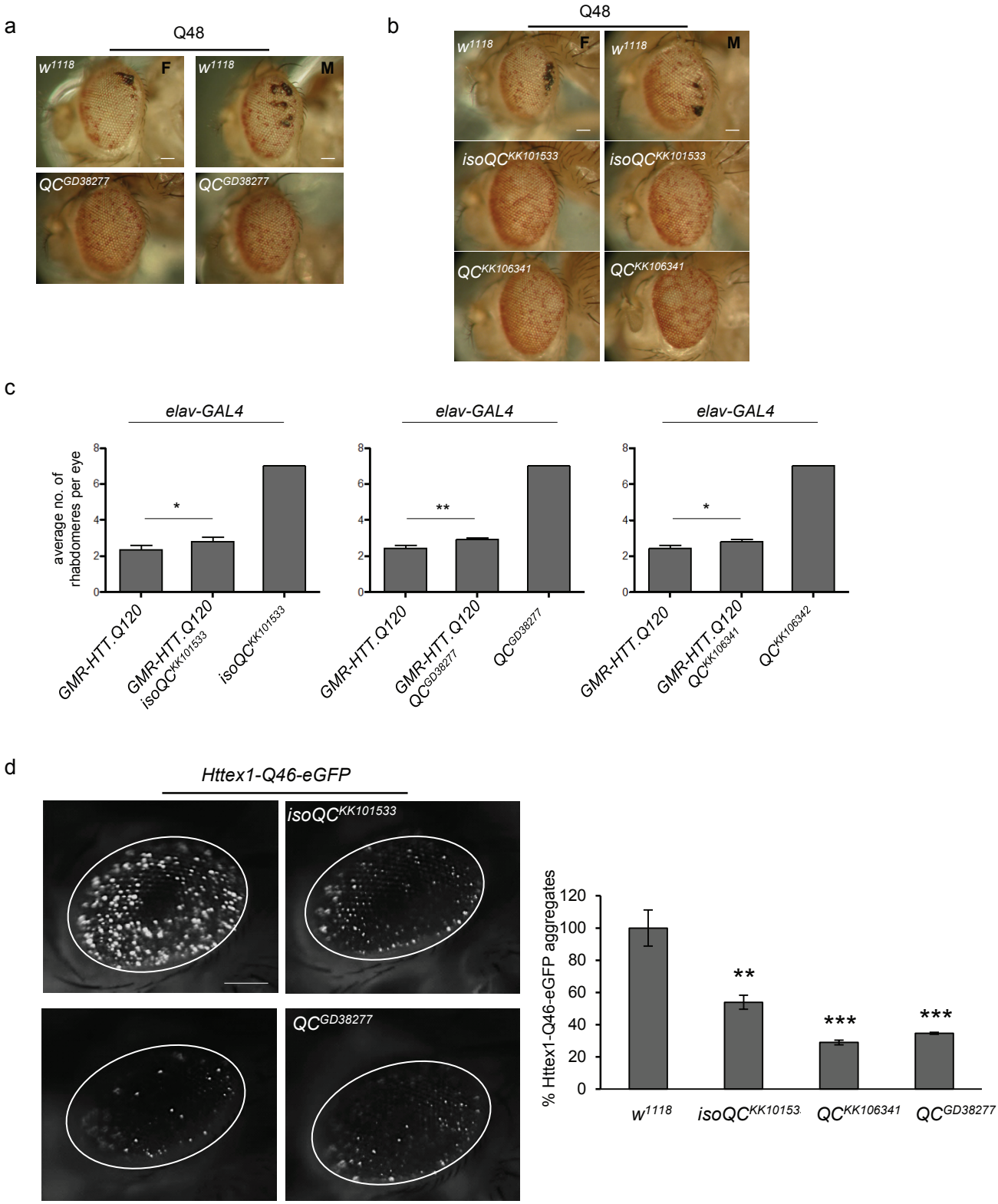
a
Q48
w1118 F
w1118 M
QCGD38277
QCGD38277
b
Q48
w1118 F
w1118 M
isoQCKK101533
isoQCKK101533
QCKK106341
QCKK106341
c
elav-GAL4
elav-GAL4
elav-GAL4
average no. of rhabdomeres per eye
0
2
4
6
8
*
**
*
GMR-HTT.Q120
GMR-HTT.Q120 isoQCKK101533
isoQCKK101533
GMR-HTT.Q120
GMR-HTT.Q120 QCGD38277
QCGD38277
GMR-HTT.Q120
GMR-HTT.Q120 QCKK106341
QCKK106342
d
Httex1-Q46-eGFP
isoQCKK101533
QCGD38277
% Httex1-Q46-eGFP aggregates
0
20
40
60
80
100
120
**
***
***
w1118
isoQCKK10153
QCKK106341
QCGD38277

Figure 2

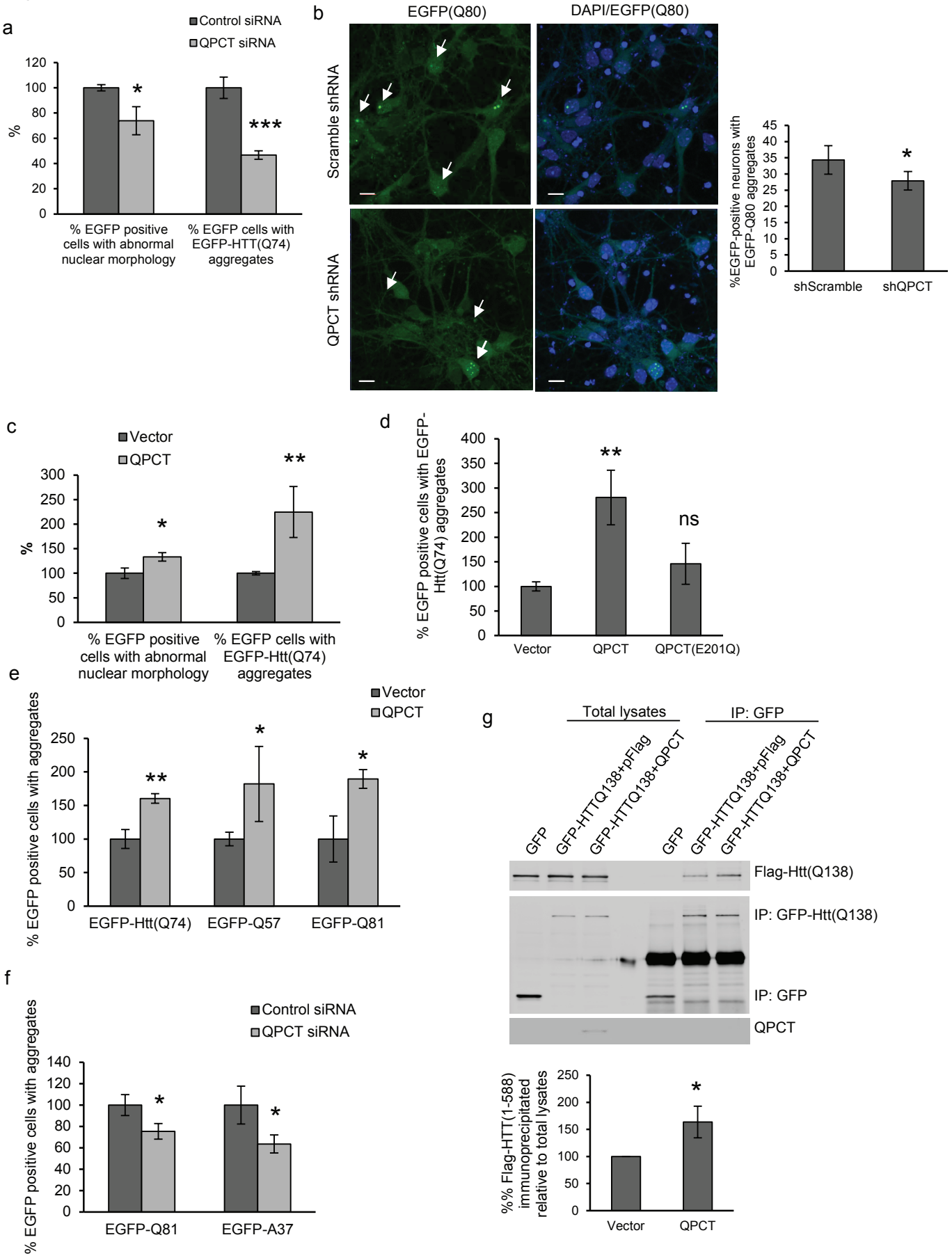
a
Control siRNA
QPCT siRNA
%
% EGFP positive cells with abnormal nuclear morphology
% EGFP cells with EGFP-HTT(Q74) aggregates
b
EGFP(Q80)
DAPI/EGFP(Q80)
Scramble shRNA
QPCT shRNA
%EGFP-positive neurons with EGFP-Q80 aggregates
shScramble
shQPCT
c
Vector
QPCT
%
% EGFP positive cells with abnormal nuclear morphology
% EGFP cells with EGFP-Htt(Q74) aggregates
d
% EGFP positive cells with EGFP-Htt(Q74) aggregates
ns
Vector
QPCT
QPCT(E201Q)
e
Vector
QPCT
% EGFP positive cells with aggregates
EGFP-Htt(Q74)
EGFP-Q57
EGFP-Q81
f
Control siRNA
QPCT siRNA
% EGFP positive cells with aggregates
EGFP-Q81
EGFP-A37
g
Total lysates
IP: GFP
GFP
GFP-HTTQ138+pFlag
GFP-HTTQ138+QPCT
Flag-Htt(Q138)
IP: GFP-Htt(Q138)
IP: GFP
QPCT
%% Flag-HTT(1-588) immunoprecipitated relative to total lysates
Vector
QPCT

Figure 3

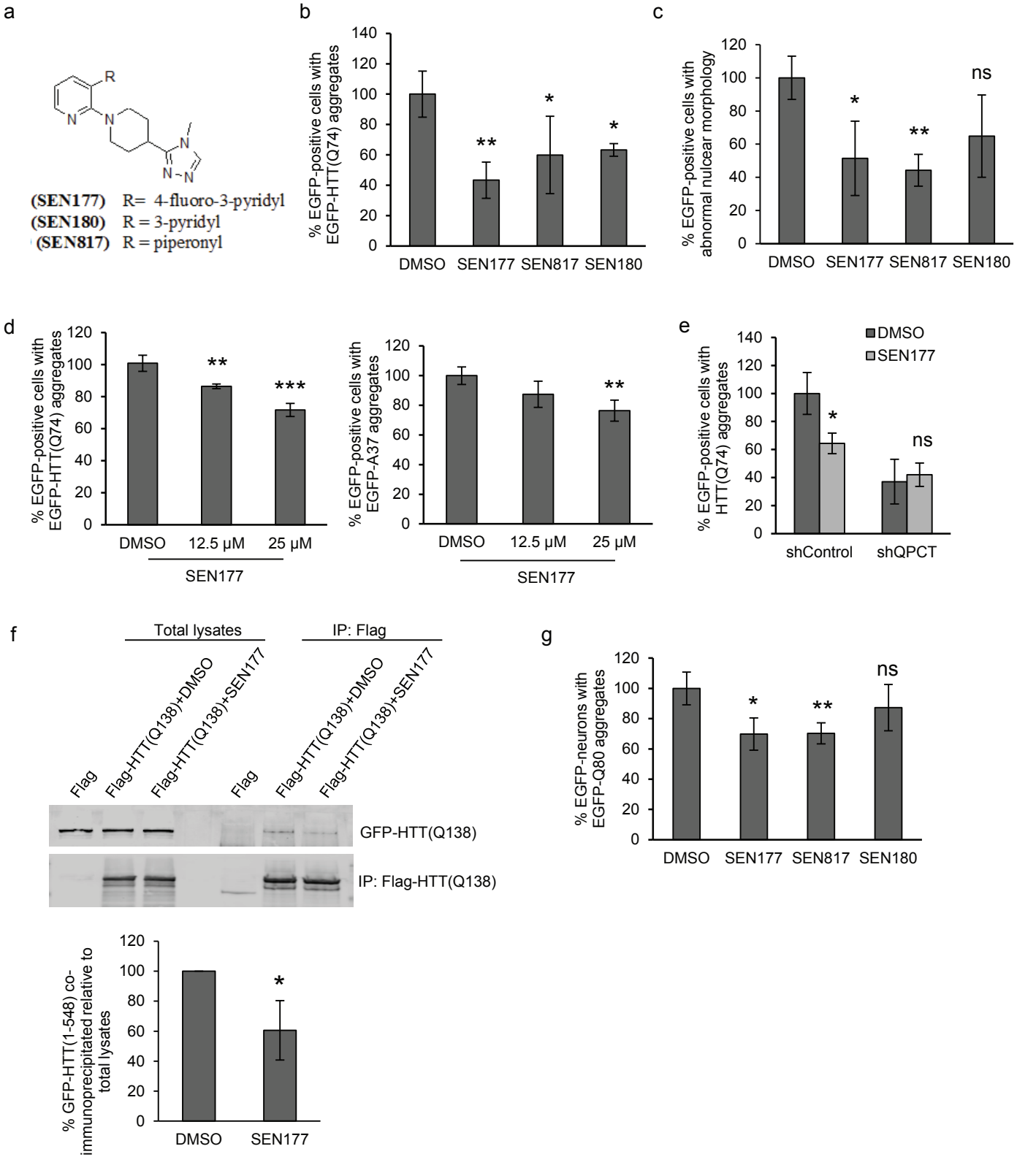
a
(SEN177) R= 4-fluoro-3-pyridyl
(SEN180) R = 3-pyridyl
(SEN817) R = piperonyl
b
% EGFP-positive cells with EGFP-HTT(Q74) aggregates
DMSO SEN177 SEN817 SEN180
c
% EGFP-positive cells with abnormal nulcear morphology
ns
DMSO SEN177 SEN817 SEN180
d
% EGFP-positive cells with EGFP-HTT(Q74) aggregates
DMSO 12.5 μM 25 μM
SEN177
% EGFP-positive cells with EGFP-A37 aggregates
e
DMSO
SEN177
% EGFP-positive cells with HTT(Q74) aggregates
ns
shControl shQPCT
f
Total lysates
IP: Flag
Flag
Flag-HTT(Q138)+DMSO
Flag-HTT(Q138)+SEN177
GFP-HTT(Q138)
IP: Flag-HTT(Q138)
% GFP-HTT(1-548) co-immunoprecipitated relative to total lysates
DMSO SEN177
g
% EGFP-neurons with EGFP-Q80 aggregates
ns
DMSO SEN177 SEN817 SEN180

Figure 4

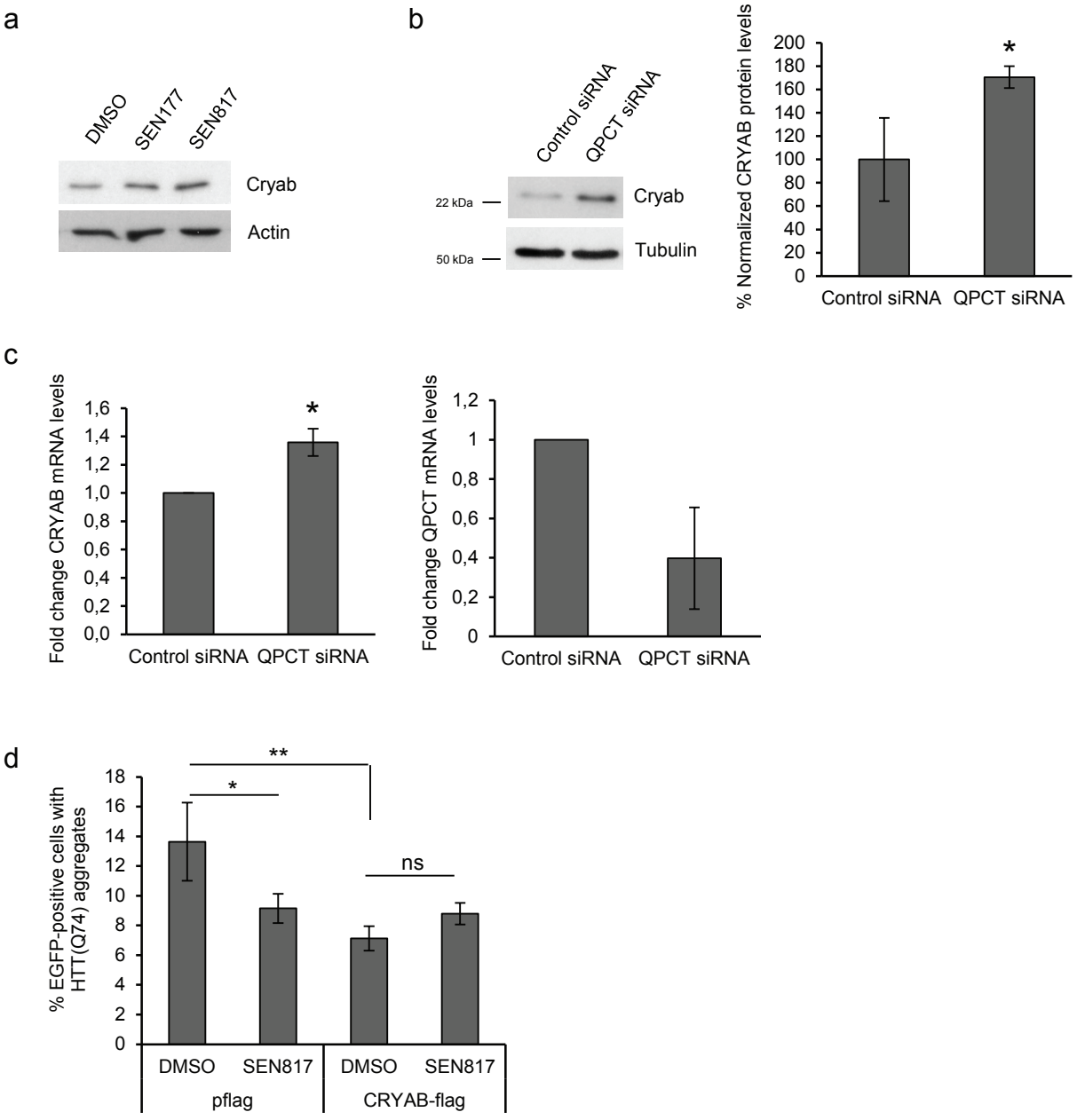
a
DMSO
SEN177
SEN817
Cryab
Actin
b
Control siRNA
QPCT siRNA
22 kDa
50 kDa
Cryab
Tubulin
% Normalized CRYAB protein levels
200
180
160
140
120
100
80
60
40
20
0
*
Control siRNA
QPCT siRNA
c
Fold change CRYAB mRNA levels
1,6
1,4
1,2
1,0
0,8
0,6
0,4
0,2
0,0
*
Control siRNA
QPCT siRNA
Fold change QPCT mRNA levels
1,2
1
0,8
0,6
0,4
0,2
0
Control siRNA
QPCT siRNA
d
% EGFP-positive cells with HTT(Q74) aggregates
18
16
14
12
10
8
6
4
2
0
**
*
ns
DMSO
SEN817
DMSO
SEN817
pflag
CRYAB-flag

Figure 5

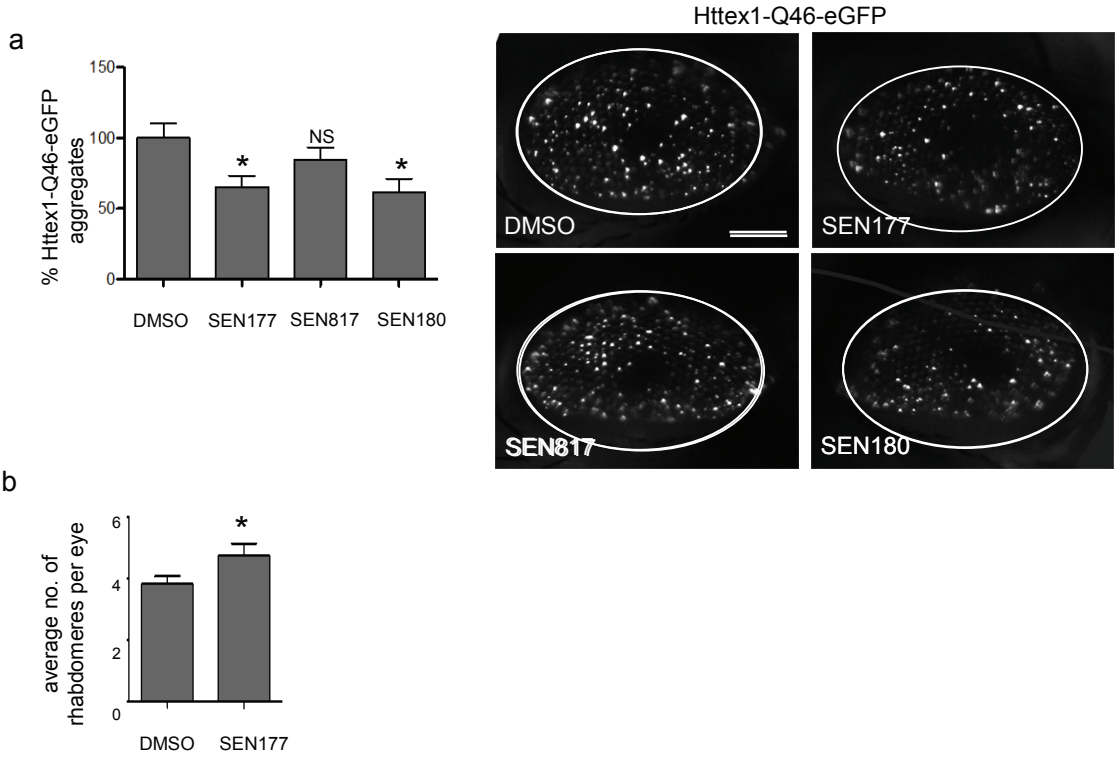
a
% Httex1-Q46-eGFP aggregates
150
100
50
0
*
NS
*
DMSO
SEN177
SEN817
SEN180
Httex1-Q46-eGFP
DMSO
SEN177
SEN817
SEN180
b
average no. of rhabdomeres per eye
6
4
2
0
*
DMSO
SEN177

Figure 6

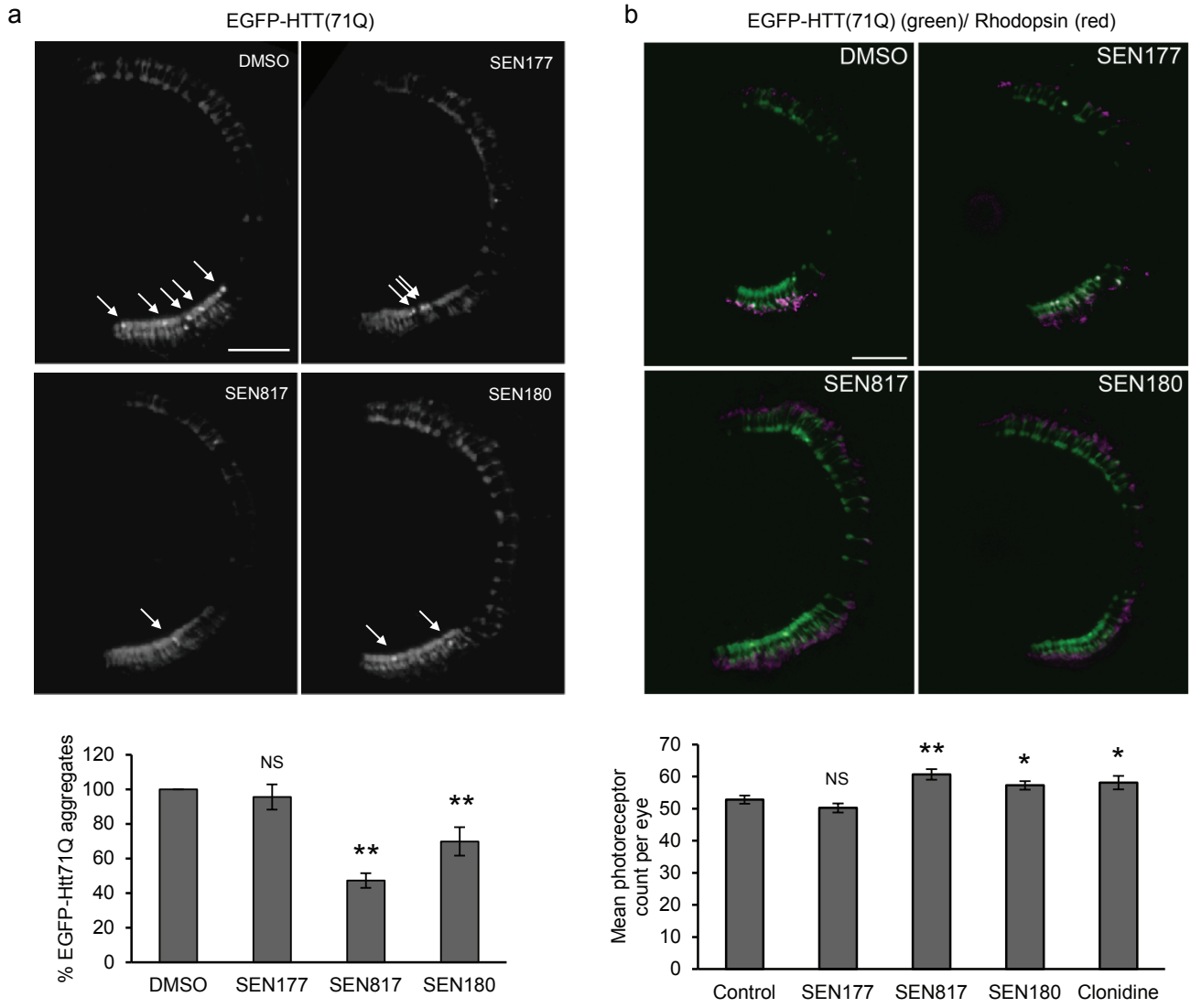
a
EGFP-HTT(71Q)
DMSO
SEN177
SEN817
SEN180
b
EGFP-HTT(71Q) (green)/ Rhodopsin (red)
DMSO
SEN177
SEN817
SEN180
% EGFP-Htt71Q aggregates
120
100
80
60
40
20
0
NS
**
**
DMSO
SEN177
SEN817
SEN180
Mean photoreceptor count per eye
70
60
50
40
30
20
10
0
NS
**
*
*
Control
SEN177
SEN817
SEN180
Clonidine

SUPPLEMENTARY INFORMATION

siRNA screen identifies QPCT as a druggable target for Huntington's disease

Maria Jimenez-Sanchez[1], Wun Lam[1,2], Michael Hannus[3,§], Birte Sönnichsen[3,§], Sara Imarisio[1,2,§,] Angeleen Fleming[1,4,§], Alessia Tarditi[6,#], Fiona Menzies[1], Teresa Ed Dami[1,4,5], Catherine Xu[1,4], Eduardo Gonzalez-Couto[6,€], Giulia Lazzeroni[6], Freddy Heitz[6,£], Daniela Diamanti[6], Luisa Massai[6], Venkata P. Satagopam[7,8], Guido Marconi[6,$], Chiara Caramelli[6,&], Arianna Nencini[6], Matteo Andreini[6], Gian Luca Sardone[6], Nicola P. Caradonna[6], Valentina Porcari[6], Carla Scali[6], Reinhard Schneider[7,8], Giuseppe Pollio[6], Cahir J. O'Kane[2], Andrea Caricasole[6,^,*] and David C. Rubinsztein[1,*]

[1]Department of Medical Genetics, University of Cambridge, Cambridge Institute for Medical Research, Addenbrooke's Hospital, Hills Road, Cambridge CB2 0XY, UK

[2] Department of Genetics, University of Cambridge, Cambridge CB2 3EH, UK

[3]Cenix BioScience GmbH, Tatzberg 47, 01307 Dresden, Germany

[4]Department of Physiology, Development and Neuroscience, University of Cambridge, Downing Street, Cambridge, UK, CB2 3EG.

[5] Department of Neuroscience, Psychology, Drug Research and Child Health, Division of Pharmacology and Toxicology, University of Florence, Florence, Italy

[6]Siena Biotech. Strada del Petriccio e Belriguardo, 35 53100 Siena, Italy

[7]Structural and Computational Biology, EMBL, Meyerhofstr.1, 69117, Heidelberg, Germany

[8]Luxembourg Centre for Systems Biomedicine (LCSB), University of Luxembourg, Campus Belval, House of Biomedicine, 7 avenue des Hauts-Fourneaux, L-4362 Esch-sur-Alzette, Luxembourg

[#]Current address: TPV GmbH, Messerschmittstr. 1+3 , D-80992 München, Germany

[£]Current address: GenKyoTex S.A.,16 Chemin des Aulx, CH-1228,Geneva, Switzerland

[€]Current address: Integromics S.L., Santiago Grisolía, 2 E-28760 Tres Cantos (Madrid)

[$]Current address: Autifony S.r.l., Via Fleming, 437135 Verona (VR), Italy

[&]Current address: Novartis Vaccines and Diagnostics srl CQ Bioprocess support unit 53018 Rosia (SI), Italy

^Current address: IRBM Promidis, Via Pontina Km 30.600, 00040 Pomezia (Rome, Italy)

[§] Authors contributed equally to this work

*Address correspondence to: David C. Rubinsztein – Tel: +44 (0)1223 762608,

Fax: +44 (0)1223 331206, E-mail: dcr1000@hermes.cam.ac.uk or to Andrea Caricasole E-mail A.Caricasole@irbm.it

Supplementary Notes

Supplementary Note 1. Details for primary high-throughput siRNA screen development and analysis

Supplementary Note 2. Detailed synthesis and characterization of QPCT inhibitors

Supplementary Data Sets

Supplementary Data Set 1. List of 257 human genes obtained in HEK293 siRNA screen and its validation in *Drosophila*

Supplementary Data Set 2. List of RNAi Drosophila lines that rescued Q48-eye degeneration and their effect on GFP levels

Supplementary Data Set 3. Complete results from Heat shock proteins PCR array.

Supplementary Results

Supplementary Figure legends

Supplementary figure 1. Characterization of full-length HTT(Q138) inducible cell line

a. HEK293/T Rex cells were stably transfected with full-length HTT with 138 polyglutamines, HTT(Q138), and expression was induced by treatment with doxycycline (1µg/ml) for 0, 24 or 48 hours. An anti-N-terminal HTT antibody recognizing amino acids 3-16 of human HTT was used to check the expression of the mutant HTT in total lysates (Input) or after immunoprecipitation with anti-Flag antibodies. Tubulin was used as a loading control.

b. HEK293/T Rex cells expressing HTT(Q138) were treated with doxycycline (1µg/ml) for 48 hours and mRNA levels of HTT transgene were assessed by QPCR using primers amplifying sequences close to 800, 2000, 4000, 6500, 8100, 9050, the Flag epitope or an untranslated region, and were compared to mRNA levels under non-induced conditions.

c. Cell viability assay with ROCK1 inhibitor (Y27632) reference compound. The ROCK1 inhibitor (Y27632) was tested at 20µM on HEK293/T Rex cells stably transfected with full-length HTT with 138 polyglutamines, HTT(Q138), and induced by treatment with doxycycline (1µg/ml) for 0 and 72 hours. Cell viability was assessed with the ATPlite Assay System and showed an increase of the ATP concentration due to the effect of the compound. The Z' factor between not induced control and doxycycline-induced condition was 0.42, Graphs shows mean values normalized to 100 with error bars representing standard deviation. Statistical analyses were performed by unpaired Student's test: ***p<0.001.

Supplementary figure 2. Primary high-throughput screening for suppressors of mutant HTT toxicity in cell cultures

a. Venn diagram representing the redundancy of the three readouts evaluated in the siRNA screen in pass 1. Each circle represents the 1000 siRNAs scoring highest in the rescue

indices of the three parameters: proliferation, aberrant nuclei index and apoptotic index. Numbers in each overlapping segment indicate the number of positive siRNAs shared by different readouts.

b. Pairwise alignment of rescue indices for proliferation (y axis) against aberrant nuclei index (x axis) obtained in pass 1. In green, control non-targeting siRNAs (negQ and negF); in light blue, non-transfected cells; red points correspond to HTT siRNA treated cells; and dark blue represent siRNA samples.

Supplementary figure 3. Secondary RNAi screen in a *Drosophila* model of HD

a, b. Examples of suppressors of Q48 eye degeneration. Flies expressing the Q48 protein in the eye (*GMR-GAL4; UAS-Q48.myc/flag*) were crossed with *UAS-RNAi* fly lines for each of the genes selected from the screen or with the corresponding background control used (w^{1118}, stock number 60000 for GD-RNAi lines and 60100 for KK-RNAi lines). Examples of suppressors from the GD-RNAi line collection (**a**) and from the KK-RNAi line collection (**b**) showed a partial rescue on the eye pigmentation and on of black necrotic-like spots respectively. F=female; M=male. Scale bars represent 200 µm.

Supplementary figure 4. Functional categorization of mutant HTT toxicity modifiers.

a. Pie chart representation of the main molecular functions of genes obtained from siRNA screen in HEK293 cells (670 primary and 257 further selected genes) (top and middle) and 66 validated genes in *Drosophila* (bottom).

b. Top functional pathways associated with the 66 hits validated in *Drosophila*. Canonical pathways were determined by an Ingenuity Pathway Analysis and were ranked by –log(p-value). The significance of the association between the data set and the canonical pathway was measured in 2 ways: 1) a ratio of the number of molecules from the data set that map to the pathway divided by the total number of molecules that map to the canonical pathway

displayed, 2) Fisher's exact test was used to calculate a *p*-value (blue bars) determining the probability that the association between the genes in the dataset and the canonical pathway is explained by chance alone (*p*-value). The threshold line represents a *p*-value of 0.05, canonical pathways below the yellow line are not statistically significant. Number and name of the genes associated with each of the top 30 pathways are shown in Supplementary Table 1b.

Supplementary figure 5. Validation of QPCT RNAi lines in *Drosophila*

a. Downregulation of QPCT fly orthologs *QC* and *isoQC* using the KK-RNAi lines (lines $QC^{KK106341}$ and $isoQC^{KK101533}$) reduced the number of black necrotic-like spots of Q48 flies. Fisher's exact test was applied for statistical comparison between the control and test genotypes. BS= black necrotic-like spots; no BS= absence of black necrotic-like spots.

b. Downregulation of QPCT fly orthologs *QC* and *isoQC* (lines $QC^{GD38277}$ and $isoQC^{KK101533}$) using GMR-GAL4 did not decrease GFP expression level. Graph represents mean ± SEM from 3 independent crosses for each genotype, with control conditions (GFP) set to 1. Statistical analyses were performed by unpaired two-tailed Student's t-test: $^{**}p<0.01$; NS, not significant. Full blot images are shown in supplementary figure 18a.

Supplementary figure 6. Validation of QPCT in mammalian cell lines

a. The number of HEK293 cells transfected with EGFP-HTT(Q74) containing HTT(Q74) aggregates relative to the number of transfected cells is reduced when QPCT is knocked down with siRNA compared to scramble siRNA treated cells. Representative images are shown andquantification is shown in figure 2a. Scale bar represents 20 µm.

b. We confirmed the efficiency of QPCT knockdown by analyzing mRNA levels by RT-PCR, due to the lack of antibodies that recognize the endogenous protein. Total RNA was extracted, cDNA synthesized and mRNA levels of QPCT and actin from HEK293 cells

transfected with control or QPCT siRNA were amplified by standard PCR and visualized in agarose gel stained with ethidium bromide. Full gel images are shown in supplementary figure 18b.

c. We confirmed that the QPCT siRNAs used in these experiments do not target QPCT-like. QPCT-like mRNA levels do not change upon QCPT siRNA treatment, measured by quantitative RT-PCR. Graph shows the mean of two independent experiments in triplicate with error bars representing standard deviation.

d. HeLa cells were transfected with scrambled or QPCT siRNA followed by transfection with EGFP-HTT(Q74) for another 48 hours. Cells were fixed and the percentage of cells with HTT(Q74) aggregates in EGFP-positive cells was scored by fluorescence microscopy.

e. As in c, we knocked down QPCT in HEK293 cells, then EGFP-HTT(Q138) was transfected for the last 48h and the percentage of green cells with aggregates was scored.

f. After knocking down QPCT, HeLa cells were split in 96 well plates and treated with 1 μM staurosporine or DMSO for the last 8 h. Caspase 3/7 activity was determined by using a luciferase reporter assay and normalized to protein levels. The average of a triplicate experiment is represented in the graph with error bars representing standard deviation.

g. QPCT mRNA levels relative to Actin mRNA was quantified using real time PCR to confirm the level of knockdown in primary cortical neurons infected with scramble or QPCT shRNA for 6 days. Graph show the fold change in QPCT mRNA levels normalized to actin in cells treated with QPCT shRNA relative to scramble shRNA treated cells from a representative experiment.

In all panels, unless indicated, graphs show mean values with control conditions set to 100 or 1, and error bars represent standard deviation from a triplicate experiment representative of at least three independent experiments. Statistical analyses were performed by two-tailed unpaired Student's t-test: $^{**}p<0.01$; $^{*}p<0.05$; NS, not significant.

Supplementary figure 7. Characterization of QPCT overexpression in mammalian cell lines

a. Percentage of EGFP-HTT(Q74) cells with aggregates was determined in HEK293 cells transfected with either pCMV6-QPCT or empty vector for 48 hours. Graphs show mean values with control conditions set to 100 and error bars represent standard deviation from a triplicate experiment representative of at least three independent experiments. Statistical analyses were performed by unpaired two-tailed Student's t-test: $^{**}p<0.01$.

b. HeLa cells expressing QCPT-Flag or empty Flag vector were split in 96 well plates and treated with 1 μM staurosporine or DMSO for the last 8 h. Caspase 3/7 activity was determined by using a luciferase reporter assay and normalized to protein levels. The average of a triplicate experiment is represented in the graph with error bars representing standard deviation. Statistical analyses were performed by two-tailed Student's t-test, ns: non- significant.

c. Substitution of E201 to glutamine or aspartic residues inactivates QPCT enzymatic activiy [1]. We generated a QPCT construct fused to a Flag epitope in which we mutagenized the aspartic 201 to glutamine (E201Q). Both, wild-type and mutant forms were expressed at similar levels in HeLa cells, as detected by western blot using anti-Flag antibodies. Full blot images are shown in supplementary figure 18c.

d. The enzymatic activity of wild type and mutant QPCT(E201Q) was assessed by fluorometric analysis representing the kinetic of pGlu-AMC formation of either cell lysates (Left panel) or conditioned media (Right panel) from HEK293 cells expressing QPCT-Flag, QPCT(E201Q)-Flag, non-transfected cells or a reaction blank, incubated with Glu-AMC and pyroglutamyl aminipeptidase at different time points. No activity above background was detected on expression of the E201 mutant.

Supplementary figure 8. Determination of QPCT mRNA levels in mouse brains

mRNA was extracted from mouse brain from six N171 mutant HD mice and four wild-type littermate controls at 20 week of age. Relative levels of QPCT mRNA of each brain detected by quantitative PCR were normalized to GAPDH mRNA and the mean values are represented in the graph with error bars representing standard deviation. Statistical analyses were performed by two-tailed unpaired Student's t-test: *p<0.05.

Supplementary figure 9. QPCT modulates aggregation of HA-tagged HTT(Q74)

a. HeLa cells were treated with scrambled or QPCT siRNA followed by a second siRNA transfection together with HA-HTT(Q74) for another 24 hours. Cells were fixed followed by inmunofluorescence with anti-HA antibodies and the number of HA-transfected cells containing aggregates was scored.

b. HeLa cells were transfected QPCT overexpression construct together with HA-HTT(Q74) for 24 hours. Cells were fixed and HA-transfected cells were detected by immunofluorescence and the percentage of cells with HA aggregates was scored.

Graphs show mean values with control conditions set to 100 and error bars represent standard deviation from a triplicate representative experiment. Statistical analyses were performed by two-tailed Student's t-test: *p<0.05.

Supplementary figure 10. No effect of PBD150 on mutant HTT aggregation

a. The effect of increased doses of a previously described QPCT inhibitor, PBD150 [2], was assessed in HeLa cells transfected with EGFP-HTT(Q74). The effect of the compound at the indicated concentrations, or DMSO as a control, was assessed after 24h by counting the number of EGFP-positive cells containing aggregates.

b. Cells expressing empty vector or QPCT together with EGFP-HTT(Q74) were treated with PBD150 for 24h. This compound was not able to inhibit the effect of QPCT increasing the number of aggregates containing cells.

Graphs show mean values and error bars represent standard deviation from a representative triplicate experiment. Statistical analyses were performed by two-tailed unpaired Student's t-test: NS, not significant.

Supplementary figure 11. Characterization of QPCT inhibitors

a. Table showing the activity and *in vitro* ADME properties of the compounds. [a]IC_{50} were determined fluorometrically for QPCT and QPCT-like by a coupled enzyme assay with 50 µM H-Gln-AMC substrate. [b]Solubility was determined at pH 7.4 at pseudothermodynamic equilibrium. [c]Metabolic stability was determined as percentage remaining after incubation for 1 h with recombinant hCYP3A4. [d]Permeability was based on measuring the permeation rate of the compound through an artificial membrane. The PAMPA-BBB assay uses a mixture of porcine brain lipids in dodecane (2% w/v).

b. A dose response effect of SEN817 on aggregation was detected in HeLa cells transfected with EGFP-HTT(Q74) and treated with increasing concentrations of QPCT inhibitor (SEN817) for 24 h and compared to DMSO treated cells.

c. A general effect of QPCT inhibitors on protein levels was discarded by transfecting HeLa cells with an EGFP expressing vector and levels were determined by western blotting after 24h treatment with the indicated compounds (50 µM). Tubulin was used as a loading control. Graph represents the average of 3 independent experiments in triplicate. Full blot images are shown in supplementary figure 18d.

d. De novo synthesis of HTT(Q23) was assessed by metabolic labeling of HeLa cells transfected with EGFP-HTTQ23 with AHA. After treating with DMSO or SEN177 (50 µM) (Time 0), AHA was added and cells collected at the indicated time points. Newly synthesized

HTT(Q23) was detected with anti-GFP antibody and relative levels are represented in the graph. Full blot images are shown in supplementary figure 18e.

e. We confirmed that the effect of the compounds was dependent on QPCT inhibition by validating their effect in cells where QPCT was downregulated using lentivirus bearing QPCT shRNA. Treatment with 50 µM SEN817 for 24 h reduced aggregation of EGFP-HTT(Q74) in HeLa cells infected with scramble shRNA, while this effect was abolished when cells were treated with QPCT shRNA.

f. We confirmed that QPCT was efficiently knocked down with shRNA by quantifying the mRNA levels of QPCT relative to actin, by real time PCR. Graph represents values obtained from 2 independent experiments.

In all panels, graphs show mean values with control conditions set to 100 and error bars represent standard deviation from a triplicate experiment representative of at least three independent experiments. Statistical analyses were performed by two-tailed unpaired Student's t-test: $**p<0.01$; $*p<0.05$; NS, not significant.

Supplementary figure 12. QPCT effect is independent on protein degradation pathways: autophagy or proteasome activity

The effect of QPCT was studied in conditions were autophagy was inhibited by removing the essential autophagy gene Atg5 (Atg5-/- MEFs) [3] (a) or by treating cells with an autophagy inhibitor, 3-methyladenine (3-MA) (b) which, as reported previously, results in higher percentages of aggregate-positive cells [4].

a. Wild-type or Atg5-null mouse embryonic fibroblasts (MEFs) were infected with lentiviral scramble or QPCT shRNA for 5 days. In the last 2 days, EGFP-HTT(Q74) was transfected and the percentage of transfected cells with aggregates was scored. QPCT knockdown in both wild-type and autophagy- deficient cells led to a reduced percentage of cells with

HTT(Q74)GFP aggregates, irrespective of whether they were autophagy-competent or -deficient.

b. Similarly, the ability of QPCT overexpression to increase the percentage of HTT-aggregate-containing cells was also independent of autophagy, since expression of QPCT together with EGFP-HTT(Q74) for 48 hours resulted in an increase in the percentages of cells with aggregates, irrespective of the treatment with 3-MA for the last 16 hours.

c. A possible effect of QPCT on autophagic activity was also dismissed by assessing the levels of LC3-II, a conjugated form of LC3 that is specifically recruited to autophagosome membranes [5]. LC3-II protein levels correlate with the number of autophagosomes per cell [6 7]. LC3-II levels depend on changes in autophagosome synthesis or degradation. To differentiate between these two possibilities, we performed these experiments in the presence of bafilomycin A1, an inhibitor of autophagosome-lysosome fusion [8]. HeLa cells were treated with QPCT siRNA or transfected with QPCT DNA constructs. For the last 4 hours, cells were treated with bafilomycin A1 and western blot analysis was performed in total cell lysates using an anti-LC3 antibody and actin as a loading control. Quantification relative to actin is shown in the graphs. Full blot images are shown in supplementary figure 18f.

d. To test whether QPCT exerts its effect by modulation of proteasome activity, we overexpressed QPCT in the presence of a proteasome inhibitor, MG132, which leads to an increase in the number of cells with HTT(Q74) aggregates. The percentage of cells with EGFP-HTT(Q74) aggregates in HeLa cells transfected with QPCT was still enhanced when cells were treated with MG132 for the last 16 hours, indicating a proteasome-independent activity of QPCT.

e. We further confirmed that QPCT cannot modify proteasome activity, which can be monitored by changes in Ub^{G76V}-GFP, an ubiquitin-proteasome system (UPS) activity reporter that is efficiently and quickly recognized by the proteasome but accumulates in the presence of MG132 [9]. HeLa cells stably expressing Ub(G76V)-GFP were transfected with

either empty vector or QPCT overexpression constructs. GFP fluorescence intensity was quantified by flow cytometry. As a control, GFP intensity was determined in cells subjected to 16 hours treatment with MG132.

These data suggest that QPCT perturbations do not influence the percentage of cells with HTT aggregates via alterations of the UPS or macroautophagy, the major intracellular protein degradation pathways.

Graphs shows mean values with control conditions set to 100 and error bars represent standard deviation from a triplicate representative experiment. Statistical analysis were performed by two-tailed unpaired Student's t-test: ***p<0.001, **p<0.01; *p<0.05; NS, not significant.

Supplementary figure 13. QPCT does not change mRNA levels or total protein levels and its effect does not depend on the secreted fraction

a. We confirmed that QPCT does not change mRNA levels of the transgene by assessing the mRNA levels of GFP in HeLa cells transfected with scramble or QPCT shRNA, along with EGFP empty vector for the last 48h. mRNA levels of GFP, QPCT or actin were quantified by quantitative real time PCR. Fold changes in GFP and QPCT mRNA levels relative to actin from 3 independent experiments are shown in the graphs.

b. We excluded any effect of QPCT on protein levels by co-transfecting HeLa cells with EGFP-HTTQ23 (this form does not aggregate and it is not a target for degradation by autophagy [4 10]) and DsRed, and either empty vector or QPCT. GFP fluorescence intensity was determined by flow cytometry in green- and red-positive cells.

c. Since QPCT is localized in the secretory pathway and it is secreted to the extracellular media [11], we assessed whether its effect on mutant HTT aggregation depends on the extracellular fraction of QPCT or QPCT-modified targets that are secreted. Cells expressing HA-HTT(Q74) were incubated in conditioned media from cells expressing QPCT for 48

hours. Incubation of cells with QPCT-containing conditioned media did not increase aggregation, suggesting that the effect of QPCT on mutant HTT aggregation is not dependent on the extracellular fraction of QPCT. As a control to check the effect of transfected QPCT on aggregation, another set of cells were transfected in parallel with QPCT-Flag together with HA-HTT(Q74).

In all panels, graphs show mean values with control conditions set to 100 and error bars represent standard deviation from a triplicate experiment representative of at least three independent experiments. Statistical analyses were performed by two-tailed unpaired Student's t-test*$p<0.05$; NS, not significant.

Supplementary figure 14. Modulation of the ER stress response does not mediate the effect of QPCT on aggregation

a, b, c. We studied whether QPCT might affect the ER stress response by measuring levels of the main regulator of this pathway, GRP78/BIP, using a GRP78 reporter-luciferase construct. We observed that both QPCT overexpression (**a**) and QPCT siRNA (**b**) resulted in an increase in the relative luciferase activity. Two of the QPCT inhibitors (SEN177 and SEN180) did not show any response and SEN817 reduced GRP78-luciferase signal (**c**). Renilla-luciferase was used as a control to normalized the GRP78-firefly luciferase activity. Treatment with 500nM of thapsigargin for 24 h was used as a control to confirm increased transcription of GRP78.

d, e. In view of this contradictory data, we measured GRP78 protein levels by western blotting, which were not altered either when QPCT was overexpressed (**d**) or knocked down (**e**), suggesting that QPCT does not affect the ER stress response. Full blot images are shown in supplementary figure 18g and 18h.

f, g. Other markers of ER stress such as eIF2α phosphorylation were not affected by QPCT overexpression (**f**) or QPCT inhibition with SEN17 or SEN180 (**g**). Only treatment with

SEN817 slightly reduced its phosphorylation. Full blot images are shown in supplementary figure 18i and 18j.

While we cannot exclude that QPCT may modulate the ER stress response, its effect on this pathway does not correlate with the effect we observe in mutant HTT aggregation.

In all panels, graphs show mean values of the firefly luciferase activity normalized to renilla and error bars represent standard deviation from a triplicate experiment representative of at least three independent experiments. Statistical analyses were performed by two-tailed unpaired Student's t-test: ***p<0.001, **p<0.01; NS, not significant.

Supplementary figure 15. Investigation of signalling pathways that may be regulated by QPCT

a, b. It has been recently reported that QPCT inhibition results in ERK and CREB phosphorylation [12]. We checked the phosphorylation levels of ERK (**a**) and CREB (**b**), which were unaltered in response to QPCT siRNA for 48 h in the presence of EGFP-HTTQ74 for the last 24h. Full blot images are shown in supplementary figure 18k and 18l.

c. QPCT inhibition did not result in changes in activation of JNK, as assessed by levels of phosphorylation relative to total levels of the protein when QPCT was knocked down either in the presence or absence of EGFP-HTTQ74. Full blot images are shown in supplementary figure 18m.

d. In response to protein misfolding, quality control systems such as the Heat Shock Response (HSR) [13], are activated and induce the expression of heat shock proteins or chaperones. Levels of Hsp70 levels, the main stress-inducible chaperone, were not altered upon QPCT knockdown or overexpression as shown by western blot analysis where Hsp70 levels were normalized to actin as a loading control. Full blot images are shown in supplementary figure 18n.

Supplementary figure 16. QPCT inhibition induces alpha B-crystallin levels

a. Fold changes in mRNA levels of an array of 84 heat shock proteins was assessed by quantitative RT-PCR in cells expressing HTT(Q74)GFP treated with 25 µM SEN177. Values greater than one indicate an up-regulation, and the fold-regulation is equal to the fold-change. Values less than one indicate a down-regulation, and the fold-regulation is the negative inverse to the fold-change. Fold-changes greater than 1.25 or below 0.75 are shown (full details in Supplementary Note 3).

b. AlphaB-crystallin protein levels were upregulated in cells treated with QPCT siRNA for 5 days. This increase was significant when HTT(Q74)GFP was also expressed for the last 24h. Graph shows quantification relative to tubulin of a triplicate experiment representative of at least 3 independent experiments. Error bars represent standard deviation. Statistical analyses were performed by two-tailed Student's t-test: $^{**}p<0.01$; NS, not significant. Full blot images are shown in supplementary figure 18o.

c. Alpha B-crystallin protein levels where detected by western blotting in HeLa cells transfected QPCT DNA together with HTT(Q23) or HTT(Q74) for 48h. Full blot images are shown in supplementary figure 18p.

d. Detection of endogenous and CRYAB-Flag by western blotting confirms efficient overexpression of alpha B-crystallin. Full blot images are shown in supplementary figure 18q.

Supplementary Figure 17. Full blots from main figures.

Blots from figure 2g (**a**), 3f (**b**). Blots were scanned using Odyssey Fc Imaging System (LI-COR Biosciences).

Blots from figure 4a (**c**), 4b (**d**). Blots were developed using ECL detection kit (Amersham).

Supplementary Figure 18. Full blots from supplementary figures.

Blots from figure 5a (**a**), 11c (**d**), 11d (**e**), 14f (**i**), 14g (**j**), 15a (**k**), 15d (**n**). Blots were scanned using Odyssey Fc Imaging System (LI-COR Biosciences).

Gels from figure 6b (**b**). Gels were stained with ethidium bromide.

Blots from figure 7c (**c**), 12c (**f**), 14d (**g**), 14e (**h**), 15b (**l**), 15c (**m**),16b (**o**), 16c (**p**), 16d (**q**). Blots were developed using ECL detection kit (Amersham).

Supplementary table 1. Ingenuity Pathway Analysis

a. Ingenuity Pathway Analysis of the 257 selected genes from high throughput-siRNA screen in HEK293 cells

Table shows the top 30 pathways in which the 257 genes selected in the siRNA screen performed in HEK293 cells were categorized by Ingenuity Pathway Analysis, ranked by –log(p-value). Number and name of the genes associated with each pathway are shown.

b. Ingenuity Pathway Analysis of the 66 hits that rescue Q48-eye degeneration in *Drosophila*

Top 30 pathways in which the 66 hits validated in *Drosophila* were categorized by Ingenuity Pathway Analysis, ranked by –log(*p*-value). Number and name of the genes associated with each pathway are shown.

References

1. Huang, K.-F., Liu, Y.-L., Cheng, W.-J., Ko, T.-P. & Wang, A. H.-J. Crystal structures of human glutaminyl cyclase, an enzyme responsible for protein N-terminal pyroglutamate formation. *Proc. Natl. Acad. Sci. U. S. A.* **102,** 13117–13122 (2005).
2. Buchholz, M. *et al.* The first potent inhibitors for human glutaminyl cyclase: synthesis and structure-activity relationship. *J. Med. Chem.* **49,** 664–677 (2006).
3. Mizushima, N. *et al.* Dissection of autophagosome formation using Apg5-deficient mouse embryonic stem cells. *J. Cell Biol.* **152,** 657–668 (2001).
4. Ravikumar, B., Duden, R. & Rubinsztein, D. C. Aggregate-prone proteins with polyglutamine and polyalanine expansions are degraded by autophagy. *Hum. Mol. Genet.* **11,** 1107–1117 (2002).

5. Kabeya, Y. *et al.* LC3, a mammalian homologue of yeast Apg8p, is localized in autophagosome membranes after processing. *EMBO J.* **19,** 5720–5728 (2000).
6. Klionsky, D. J. *et al.* Guidelines for the use and interpretation of assays for monitoring autophagy in higher eukaryotes. *Autophagy* **4,** 151–175 (2008).
7. Rubinsztein, D. C. *et al.* In search of an 'autophagomometer'. *Autophagy* **5,** 585–589 (2009).
8. Yamamoto, A. *et al.* Bafilomycin A1 prevents maturation of autophagic vacuoles by inhibiting fusion between autophagosomes and lysosomes in rat hepatoma cell line, H-4-II-E cells. *Cell Struct. Funct.* **23,** 33–42 (1998).
9. Dantuma, N. P., Lindsten, K., Glas, R., Jellne, M. & Masucci, M. G. Short-lived green fluorescent proteins for quantifying ubiquitin/proteasome-dependent proteolysis in living cells. *Nat. Biotechnol.* **18,** 538–543 (2000).
10. Shibata, M. *et al.* Regulation of intracellular accumulation of mutant Huntingtin by Beclin 1. *J. Biol. Chem.* **281,** 14474–14485 (2006).
11. Cynis, H., Scheel, E., Saido, T. C., Schilling, S. & Demuth, H.-U. Amyloidogenic processing of amyloid precursor protein: evidence of a pivotal role of glutaminyl cyclase in generation of pyroglutamate-modified amyloid-beta. *Biochemistry (Mosc.)* **47,** 7405–7413 (2008).
12. Song, H. *et al.* Inhibition of Glutaminyl Cyclase Ameliorates Amyloid Pathology in an Animal Model of Alzheimer's Disease via the Modulation of γ-Secretase Activity. *J. Alzheimers Dis. JAD* (2014). doi:10.3233/JAD-141356
13. Morimoto, R. I. Proteotoxic stress and inducible chaperone networks in neurodegenerative disease and aging. *Genes Dev.* **22,** 1427–1438 (2008).

Supplementary figure 1

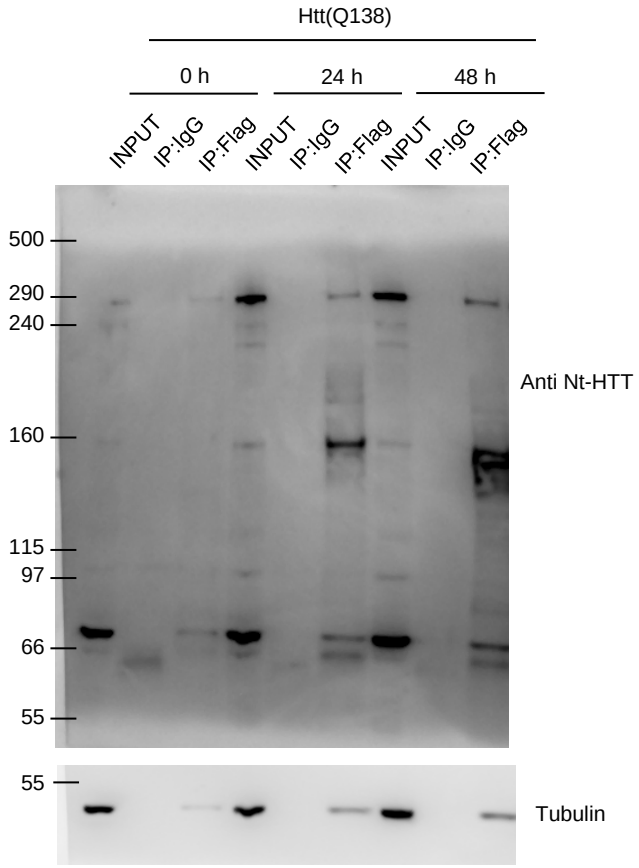

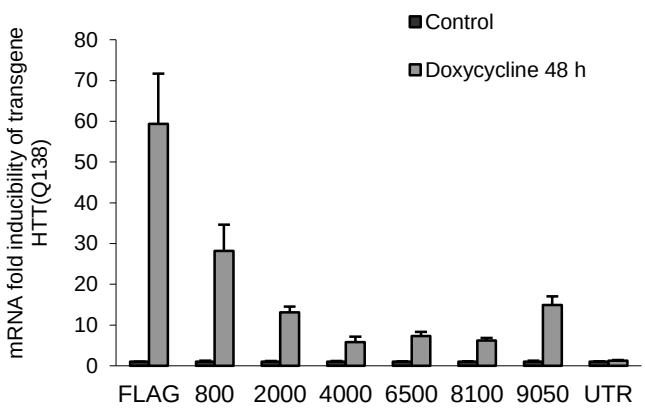

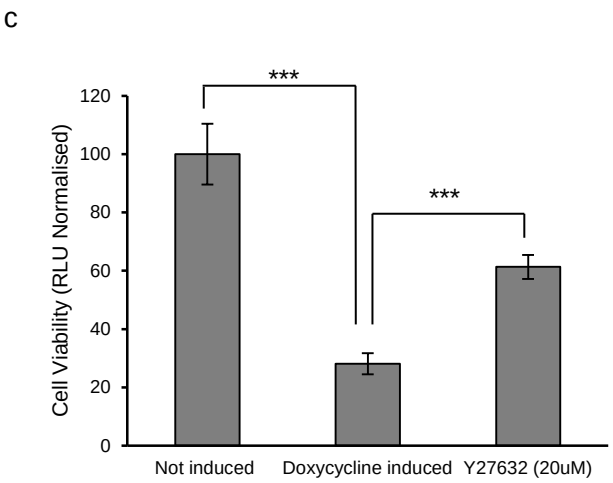

Supplementary figure 2

a

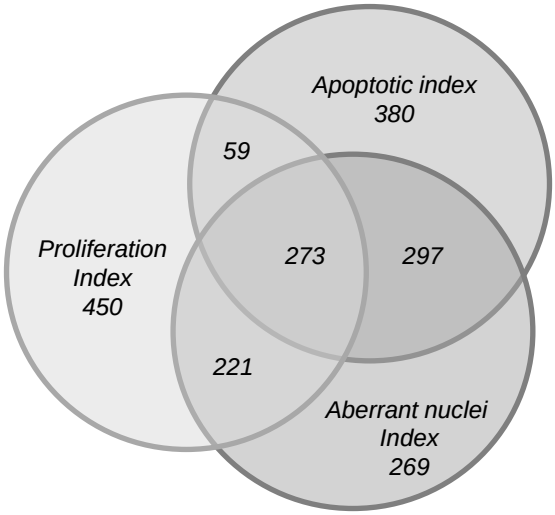

b

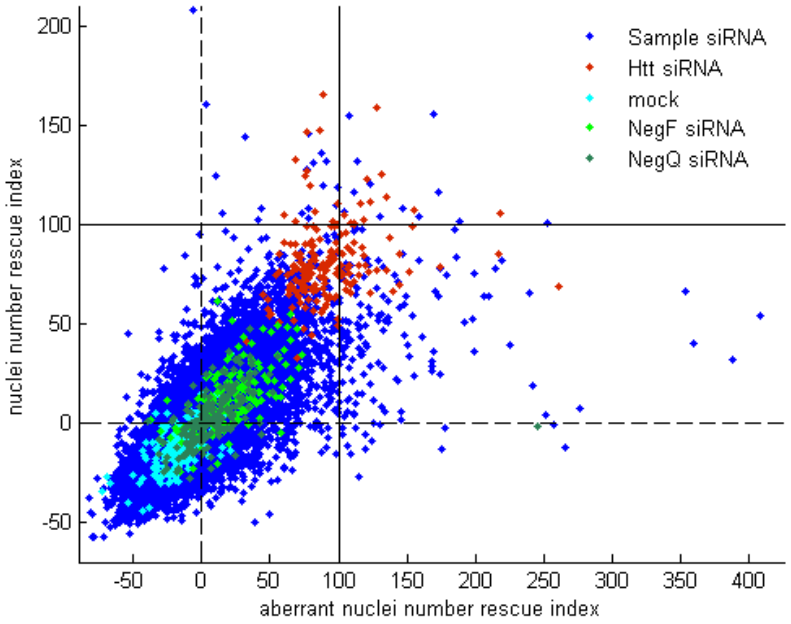

Supplementary figure 3

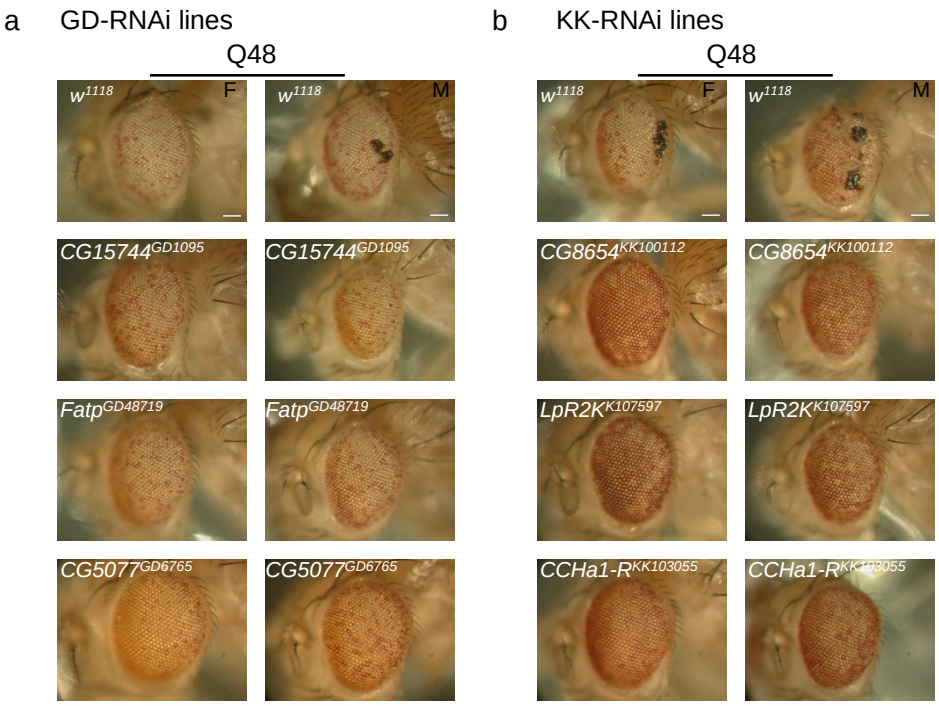

Supplementary figure 4

a

670 primary genes from mammalian cells HT-siRNA screen

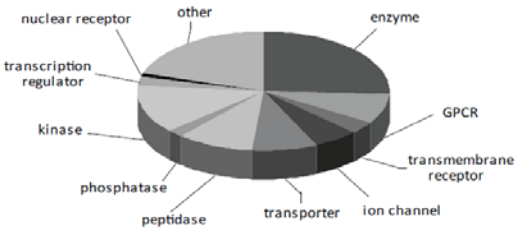

257 selected genes from mammalian cells HT-siRNA screen

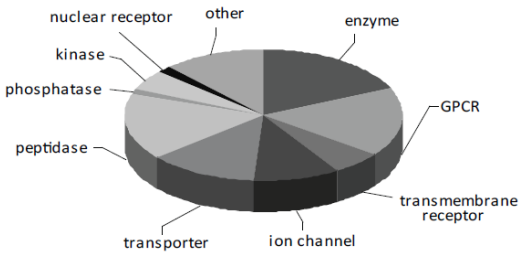

66 genes validated in Drosophila

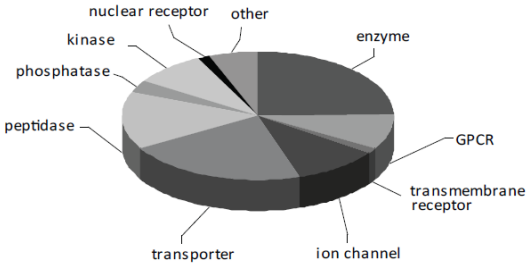

b

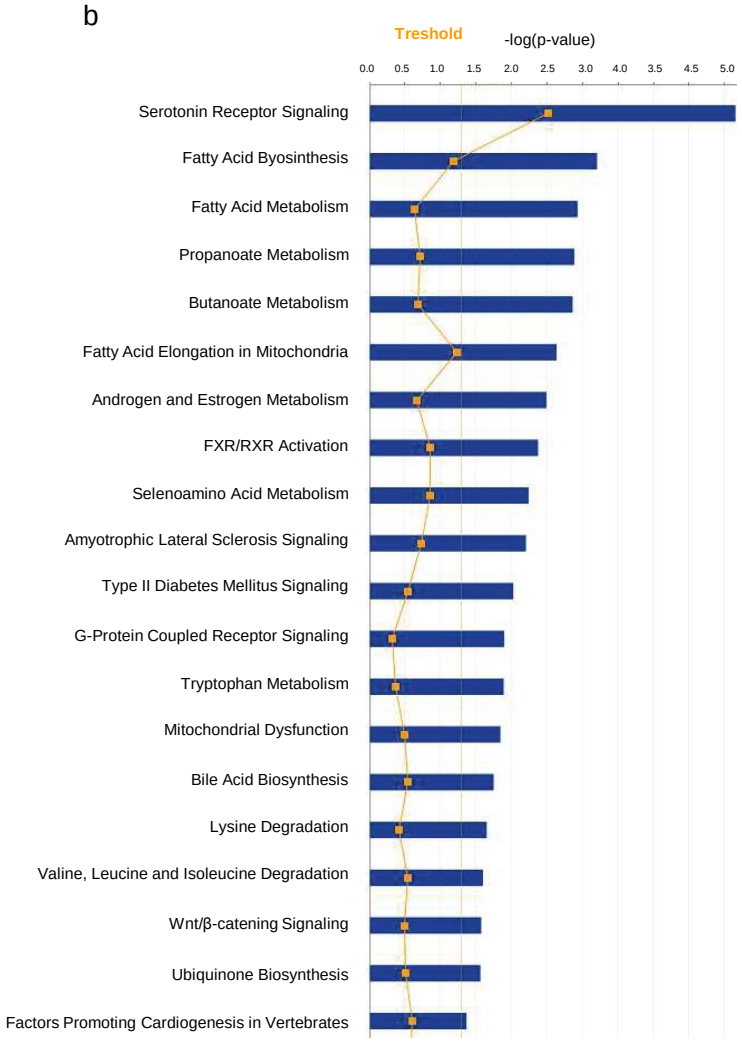

Supplementary figure 5

a

	Q48 x	BS	no BS	P-value Fisher's exact test
Female	w^{1118}	22	13	
	isoQC^{KK101533}	0	74	2.42 e-14
	QC^{KK106341}	1	65	3.05 e-12
Male	w^{1118}	9	0	
	isoQC^{KK101533}	5	55	3.53 e-0.8
	QC^{KK106341}	2	54	1.72 e-0.9

b

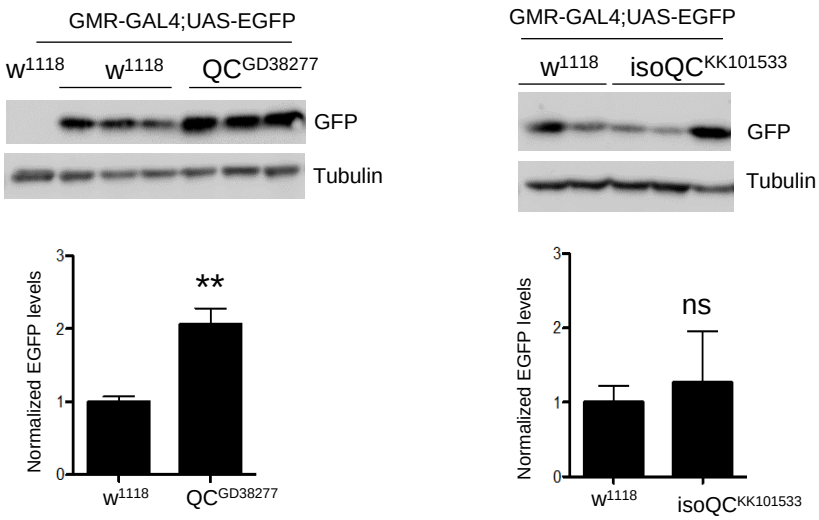

Supplementary Figure 6

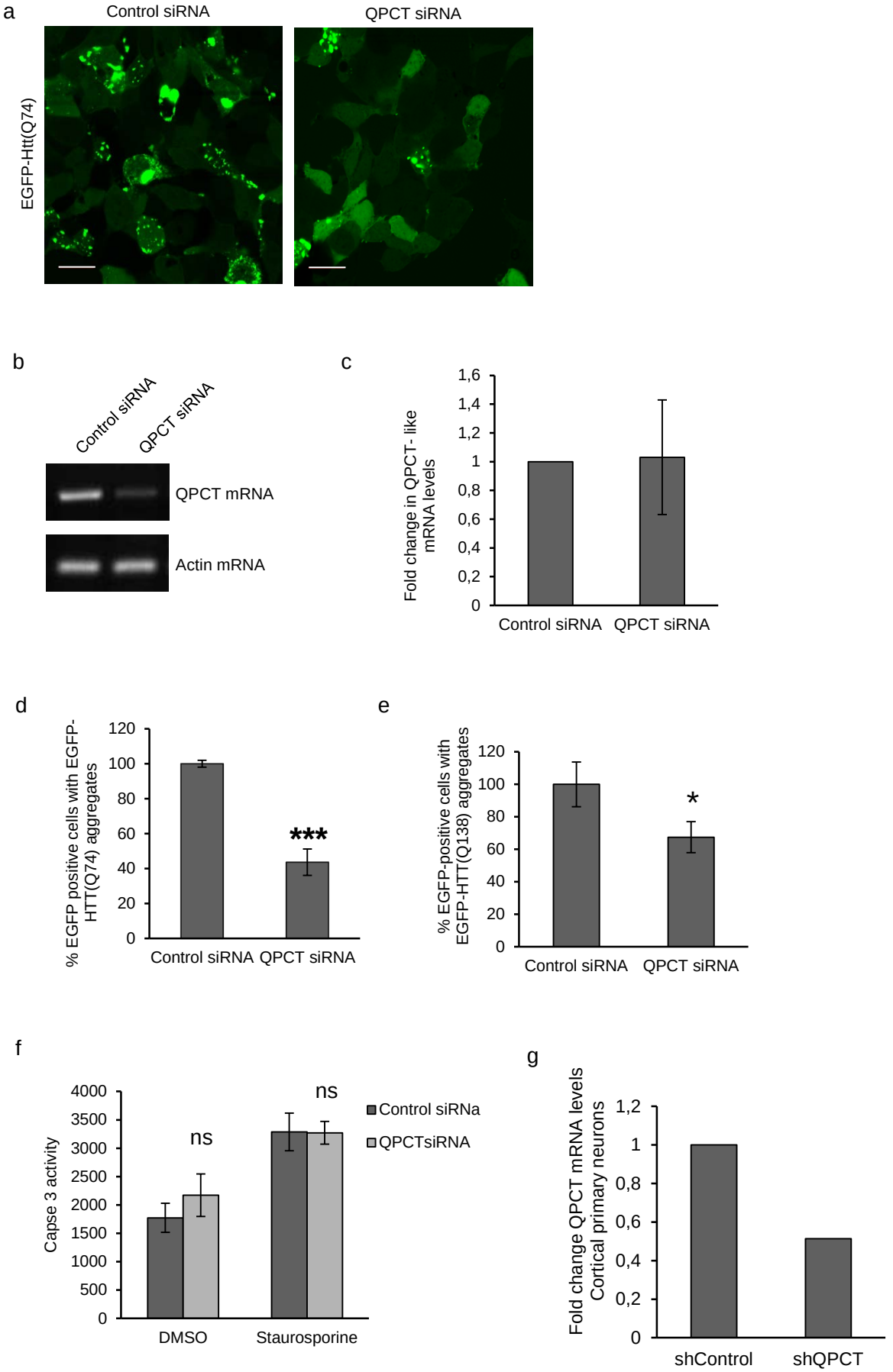

Supplementary Figure 7

a

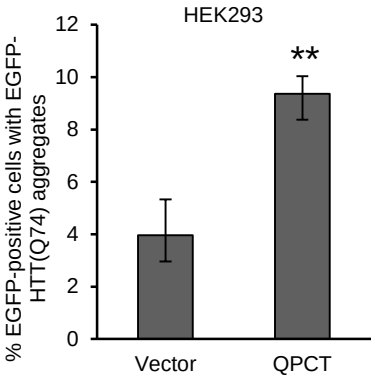

b

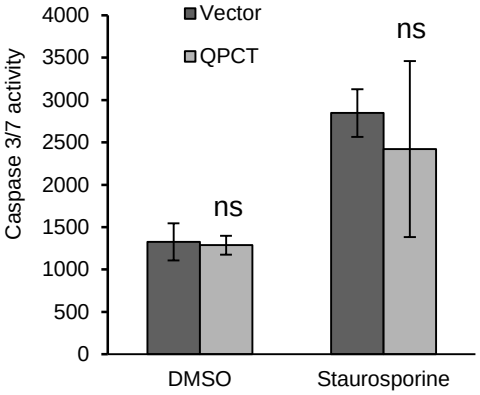

c

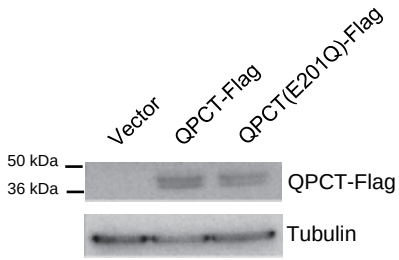

d

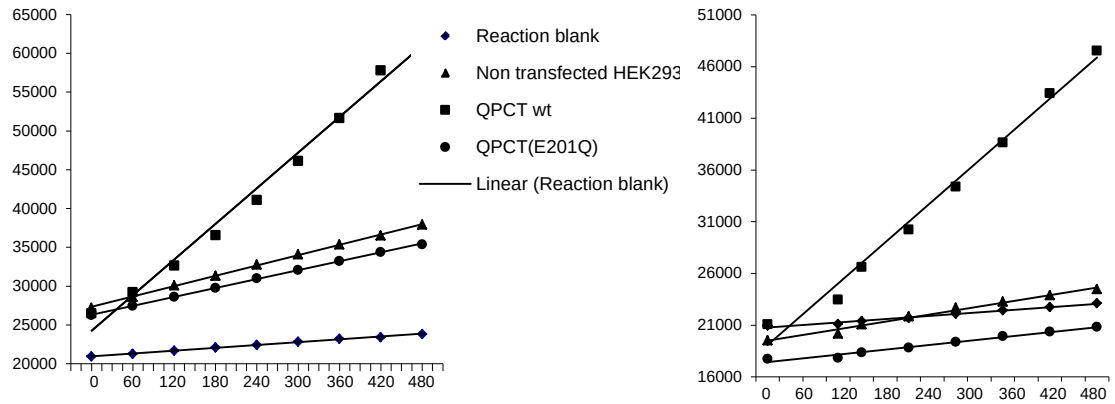

Supplementary Figure 8

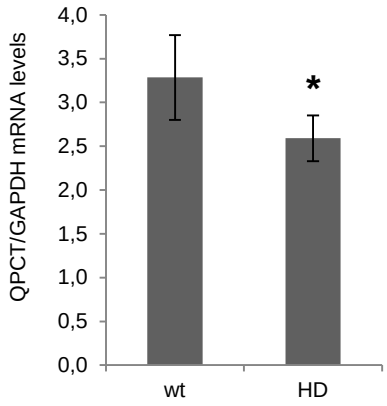

Supplementary Figure 9

a

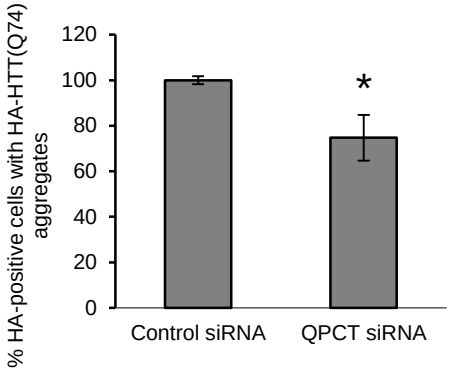

B

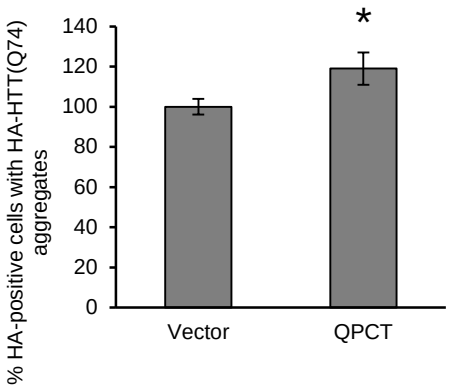

Supplementary figure 10

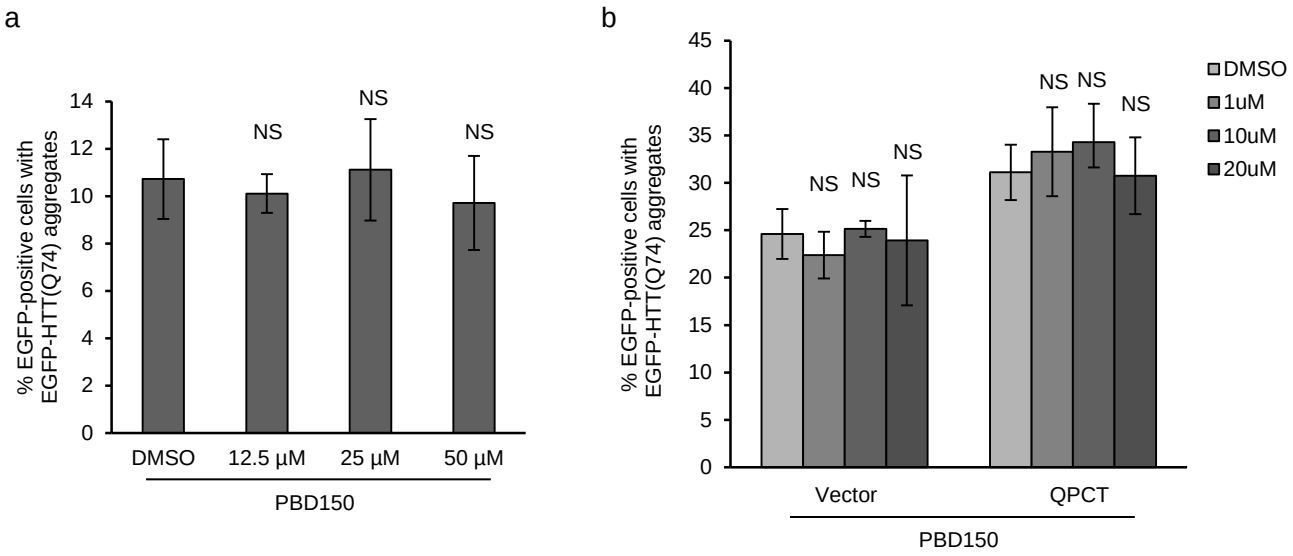

Supplementary Figure 11

a

	SEN ID short	SEN177	SEN817	SEN180
Enzymatic Assay	QPCT IC_{50} (µM)[a]	0.053	1.8	0.17
	QPCT-like IC_{50} (µM)[a]	0.013	2.3	0.058
Preliminary *in vitro* ADME	Solubility (µM)[b]	227	160	234
	Metabolic stability[c]	90	85	93
	Pampa-BBB Permeability (10^{-6} cm/s)[d]	1.7	16.5	0.9

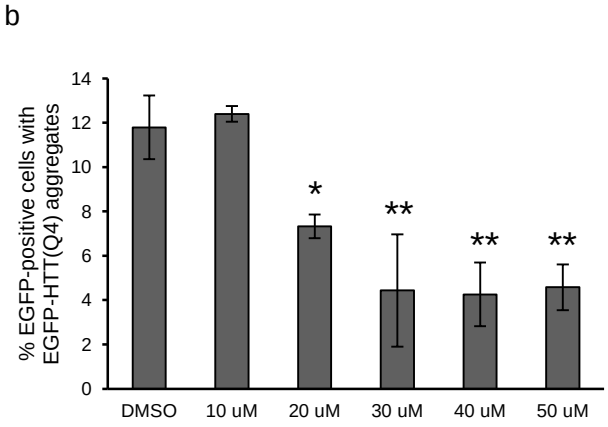

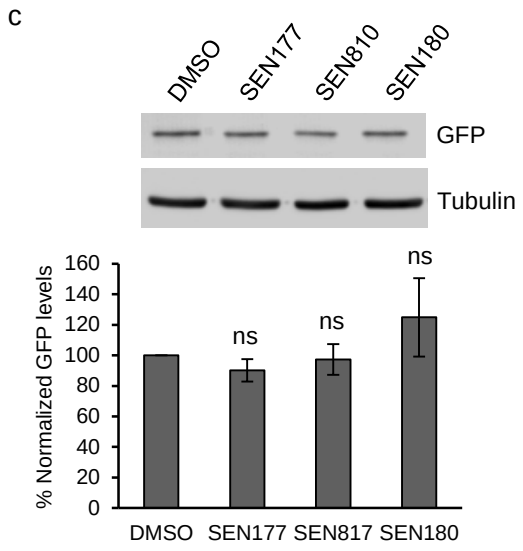

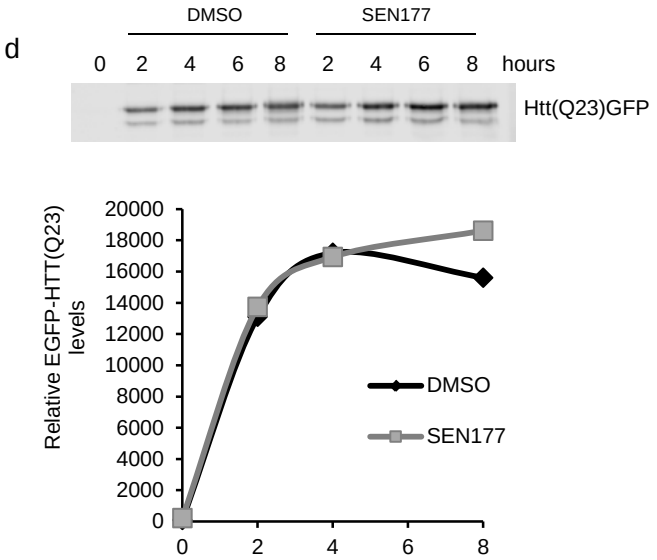

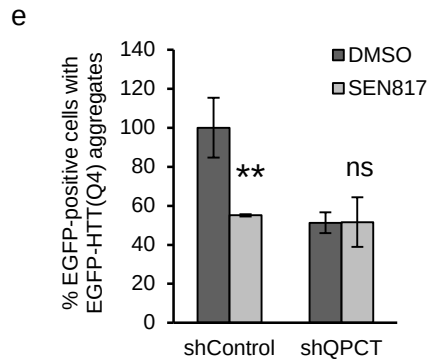

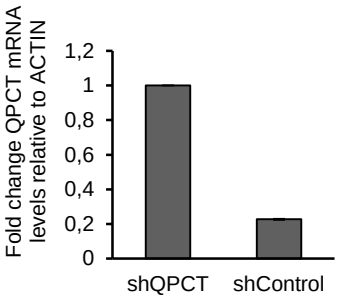

Supplementary figure 12

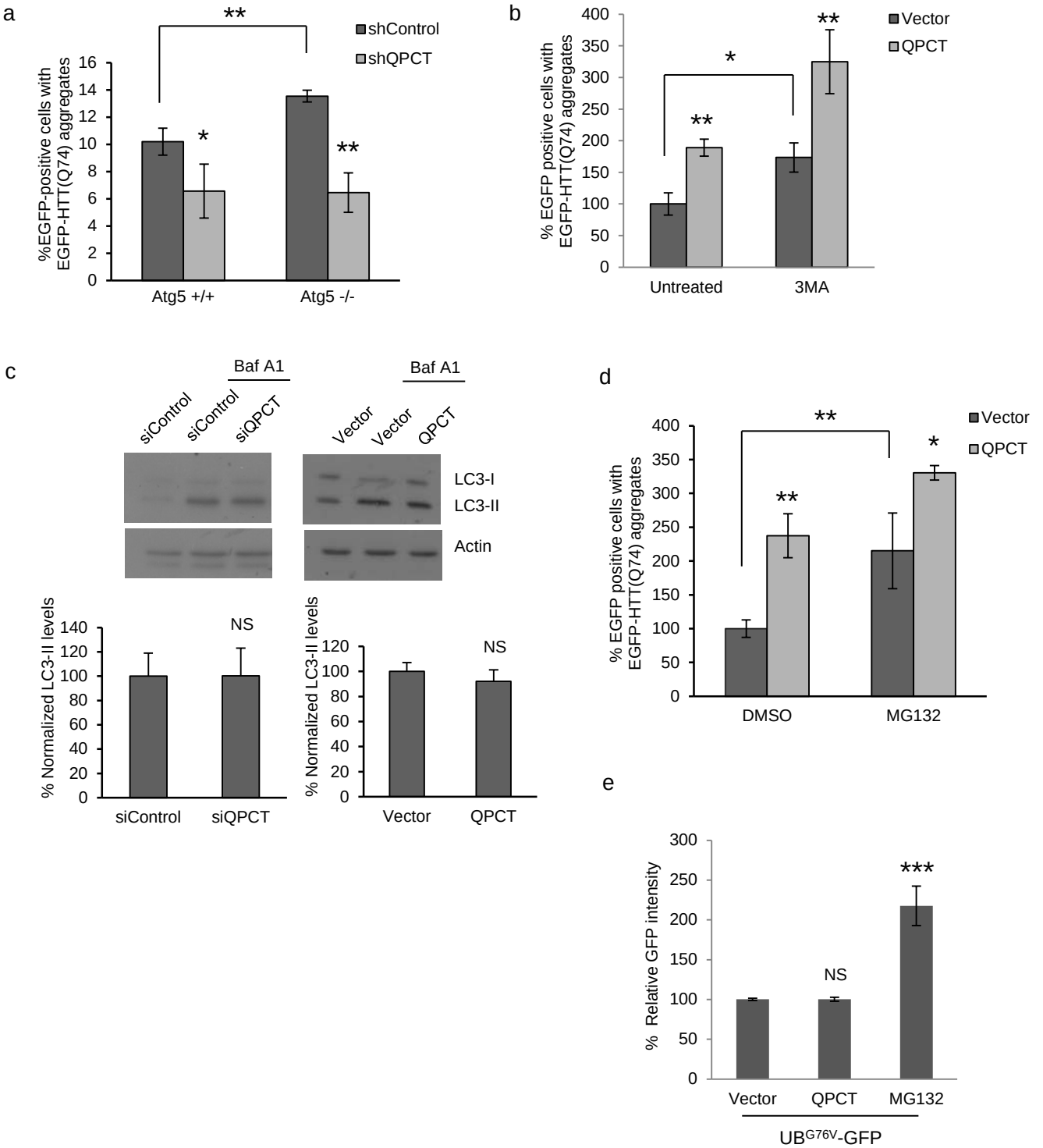

Supplementary figure 13

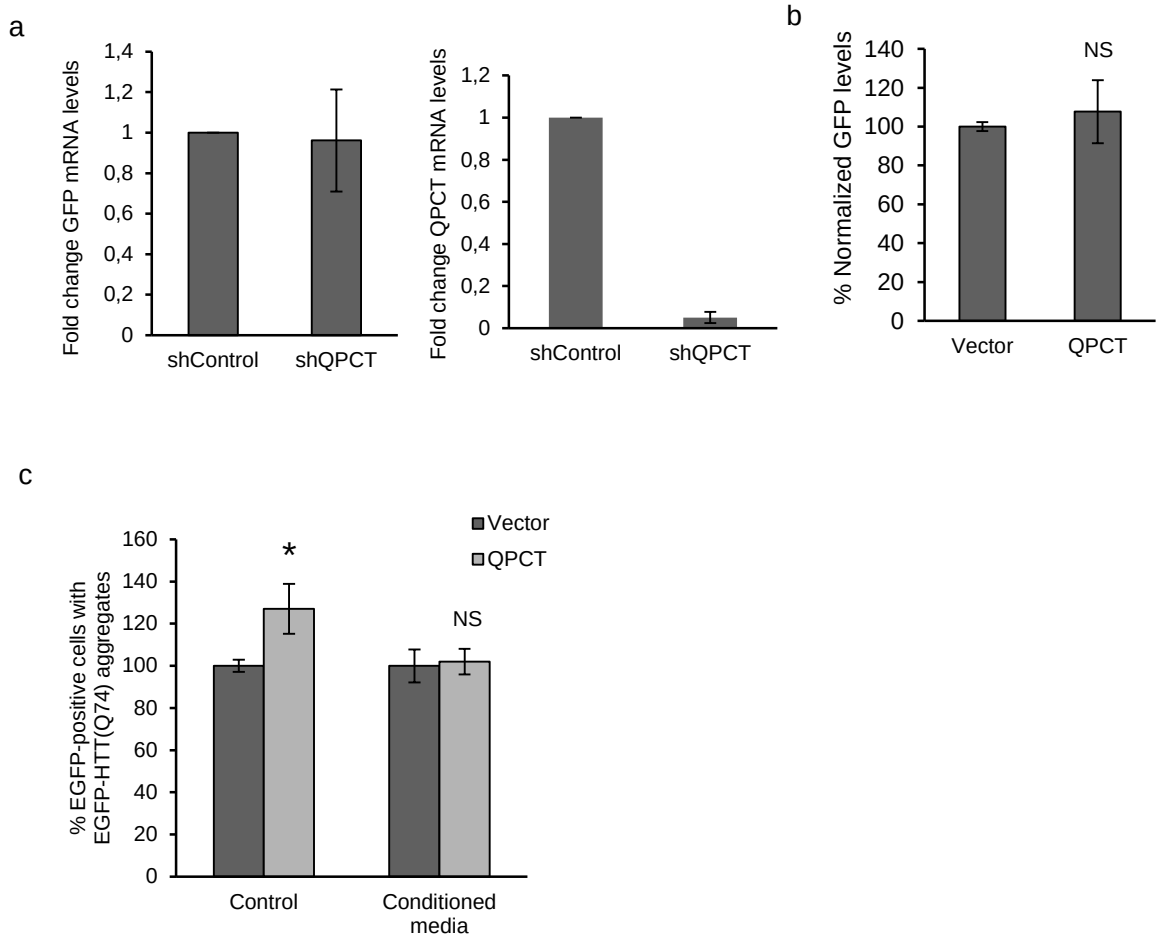

Supplementary figure 14

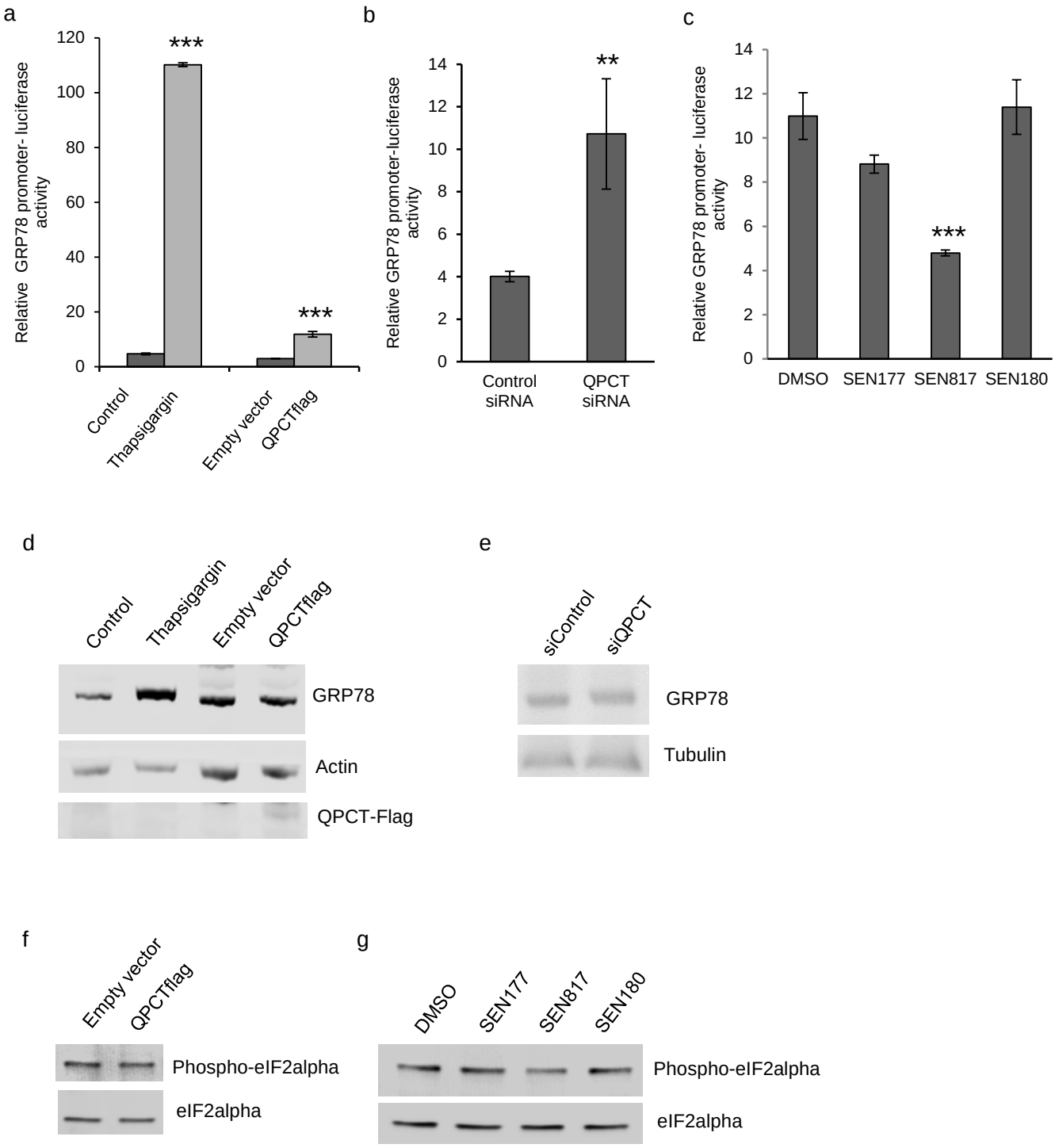

Supplementary figure 15

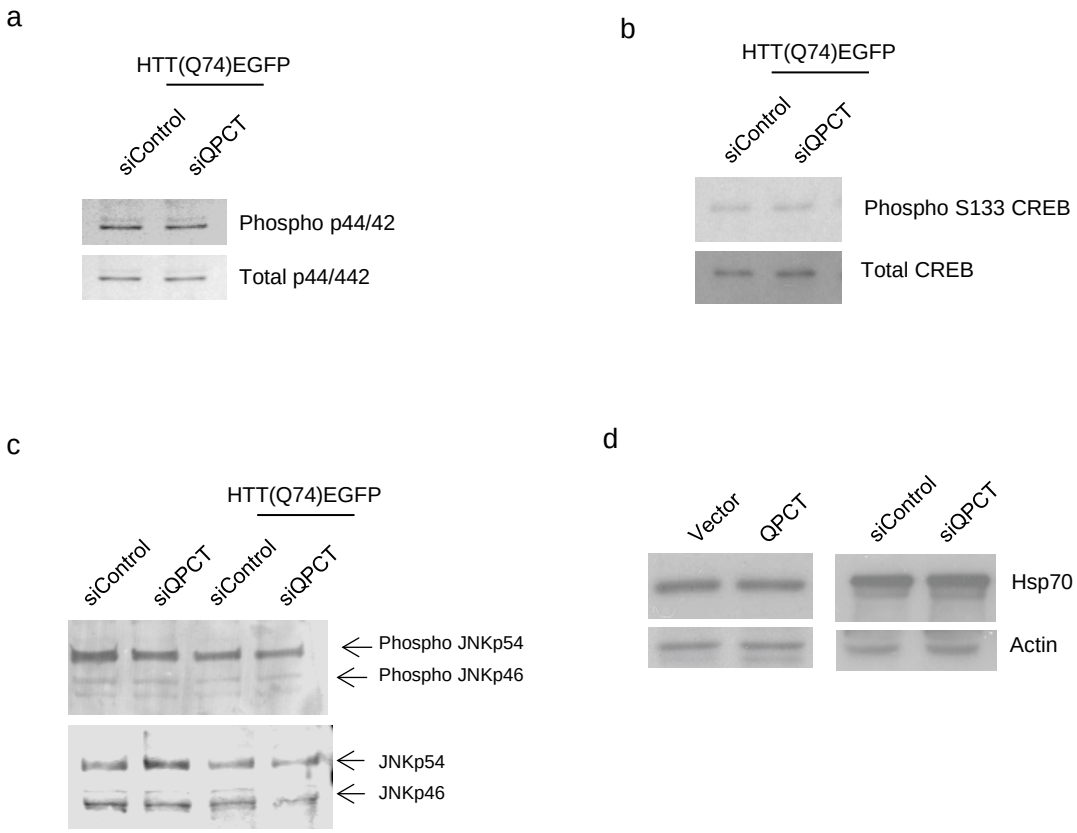

Supplementary Figure 16

a

Gene Name	Description	Fold change
CRYAB/HSPB5	Crystallin, alpha B	2.5924
HSPB7	Heat shock 27kDa protein family, member 7 (cardiovascular)	1.4979
BAG1	BCL2-associated athanogene	1.421
HSPB3	Heat shock 27kDa protein 3	1.3923
DNAJC5	DnaJ (Hsp40) homolog, subfamily C, member 5	1.3822
DNAJA4	DnaJ (Hsp40) homolog, subfamily A, member 4	1.376
HSPB6	Heat shock protein, alpha-crystallin-related, B6	1.3377
DNAJC4	DnaJ (Hsp40) homolog, subfamily C, member 4	1.253
DNAJB9	DnaJ (Hsp40) homolog, subfamily B, member 9	0.5872
BAG4	BCL2-associated athanogene 4	0.6602
DNAJC5B	DnaJ (Hsp40) homolog, subfamily C, member 5 beta	0.7327
DNAJB6	DnaJ (Hsp40) homolog, subfamily B, member 6	0.7307
HSPB2	Heat shock 27kDa protein 2	0.7428

b

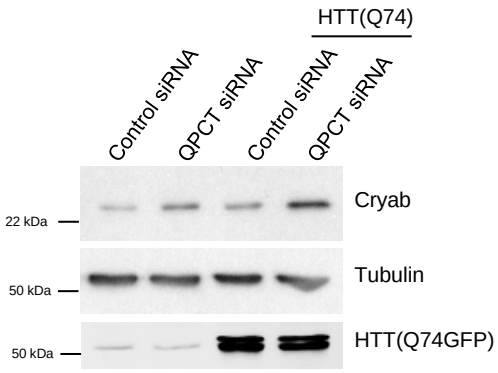

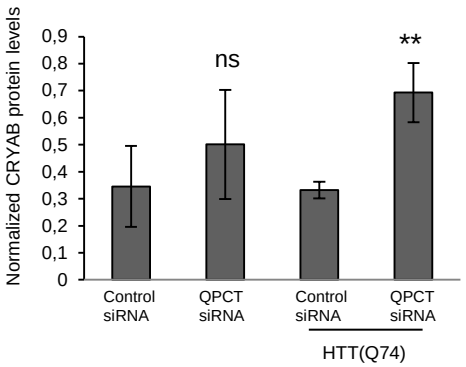

c

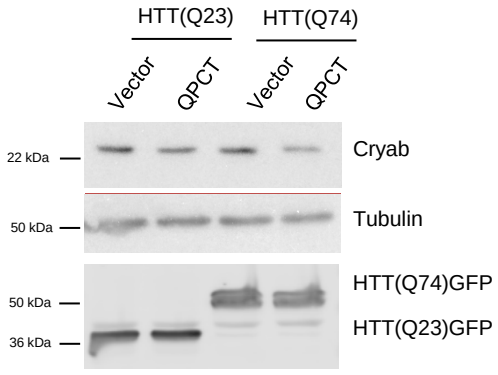

d

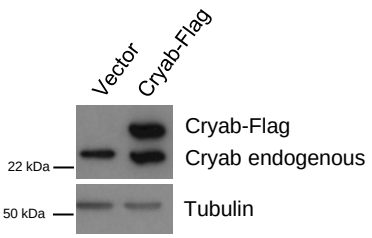

Supplementary figure 17. Full blot images. Main figures.

a. Blots from Figure 2g

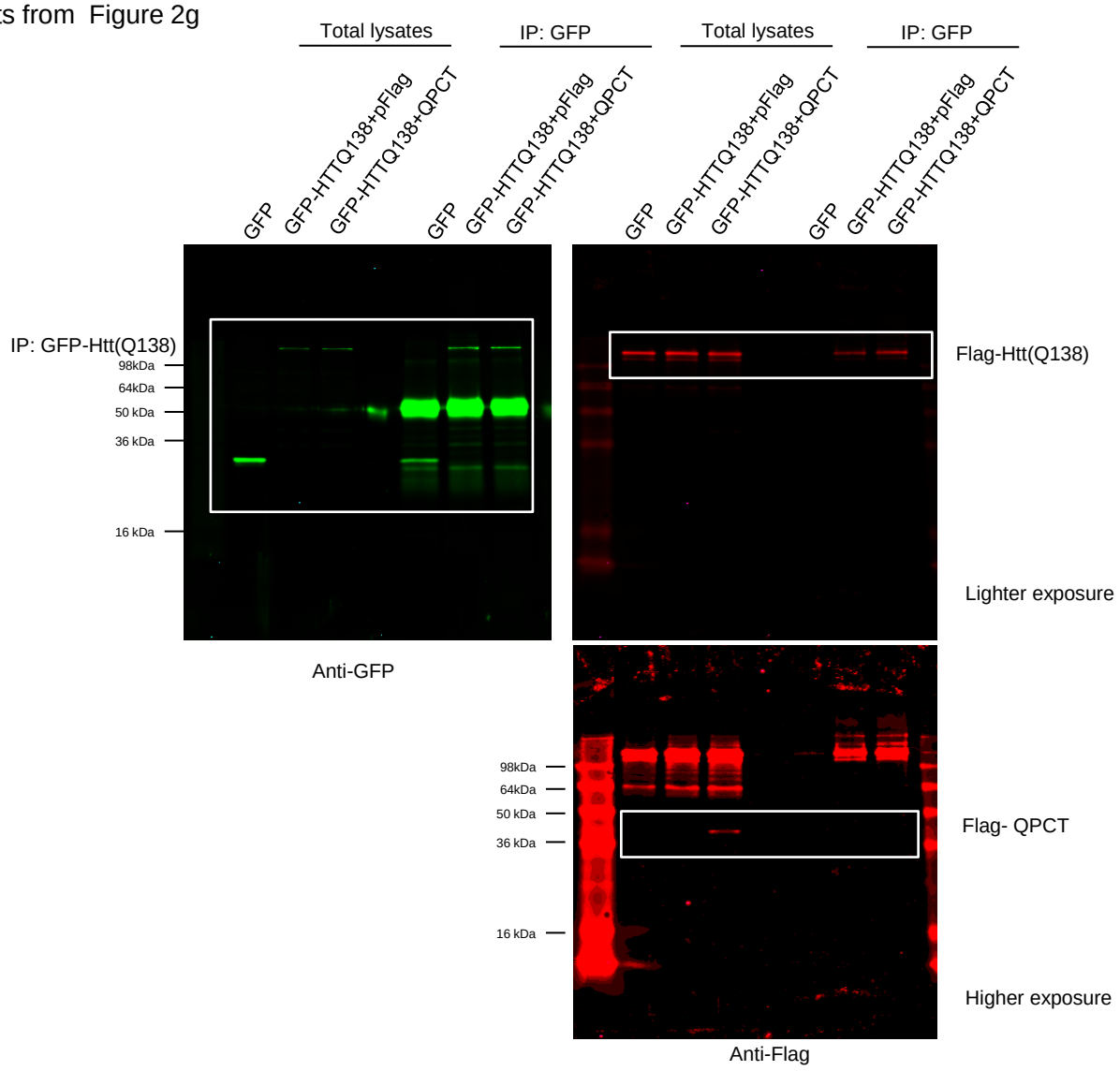

b. Blots from Figure 3f

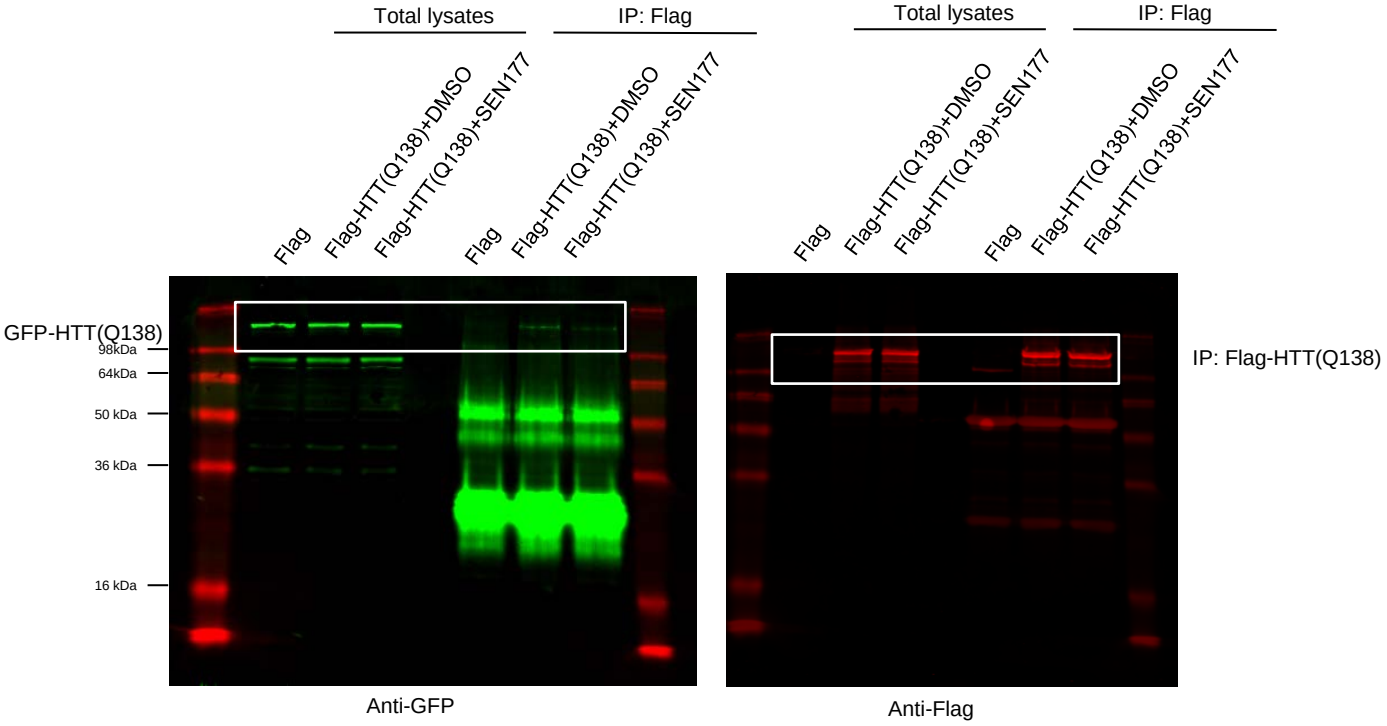

c. Blots from figure 4a

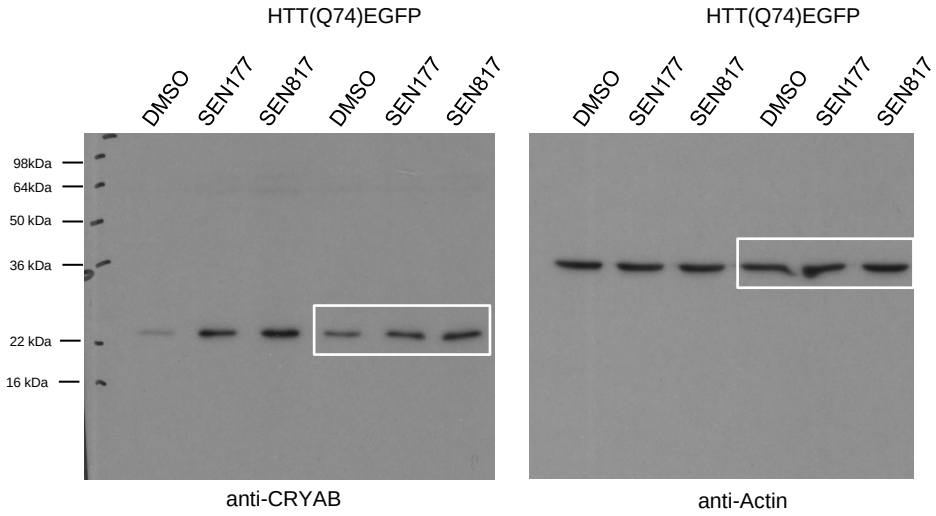

d. Blots from figure 4b

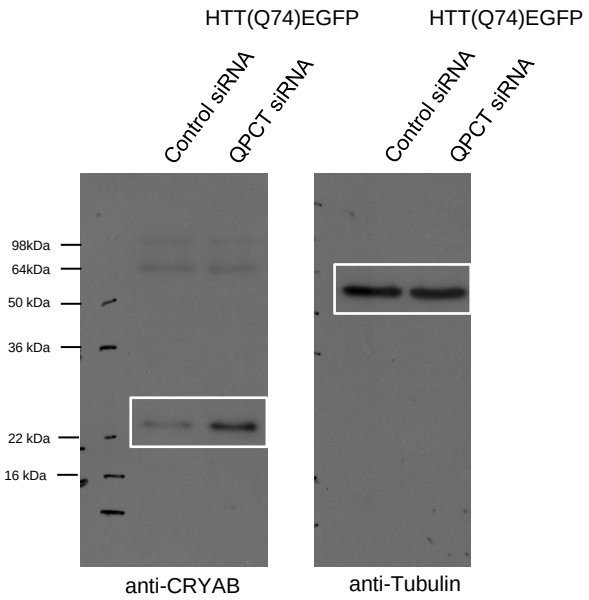

Supplementary figure 18. Full blot images from supplementary figures

a. Blots from supplementary figure 5b

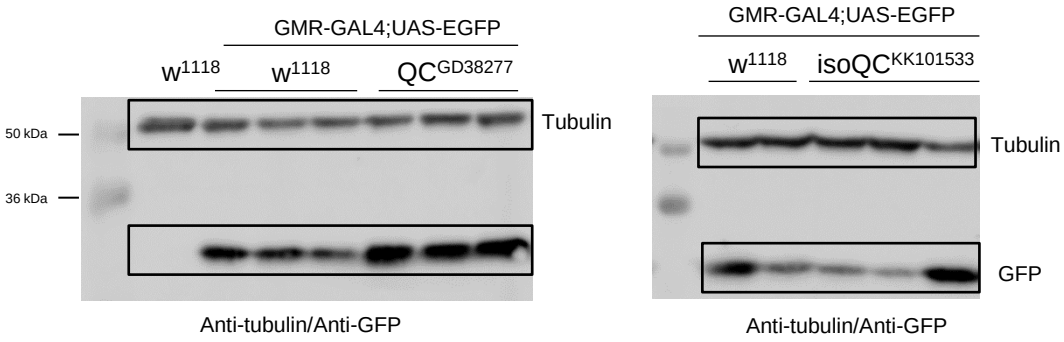

b. Gels from supplementary figure 6b

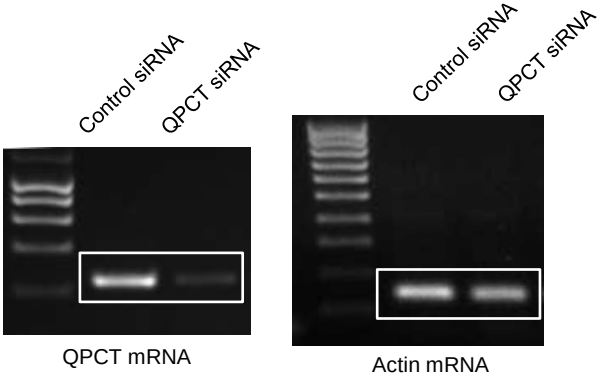

c. Blot from supplementary figure 7c

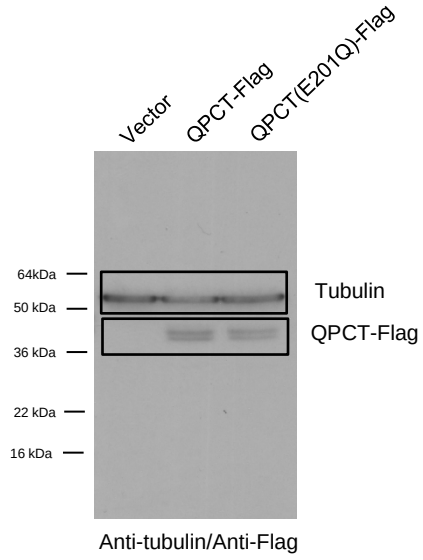

d. Blots from supplementary figure 11c

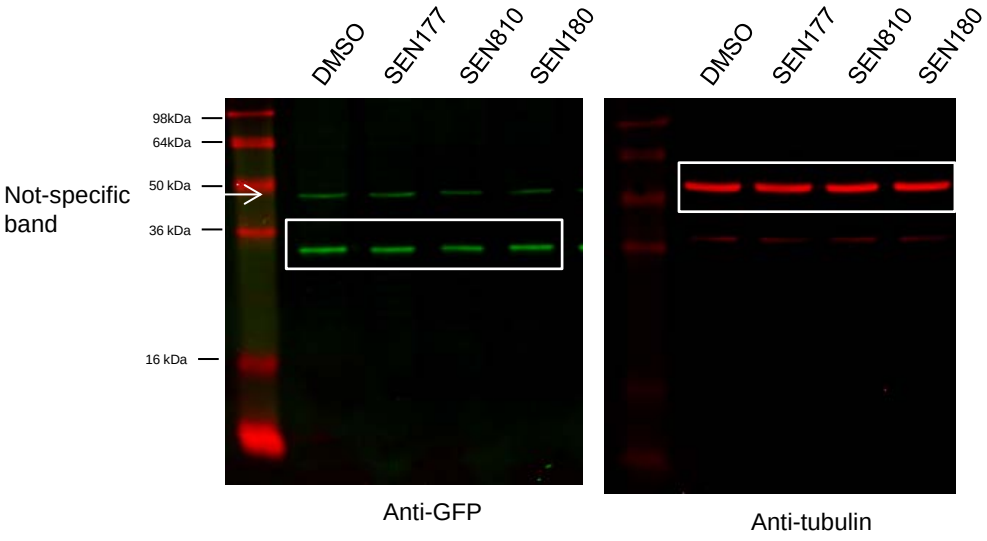

Supplementary figure 18. Continuation.

e. Blots from supplementary figure 11d

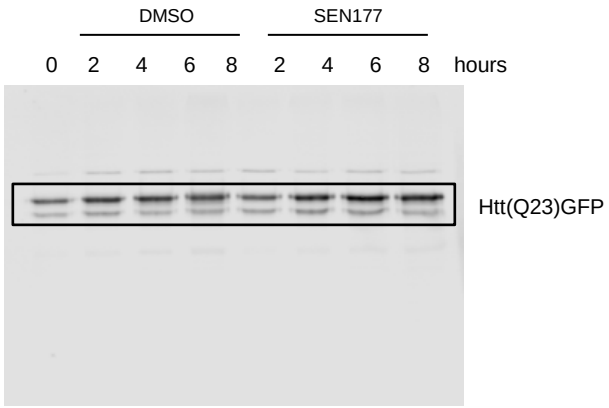

f. Blots from supplementary figure 12c

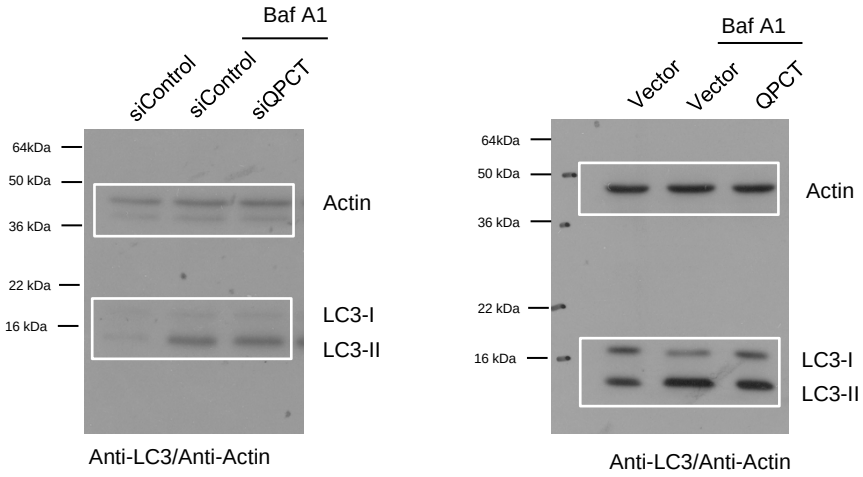

g. Blots from supplementary figure 14d

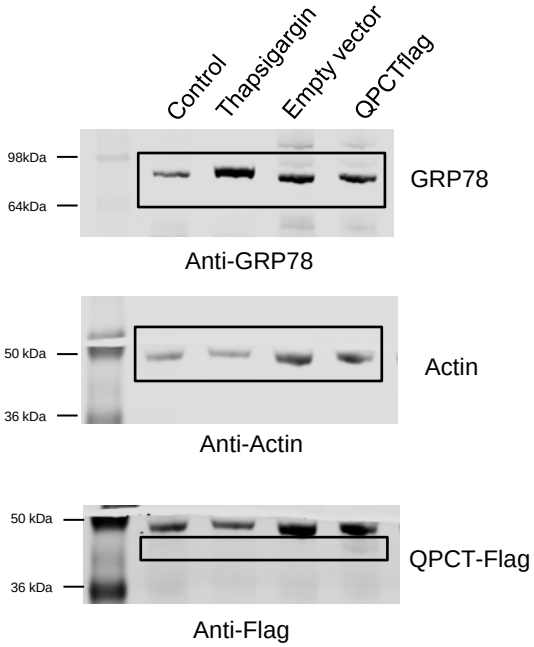

h. Blots from supplementary figure 14e.

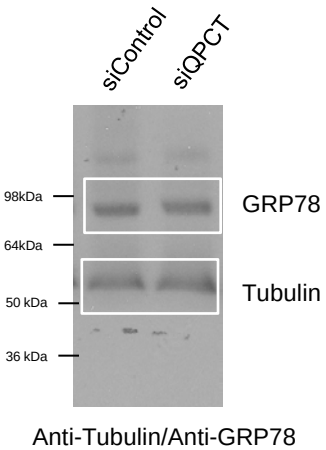

Supplementary figure 18. Continuation.

i. Blots from supplementary figure 14f

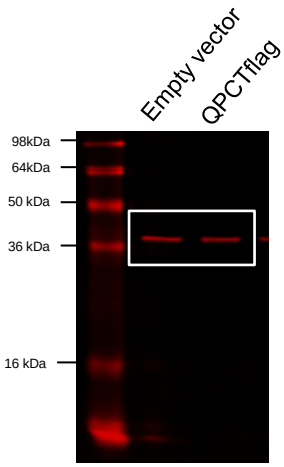

Anti-eIF2alpha

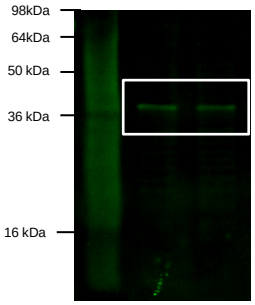

Anti-phospho-eIF2alpha

j. Blots from supplementary figure 14g

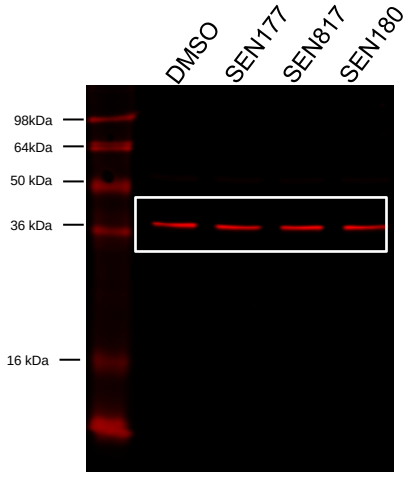

Anti-eIF2alpha

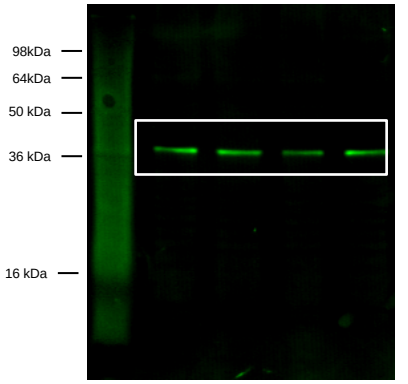

Anti-phospho-eIF2alpha

k. Blots from supplementary figure 15a

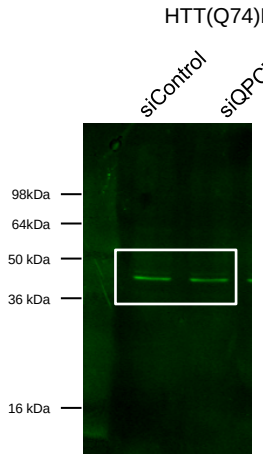

Anti-p44/442

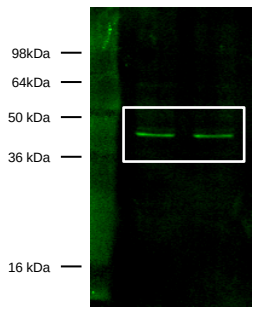

Anti-Phospho p44/42

l. Blots from supplementary figure 15b

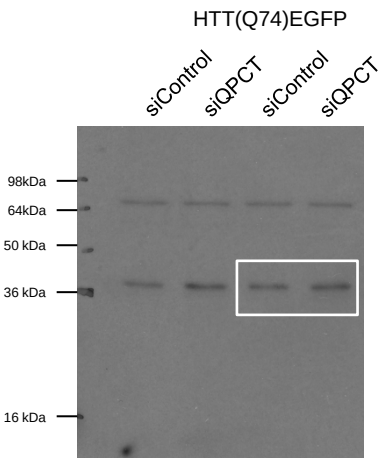

Anti-CREB

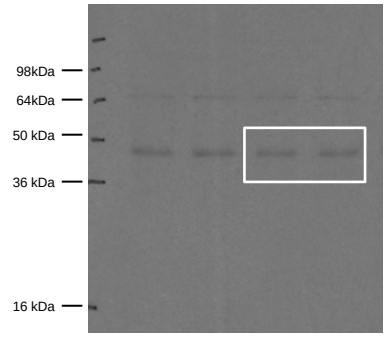

Anti-Phospho S133 CREB

Supplementary figure 18. Continuation.

m. Blots from supplementary figure 15c

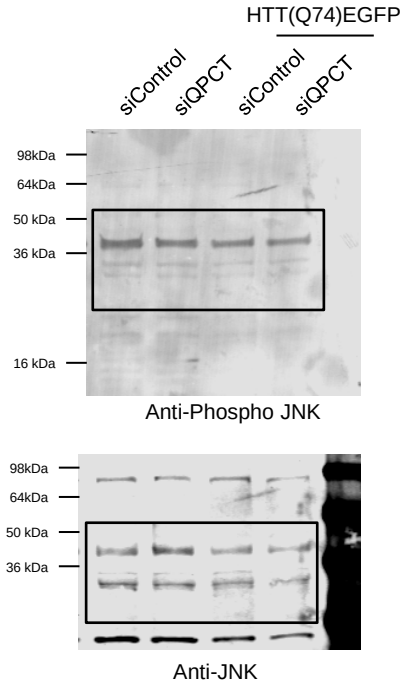

n. Blots from supplementary figure 15d

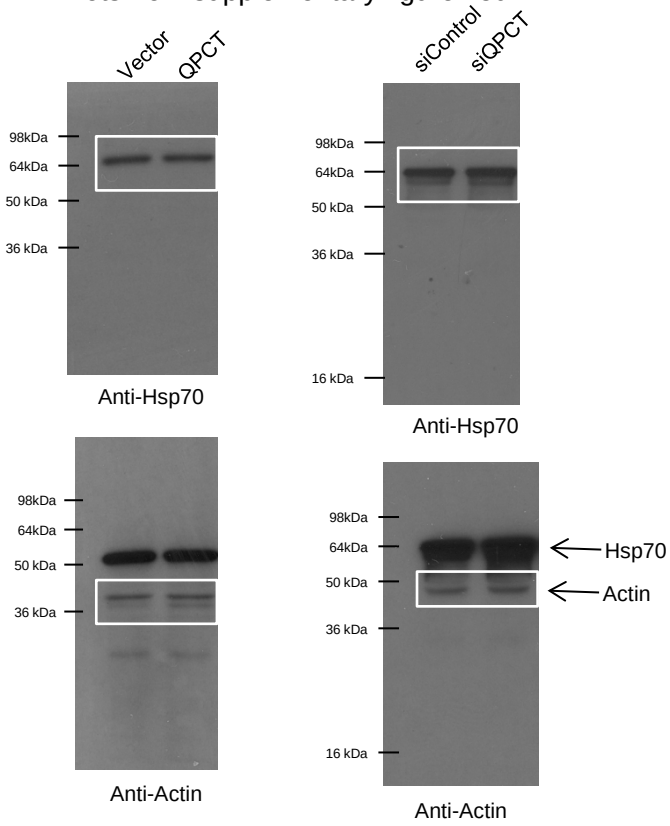

o. Blots from supplementary figure 16b

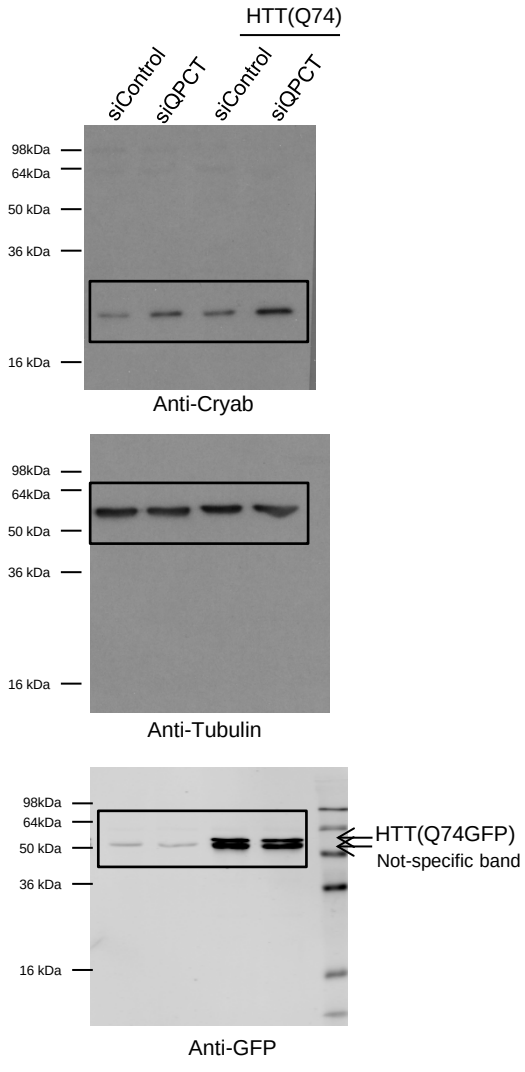

p. Blots from supplementary figure 16c

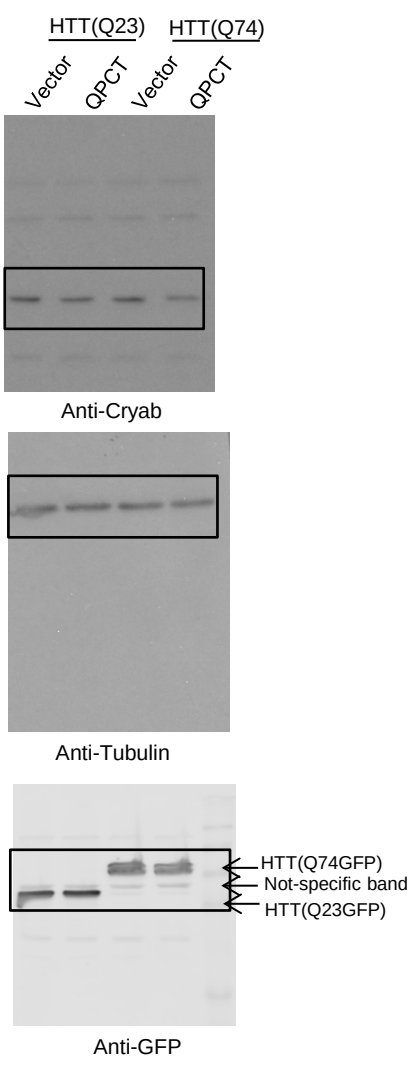

Supplementary figure 18. Continuation.

q. Bltos from supplementary figure 16c

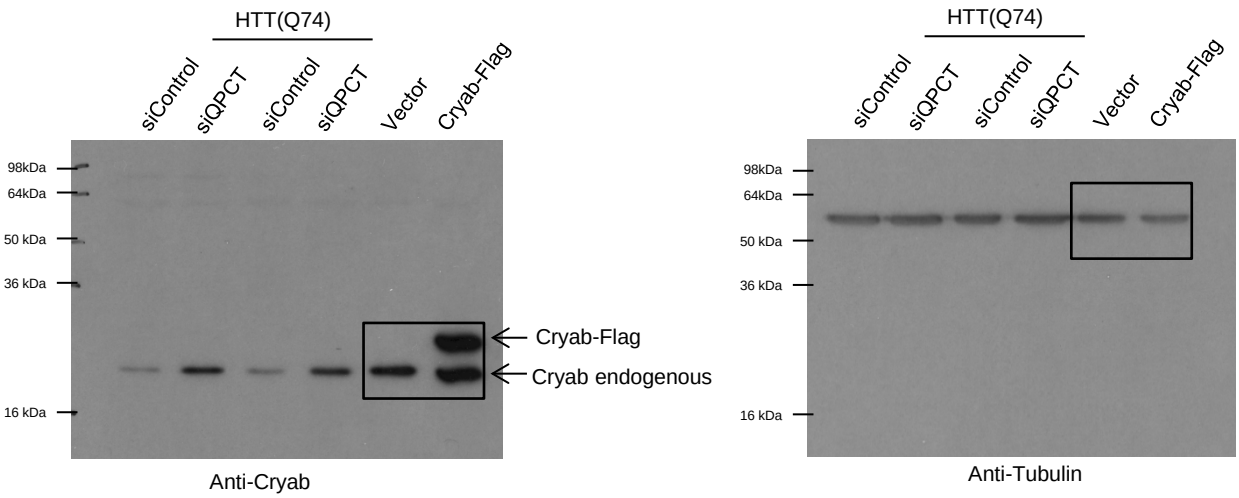

Supplementary Note 1. High-throughput siRNA screen

Detailed methodology and analysis for the siRNA screen in HEK293 cells.

Generation and maintenance of HEK293 recombinant cell lines for siRNA screen

The full length human huntingtin (*HTT*) cDNA containing 138 CAG repeats was subcloned from the plasmid pTre2Hyg:3xFLAG:HD138Q into the Invitrogen tetracycline-inducible vector pCDNA5/TO (cat.# V103320) by standard restriction enzymes digestion and ligation. The derived plasmids were then transfected using FuGENE® 6 transfection reagent (Roche, Cat. No. 11 815 091 001) into HEK293/T-Rex cells stably expressing the tetracycline-repressor protein (Invitrogen). Clones were identified using dilution and ring cloning methods [52].

Stably transfected cells were maintained in DMEM (Invitrogen GIBCO) containing 10% Fetal Bovine Serum Certified (Invitrogen GIBCO), 1% Glutamax (Invitrogen GIBCO) and 1% Penicillin/Streptomycin (Cat 15140-122), in the presence of the antibiotics used for plasmid selection: 0.25 mg/ml hygromycin B (Invitrogen), 5ug/ul of Blasticidin (Invitrogen, ant-bl-1). Cells were grown at 37°C in a 5% carbon dioxide fully humidified environment, and used for up to 4-5 passages after thawing.

Y27632 Rho kinase inhibitor was obtained from TOCRIS (#1254; Bristol, UK).Cell viability was measured with the PerkinElmer ATPlite Assay System (#6016949, PerkinElmer, Walthman, MA) plating 5000 cells/well and inducing HTT(Q138) expression with 1ug/mL doxyxycline for 0 and 72h.

RNA extraction and quantitative RT-PCR*:* Total RNA was purified from plated cells using the RNeasy Plus mini kit (QIAGEN), following manufacturer's instructions. 1 µg of purified RNA was converted to cDNA for subsequent RT-QPCR, using SuperScript II (Invitrogen) and Oligo (dT) primer. RT-QPCRs were performed using an iCycler instrument (BioRad) with SYBR green master mix (BioRad). All PCRs were run under the same cycling conditions and normalized to βActin. Primers used were Hs-HD_TAQ1_800-F(AAGCTCCCCCACCATTCG),Hs-HD_TAQ1_800-R(TCTTGAGTGCTGGCAGATGCT),Hs-HD_TAQ3_2000-F(TCCATTGTGTCCGCCTTTTAT),Hs-HD_TAQ3_2000 R (TCCGGAA CC AGCACATTTTT), Hs-HD_TAQ7_4000-F (TGAGGCCAGGCTTGTACCA), Hs-HD_TAQ7_4000-R(CGAGGGCCTGGGTGAAG),Hs-HD-TAQ12-6500-F(GCCGGCGGCCTACTG),Hs-HD_ TAQ12_6500-R(CAGAGTGGGCAGGGACTGATA),Hs_HD_TAQ15_8100-F(CAACCAGTTTGA GCTGATGTATGTG),Hs_HD_TAQ15_8100-R(GCGAGGATCTCGTCTTCTGAA), Hs_HD_

TAQ17_9050-F(CCGTGGTGTATAAGGTGTTTCAGA),Hs_HD_Q17_050-R(GACCCAGTCCCG GACCAT),Hs_HD_TAQ_3UTR-F(GTGGAGTCAGGCTTCTCTTGCT), Hs_ HD_TAQ_3UTR-R (AGGGACAAAGCCCGATGAG), Hs-Act-for (CTGGAACGGTGAAGGTGACA), Hs-Act-R (AAGGGACTTCCTGTAACAATGCA).

***Western blotting and inmunoprecipitation**:* Cell pellets were resuspended in ice- cold Ripa buffer (NaCl 150 mM, EDTA 2mM, Tris 50 mM pH 7.5, 1% Triton X-100) containing protease inhibitor mixture (mini-complete, ROCHE) and incubated at 4°C for 1h, followed by pre-clearing of the cell lysate with ProteinG/sepharose slurry (50%) for 1h at 4°C in an orbital shaker. The supernatant was incubated with Flag antibody overnight at 4°C followed by incubation with protein G sepharose bead slurry (50%) and gently mixed on an orbital shaker for 2h at 4°C. The sepharose beads were separated by centrifugation, washed 2 times in RIPA buffer, and finally resuspended in 30 µl of Laemmli sample buffer and boiled for 10 minutes. Total lysates or immunoprecipitates were separated in a 3-8% Tris Acetate precast gel (Invitrogen) and electrotransferred onto pvdf membrane. FLAG-tag was detected using anti-HTT (Sigma, H7540) diluted at 1µg/ml in 3% milk in PBS-Tween 0.1% and anti-rabbit (Biorad) 1:30000. The signal was revealed by ECL plus (GE) and acquired with VersaDoc4000 system.

High-throughput siRNA screen

***siRNA library**:* Initial library included 16,869 siRNAs (*Silencer Select* from Ambion) targeting 5,623 genes based on the RefSeq annotation of the human genome. The library was arrayed on 60 384-well plates, each containing a maximum of 287 sample siRNAs and a set of controls in triplicate, each consisting on two non-gene targeting negative control siRNAs, HTT positive control siRNA and mock (transfection reagent only). Edge wells were not transfected.

***Screening assay**:* 1,500 to 1,650 HEK293 HTT(Q138) cells per well were seeded in collagen I coated Greiner MicroClear 384-well optical plates in complete medium without antibiotics. A final concentration of 33 nM siRNA was transfected in 4 identical plates, using 0.063 µl/well of Dharmafect 3 (Dharmacon/Thermo) as transfection reagent. At 30h after siRNA transfection, two identical plates were induced for mutant HTT expression by addition of doxycycline to a final concentration of 0.5 µg/ml and the two remaining plates were treated with the identical volume of medium in the abscence of doxycycline. Thus, each siRNA was screened in duplicate in presence and absence of induced mutHTT. At 72h after induction, cells were fixed in 4.6 % PFA and stained with 5 µg/ml Hoechst 33342.

***Image analysis**:* Fluorescence microscopy images of cell nuclei were acquired on an *ImageXpress Micro* automated fluorescence microscope (Molecular Devices), using a 10x objective with a binning of 2 at four non-neighbouring sites per well. Automated Image analysis was performed by a custom algorithm using the Definiens *Cellenger* image analysis software package. Three different readouts were extracted: 1) *Number nuclei*: Number of cell nuclei per image field (#nuclei); 2) *Apoptotic/mitotic index (%)*: Relative number of nuclei with strongly aggregated, brightly fluorescent and/or heterogeneous chromatin (which also includes mitotic nuclei), calculated as (number of apoptotic and mitotic nuclei/number of nuclei)*100; and 3) *Aberrant nuclei index (%):* Relative number of nuclei aberrant in shape, size and chromatin texture, as defined as ((number of non-aberrant nuclei)/(number of aberrant shaped nuclei + number of small and large nuclei + all apoptotic nuclei)*100. Furthermore, the algorithm performed an automated image QC, monitoring each image for background intensity, focus and presence of large artefacts.

Data processing: Raw image analysis data was further processed in *Spotfire* (Tibco) applying the following steps: 1) Exclusion of images failed in Image QC. 2) Calculation of inter-replicate plate duplicate mean for each plate position and readout. 3) Calculation of a "rescue index" for each duplicate mean and readout as a dual normalized measure for the rescue of mutant HTT induced cell toxicity phenotype, computed as (1-y/x)*100 (%) where y= ($sample_i$ non induced) - ($sample_i$ induced)) and, for pass 1, x= plate mean (($sample_n$ non induced) - ($sample_n$ induced)) or for pass 2 to 3, x = plate mean (neg controls non induced) – (neg controls induced). 4) Gene-wise aggregation of the phenotypic results from each of three siRNAs screened per gene was performed by the RSA method [2], using an iterative hypergeometrical distribution formula to calculate the statistical significance of the phenotypic readout ranks obtained for each siRNA and rescue index. Log P values obtained for each gene and rescue index are based on non-parametric readout ranks and therefore do not assume any (e.g., Gaussian) data distribution. 5) Aggregation over the results from the three readouts, obtained for each gene was performed by the identical mathematical method as in 4), calculating a "meta" logP value on the ranked logP values of each gene in three rescue indices.

Screen consecutive passes: In an initial screen (pass 1), 16,869 siRNAs targeting 5,623 genes were tested, from which 670 genes were selected. The effect of each individual siRNA on cellular toxicity was expressed in rescue indices for each parameter analysed, which indicates the effect of an individual siRNA relative to the plate average phenotype of the samples. To avoid any bias due to the pre-selection of siRNAs screened, in consecutive rounds indices were calculated using the plate mean of non-targeting negative controls. Rescue indices from the three siRNAs targeting each gene, were aggregated into one

single, gene specific, logP value applying the Redundant siRNA Analysis (RSA) method [2] for each readout and a “meta” logP value for each gene was calculated based on the rescue indices of the three readouts. Genes were ranked by the logP #nuclei rescue index as a primary criterion and other logP rescue indices were used to refine the selection. Genes with logP lower than –1.7 were selected and a total of 1,125 siRNas, targeting 670 genes, were chosen for a second pass 2 validation.

Based on a combination of datasets from passes 1 and 2, 256 genes with logP lower than –1.7 were selected, considering the three readouts as previously, as well as tractability of the genes in terms of assay feasibility. In order to rank these genes, we performed a third screen (pass 3) in which those genes that presented two positive siRNAs were re-screened and genes with one single positive siRNA were tested with two additional new siRNAs, resulting in a library of 566 siRNAs. The mean rescue indices of all samples did not increase significantly as compared to pass 2, presumably due to the addition of 120 new siRNAs that had not undergone selection by passes 1 and 2. Gene-wise aggregation of results from pass 1, 2 and 3 and ranking of positive hits was again performed by RSA. Genes were ranked based on the three rescue indices and using # nuclei as primary criteria.

References

1. König, R. *et al.* A probability-based approach for the analysis of large-scale RNAi screens. *Nat. Methods* **4,** 847–849 (2007).

Supplementary Note 2. Synthesis and Characterization of QPCT Inhibitors

General Methods: All chemicals were purchased by commercial suppliers (Sigma Aldrich, Fluorochem) and employed as received. All nuclear magnetic resonance spectra were recorded using a Varian Mercury Plus 400 MHz spectrometer equipped with a PFG ATB broadband probe. UPLC-MS analyses were run using an Acquity Waters UPLC equipped with a Waters SQD (ES ionization) and Waters Acquity PDA detector, using a BEH C18 1,7 µm, 2,1 x 50 mm column. Gradients were run using 0.05% formic acid water/acetonitrile 95/5 and acetronitrile with a gradient 95/5 to 100, flow: 0.8 ml/min. Temperature: 40 °C. UV detection at 215 nm and 254. ESI+ detection in the 80-1000 m/z range. Retention times were expressed in minutes. The purity of compounds submitted for screening were > 95% as determined by integrating at 215 nm the peak area of the LC chromatograms. To further support the purity statement, all compounds were also analyzed at a different wavelength (254 nm), and total ion current (TIC) chromatogram and NMR spectra were used to further substantiate results. HRMS (140.000) values are given for final compounds, employing Q ExactiveTM Plus (Thermo Fisher). All column chromatography was performed following small modifications of the original method described in [1]. All TLC analyses were performed on silica gel (Merck 60 F254) and spots revealed by UV visualization at 254 nm and KMnO4 or ninhydrin stain.

Detailed synthesis methods (See Supplementary Note 2 Figure)**:**

4-(5-Mercapto-4-methyl-4H-[1,2,4]triazol-3-yl)-piperidine-1-carboxylic acid benzyl ester (6): To a solution of 1-[(benzyloxy)carbonyl]piperidine-4-carboxylic acid (**4**) (5.00 g, 19.01 mmol, 1.0 eq) in acetonitrile (40 mL), was added N,N-carbonyldiimidazole (3.08 g, 19.01 mmol, 1.0 eq) and the mixture was stirred at 50°C for 2 hours. Then N-methyl-thiosemicarbazide (**5**) (2.10 g, 19.96 mmol, 1.1 eq) was added and the reaction stirred at 50°C for 18 hours. Solvent was removed under reduced pressure; the residue was dissolved in dichloromethane and washed with a saturated NH_4Cl solution. The organic phase was collected and concentrated under reduced pressure. The residue was purified by silica column eluting with cyclohexane/ethyl acetate (1:1), affording 2.60 g of title compound (yield, 41%). Mass (ES) m/z: = 333 (M+1). UPLC Rt = 1.20 min. ^{1}H NMR (400 MHz, $CDCl_3$) δ 7.41 – 7.06 (m, 5H), 5.08 (s, 2H), 4.35 – 4.10 (m, 2H), 3.51 (s, 3H), 3.04 – 2.84 (m, 2H), 2.83 – 2.65 (m, 1H), 1.95 – 1.82 (m, 2H), 1.80 – 1.62 (m, 2H).

4-(4-Methyl-4H-[1,2,4]triazol-3-yl)-piperidine-1-carboxylic acid benzyl ester (7): To a solution of 4-(5-mercapto-4-methyl-4H-[1,2,4]triazol-3-yl)-piperidine-1-carboxylic acid benzyl

ester (**6**) (2.60 g, 7.83 mmol, 1.0 eq) in dichloromethane (4mL) cooled at 0°C, hydrogen peroxide (30% water solution, 0.48 mL, 15.66 mmol, 2.0 eq) was added followed by acetic acid (4mL). The reaction was allowed to warm up to room temperature and stirred for 18 hours. 15% NaOH solution was added, bringing the reaction to pH 10 then 15 mL of dichloromethane were added and the organic phase was collected. Solvent was evaporated under reduced pressure, affording 1.2 g of title compound that was used in the next step without further purification (yield, 52%). Mass (ES) m/z: = 301 (M+1). UPLC Rt = 0.95 min.

4-(4-Methyl-4H-[1,2,4]triazol-3-yl)-piperidine (8): 4-(4-Methyl-4H-[1,2,4]triazol-3-yl)-piperidine-1-carboxylic acid benzyl ester (**7**) (1.20 g, 3.99 mmol) was dissolved in 6N HCl solution (5 mL) and the mixture was heated at 100°C for 6 hours. The reaction was then allowed to cool down to room temperature. The aqueous phase was washed with 10 mL of dichloromethane and was concentrated under reduced pressure, affording 0.55 g of the desired compound as its hydrochloride salt (yield, 83%). Mass (ES) m/z: = 189 (M+1). UPLC Rt = 0.25 min. ^{1}H NMR (400 MHz, DMSO-d6) δ 8.29 (s, 1H), 3.58 (s, 3H), 3.02 – 2.89 (m, 2H), 2.87 – 2.73 (m, 1H), 2.62 – 2.50 (m, 2H), 1.77 – 1.65 (m, 2H), 1.66 – 1.47 (m, 2H).

3'-Bromo-4-(4-methyl-4H-[1,2,4]triazol-3-yl)-3,4,5,6-tetrahydro-2H-[1,2']bipyridinyl (10): 4-(4-Methyl-4H-[1,2,4]triazol-3-yl)-piperidine (**8**) (1.67 g, 10.1 mmol, 1.0 eq) was dissolved in N,N-dimethylformamide (24 mL). Potassium carbonate (2.09 g, 15.2 mmol, 1.5 eq) and 3-bromo-2-chloro-pyridine (**9**) (2.33 g, 12.1 mmol, 1.2 eq) were added and the mixture was heated at 100°C for 18 hours under vigorous stirring. The reaction was allowed to cool to room temperature, inorganic salts were filtered, and the resulting solution was concentrated under reduced pressure. The residue was suspended in ethyl acetate and washed with water. The organic phase was collected and concentrated under reduced pressure. The residue was purified by silica column, eluting with dichloromethane/methanol (9:1). 1.35 g of the desired compound was obtained (yield, 41%). Mass (ES) m/z: = 322-324 (M+1); bromine pattern. UPLC Rt = 0.87 min. ^{1}H NMR (400 MHz, DMSO-d6) δ 8.34 (s, 1H), 8.28 – 8.23 (m, 1H), 8.00 – 7.91 (m, 1H), 6.98 – 6.85 (m, 1H), 3.84 – 3.69 (m, 2H), 3.63 (s, 3H), 3.08 – 2.97 (m, 1H), 2.96 – 2.83 (m, 2H), 2.05 – 1.79 (m, 4H).

General procedure for Suzuki couplings: 3'-Bromo-4-(4-methyl-4H-[1,2,4]triazol-3-yl)-3,4,5,6-tetrahydro-2H-[1,2']bipyridinyl (**10**) (0.45 g, 1.40 mmol, 1 eq), K_3PO_4 (0.53 g, 2.52 mmol, 1.8 eq) and the appropriate boronic acid (1.87 mmol, 1.3 eq) were dissolved in dioxane (3.5 mL) and H_2O (3.5 mL) and the resulting mixture was degassed under N_2 flux. $Pd_3(dba)_2$ (0.06 g, 0.07 mmol, 0.05 eq) and tricyclohexyl phosphine (0.01 g, 0.04 mmol, 0.03 eq) were added and the reaction was heated at 100°C for 48 hours under inert atmosphere.

The mixture was allowed to cool to room temperature and then was diluted with H_2O (2 mL) and extracted with ethyl acetate (3mL). The organic layer was concentrated and the residue was purified.

6''-Fluoro-4-(4-methyl-4H-[1,2,4]triazol-3-yl)-3,4,5,6-tetrahydro-2H-[1,2';3',3'']terpyridine (1) –SEN177. Following general procedure for Suzuki coupling, and using 4-fluoro-3-pyridyl-boronic acid, 0.07 g of compound **SEN177 (1)** were recovered (yield, 15%) after purification on silica column, eluting with DCM/MeOH (9:1). Mass (ES) m/z: = 339 (M+1). UPLC Rt = 0.69 min. ^{1}H NMR (400 MHz, DMSO-d6) δ 8.46 (s, 1H), 8.35 – 8.22 (m, 3H), 7.63 (dd, *J* = 7.4, 1.4 Hz, 1H), 7.29 (dd, *J* = 8.5, 2.5 Hz, 1H), 7.05 (dd, *J* = 7.3, 4.9 Hz, 1H), 3.56 (s, 3H), 3.50 – 3.35 (m, 4H), 2.96 – 2.82 (m, 1H), 2.81 – 2.67 (m, 2H), 1.86 – 1.71 (m, 2H), 1.72 – 1.53 (m, 2H). ^{13}C NMR (101 MHz, DMSO-d6) *δ* 163.95, 161.60, 160.59, 156.89, 147.91, 146.99 (d, J_{CF} = 15.0 Hz), 145.30, 141.99 (d, J_{CF} = 8.0 Hz), 140.27, 134.37 (d, J_{CF} = 4.6 Hz), 123.13, 118.19, 110.19 (d, J_{CF} = 37.7 Hz), 49.60, 31.69, 30.70, 30.18. HRMS calculated for C18H19N6F [M+H]+: 339.17254, found 339.17280. Mass difference (mDa): -0.26; mass error (ppm): -0.7666.

4-(4-Methyl-4H-[1,2,4]triazol-3-yl)-3,4,5,6-tetrahydro-2H-[1,2';3',3'']terpyridine (2) – SEN180. Following general procedure for Suzuki coupling and using 3-pyridyl-boronic acid, 0.21 g of compound **SEN180 (2)** (yield, 48%) were recovered after purification on reverse phase C-18 silica column, eluting with of H_2O (0.1% HCOOH)/MeOH gradient (from 80:20 to 100% MeOH). Mass (ES) m/z: = 321(M+1). UPLC Rt = 0.54 min. ^{1}H NMR (400 MHz, DMSO-d6) *δ* 8.80 (d, *J* = 2.2 Hz, 1H), 8.52 (dd, *J* = 4.8, 1.6 Hz, 1H), 8.29 (s, 1H), 8.24 (dd, *J* = 4.8, 1.8 Hz, 1H), 8.12 (s, 1H), 8.04 (dt, *J* = 7.9, 1.9 Hz, 1H), 7.61 (dd, *J* = 7.4, 1.8 Hz, 1H), 7.47 (dd, *J* = 7.9, 4.8 Hz, 1H), 7.04 (dd, *J* = 7.4, 4.9 Hz, 1H), 3.56 (s, 3H), 3.49 – 3.40 (m, 3H), 2.93 – 2.80 (m, 1H), 2.80 – 2.66 (m, 2H), 1.80 – 1.70 (m, 2H), 1.70 – 1.55 (m, 2H). ^{13}C NMR (101 MHz, DMSO-d6) *δ* 163.80, 160.50, 156.91, 149.08, 149.02, 147.73, 145.28, 140.30, 136.06, 135.64, 124.38, 124.05, 118.05, 49.55, 31.70, 30.69, 30.17. HRMS calculated for C18H20N6 [M+H]+: 321.18197, found 321.18222. Mass difference (mDa): -0.25; mass error (ppm): -0.7784.

3'-Benzo[1,3]dioxol-5-yl-4-(4-methyl-4H-[1,2,4]triazol-3-yl)-3,4,5,6-tetrahydro-2H-[1,2']bipyridinyl (3) – SEN817: Following general procedure for Suzuki coupling and using Benzo[1,3]dioxole-5-boronic acid, 0.18 g of compound **SEN817 (3)** were recovered (yield, 41%) after purification on silica column, eluting with DCM/MeOH (9:1). Mass (ES) m/z: = 364 (M+1). UPLC Rt = 0.78 min. ^{1}H NMR (400 MHz, DMSO-d6) *δ* 8.30 (s, 1H), 8.19 – 8.13 (m, 1H), 7.53 – 7.44 (m, 1H), 7.18 (s, 1H), 7.13 – 7.03 (m, 1H), 7.03 – 6.87 (m, 2H), 6.04 (s,

2H), 3.56 (s, 3H), 3.42 – 3.34 (m, 2H), 2.93 – 2.81 (m, 1H), 2.77 – 2.63 (m, 2H), 1.86 – 1.74 (m, 2H), 1.73 – 1.57 (m, 2H). ^{13}C NMR (101 MHz, DMSO-d6) δ 160.00, 156.98, 148.17, 147.06, 146.64, 145.30, 139.88, 134.23, 126.65, 121.64, 117.62, 112.49, 109.41, 108.46, 101.76, 49.24, 31.88, 30.70, 30.30. HRMS calculated for C20H21N5O2 [M+H]+: 364.17647, found 364.1768. Mass difference (mDa): -0.33; mass error (ppm): -0.9062.

Glutaminyl cyclase and iso Glutaminyl cyclase enzymatic assay: The activity of the two enzymes was estimated fluorometrically by a coupled assay using pyroglutamyl aminopeptidase (from Bacillus amyloliquefaciens, expressed in E. Coli, purchased from QIAGEN, Hilden, Germany) as auxiliary enzyme and H-Gln-AMC (7-amino-4-methylcoumaride) as substrate (Bachem AG, Switzerland) [2]. The assay was conducted in 384 well non-binding surface plates (Corning Costar) in 50 mM Tris HCl pH 8.0, in a final 50 µl volume. For the QPCT assay, the reaction mixture contained 50 µM H-Gln-AMC, 1 nM QPCT human recombinant expressed in HEK293 (OriGene, MD, USA) and 0.2 U/ml pyroglutamyl aminopeptidase, whereas for the isoQPCT the reaction mixture contained 50 µM H-Gln-AMC, 10 nM isoQPCT human recombinant expressed in HEK293 (Genscript, Piscataway, USA) and 0.2 U/ml pyroglutamyl aminopeptidase. For QPCT and QPCT (E201Q) activity assay, reaction mixture was incubated with either cells lysates or supernatants from HEK293. For compound inhibition tests, the assay was conducted in concentration response in a 10 concentrations range (100 µM to 0.005 µM), with a final 1% DMSO. As a reference compound the compound PBD150 was used [3]. The product development was followed at 25°C by repeated kinetic fluorescence readings on a TECAN Safire2 plate reader with excitation/emission wavelengths of 380/465 nm. Fluorescence was read every 2 minutes for 40 minutes and enzyme activity was calculated as RFU/min from the linear part of the product development curve

***Solubility Assay*.** Standard and sample solutions were prepared from a 10 mM DMSO stock solution using an automated dilution procedure. For each compound, three solutions were prepared; one to be used as standard and the other two as test solutions. Standard: 250 µM standard solution in acetonitrile/buffer, with a final DMSO content of 2.5% (v/v). Test sample for pH 3.0: 250 µM sample solution in acetic acid 50 mM, pH = 3, with a final DMSO content of 2.5% (v/v). Test sample for pH 7.4: a 250 µM sample solution in ammonium acetate buffer 50 mM, pH = 7.4, with a final DMSO content of 2.5% (v/v). The 250 µM product suspensions/solutions in the aqueous buffers were prepared directly in Millipore MultiScreen-96 filter plates (0.4 µm PTCE membrane) and sealed. Plates were left for 24 h at room temperature under orbital shaking to achieve “pseudo-thermodynamic equilibrium” and to presaturate the membrane filter. Product suspensions/solutions were

then filtered using centrifugation, diluted 1:2 with the same buffer solution, and analyzed by UPLC/UV/TOF-MS, using UV detection at 254 nm for quantitation. Solubility was calculated by comparing the sample and standard UV areas: $S = (A_{smp} \times FD \times C_{st})/A_{st}$, where S was the solubility of the compound (μM), A_{smp} was the UV area of the sample solution, FD was the dilution factor (2), C_{st} was the standard concentration (250 μM), and A_{st} was the UV area of the standard solution.

Metabolic Stability Assay. Compounds in 10 mM DMSO solution were added to an incubation mixture in a 96-well microplate containing 20 pmol/mL of hCYP3A4 (0.1-0.2 mg/mL protein). The mixture was split in two aliquots: one receiving a NADPH regenerating system, the other an equal amount of phosphate buffer. The final substrate concentration was 1 μM along with 0.25% of organic solvent. Incubation proceeded for 1 h at 37 ºC and was stopped by addition of acetonitrile to precipitate proteins. Metabolic stability was given as the percent remaining following incubation with cofactor (NADPH) with reference to the incubation mixture without NADPH: % remaining = $Area_{NADPH} \times 100/Area_{ctrl}$ where $Area_{ctrl}$ was the MS peak area of the sample solution without NADPH and $Area_{NADPH}$ was the MS area of the sample solution with NADPH.

Permeability Assay**.** The assay was run in a PAMPA filter plate onto which is deposited a mixture of porcine pig brain lipids in dodecane (2% w/v), and compounds (10 μM in HBSS + Hepes buffer pH = 7.4) were added to the donor chamber and incubated for 4 h at 37 °C and 80% humidity. Warfarin was used in each well as control for membrane integrity. Concentrations of reference t(0), donor, and acceptor solutions were measured by UPLC-MS-TOF. The passive permeability was calculated according to the following expression:

$$CA(t) = \left(\frac{M}{V_D + V_A}\right) + \left(Ca(0) - \frac{M}{V_D + V_A}\right) e^{-PeA\left(\frac{1}{V_D}+\frac{1}{V_A}\right)t}$$

where M refers to the total amount of drug in the system minus the amount of sample lost in membrane (and surfaces), $C_A(t)$ was the concentration of the drug in the acceptor well at time t, $C_A(0)$ was the concentration of the drug in the acceptor well at time 0, V_A was the volume of the acceptor well, V_D was the volume of the donor well, P_e was the effective permeability, A was the membrane area, and t was the permeation time. Compounds were defined as low, medium, or highly permeable following the following classification: $>10 \times 10^{-6}$ cm/s, high (passive permeability was unlikely to be limiting for passive diffusion); between 2 and 10×10^{-6} cm/s, medium (permeability may be limiting in the case of low solubility, high metabolic turnover rate or active secretion); between 0 and 2×10^{-6} cm/s, low (high risk that permeability was limiting for passive diffusion).

Supplementary Note 2 Figure

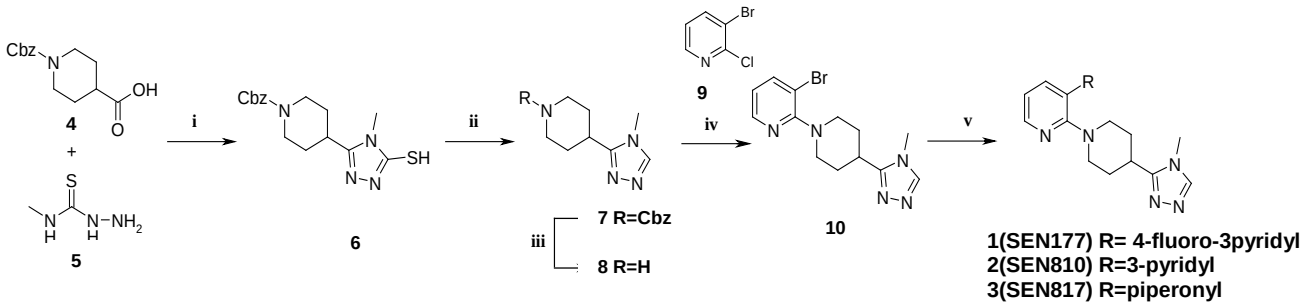

Supplementary Note 2 Figure. Synthetic scheme for SEN177, SEN817 and SEN180. Reagents and conditions: (i) CDI, CH_3CN, 90°C, 18 h (41%); (ii) H_2O_2, CH_3COOH, rt, 18 h (54%); (iii) 6N HCl, 100°C, 6 h (quantitative); (iv) DMF, K_2CO_3, 100°C, 18 h (41%); (v) $Pd_2(dba)_3$, tricyclohexyl phosphine, R-$B(OH)_3$, K_3PO_4, H_2O/Dioxane (1:1), 100°C , 48 h (15-48%). Reaction of N-protected isonipecotic acid (**4**) and N-methyl-thiosemicarbazide (**5**) afforded triazole derivative **6**, which was desulfurised in the presence of hydrogen peroxide to give intermediate **7**. Nitrogen deprotection in acidic conditions, followed by nucleophilic aromatic substitution on 3-bromo-2-chloro-pyridine (**9**), gave compound **10**, which underwent a Suzuki-Miyaura coupling with the desired boronic acids yielding final compounds **SEN177 (1)**, **SEN180 (2)** and **SEN817 (3)**.

References

1. Still, W. C., Kahn, M. & Mitra, A. Rapid chromatographic technique for preparative separations with moderate resolution. *J. Org. Chem.* **43,** 2923–2925 (1978).
2. Schilling, S. *et al.* Continuous spectrometric assays for glutaminyl cyclase activity. *Anal. Biochem.* **303,** 49–56 (2002).
3. Buchholz, M. *et al.* The first potent inhibitors for human glutaminyl cyclase: synthesis and structure-activity relationship. *J. Med. Chem.* **49,** 664–677 (2006).

Supplementary Data Set 1. List of 257 human genes obtained in HEK293 siRNA screen and validation in *Drosophila*

Top 257 genes selected from the high-throughput siRNA screen performed in HEK293 cells for rescuing HTT(138) toxicity were ranked by logP #nuclei rescue index. In column 5, the existence of *Drosophila* orthologs for each mammalian gene is indicated. Those genes for which RNA lines were available as GD and/or KK constructs and for which there were no declared off-target effects were tested (http://stockcenter.vdrc.at/control/main). RNAi lines that did not rescue the Q48-eye degeneration phenotype in Drosophila (-), or those that showed significant rescue (+) are indicated in column 6. RNAi lines that show a general effect on GFP levels. Hits positive in both high-throughput and *Drosophila* screen are highlighted in grey.

HEK293T HT-siRNA screen ranking	*Gene symbol*	*Annotation*	*RefSeq transcripts*	*Fly ortholog*	*Rescue Drosophila Q48-eye degeneration*
1	**SLC25A22**	solute carrier family 25 (mitochondrial carrier: glutamate), member 22	NM_024698	CG18347	+
				CG12201	+
2	**MPST**	mercaptopyruvate sulfurtransferase	NM_021126,NM_001013440,NM_001013436	none	
3	**TLR2**	toll-like receptor 2	NM_003264	CG6890	-
4	**KCNK3**	potassium channel, subfamily K, member 3	NM_002246	CG9637	-
5	**GABRR1**	gamma-aminobutyric acid (GABA) receptor, rho 1	NM_002042	none	
6	**PIGR**	polymeric immunoglobulin receptor	NM_002644	none	
7	**LILRB2**	leukocyte immunoglobulin-like receptor, subfamily B (with TM and ITIM domains), member 2	NM_005874	none	
8	**GCNT2**	glucosaminyl (N-acetyl) transferase 2, I-branching enzyme (I blood group)	NM_145655,NM_001491, NM_145649	none	
9	**TPSB2**	tryptase alpha/beta 1; tryptase beta 2	NM_024164	none	
10	**EDG3**	sphingosine-1-phosphate receptor 3	NM_005226	none	
11	**CPA1**	carboxypeptidase A1 (pancreatic)	NM_001868	CG17633	-
12	**GLRX**	glutaredoxin (thioltransferase)	NM_002064	CG6852	-
				CG7975	-
13	**FCER1G**	Fc fragment of IgE, high affinity I, receptor for; gamma polypeptide	NM_004106	none	
14	**NDUFS8**	NADH dehydrogenase (ubiquinone) Fe-S protein 8, 23kDa (NADH-coenzyme Q reductase)	NM_002496	CG3944	-
15	**BUB1**	budding uninhibited by benzimidazoles 1 homolog (yeast)	NM_004336	CG7838	-
				CG14030	-
16	**SLC16A6**	solute carrier family 16, member 6 (monocarboxylic acid transporter 7); similar to solute carrier family 16, membe	NM_004694	none	
17	**SLC27A4**	solute carrier family 27 (fatty acid transporter), member 4	NM_005094	CG7400	+
				CG30194	+
18	**ACACA**	acetil-CoA carboxilase A alpha	NM_198838,NM_198837, NM_198835,NM_198836, NM_198839,NM_000664, NM_198834	CG11198	+
19	**TRPC3**	transient receptor potential cation channel, subfamily C, member 3	NM_003305	none	
20	**OSBPL11**	oxysterol binding protein-like 11	NM_022776	CG1513	+
				CG5077	+
21	**BHMT2**	betaine-homocysteine methyltransferase 2	NM_017614	none	
22	**USP9Y**	ubiquitin specific peptidase 9, Y-linked	NM_004654	CG1945	+
23	**QPCT**	glutaminyl-peptide cyclotransferase	NM_012413	CG32412	+
				CG5976	+
24	**TBXA2R**	thromboxane A2 receptor	NM_001060,NM_201636	none	
25	**LDHD**	lactate dehydrogenase D	NM_153486,NM_194436	none	
26	**FADS2**	fatty acid desaturase 2	NM_004265	none	
27	**KREMEN2**	kringle containing transmembrane protein 2	NM_024507,NM_172229,NM_145347,NM_145348	none	
28	**NTSR2**	neurotensin receptor 2	NM_012344	none	
29	**SLC9A3R2**	solute carrier family 9 (sodium/hydrogen exchanger), member 3 regulator 2	NM_004785	none	
30	**BACH/ACOT7**	acyl-CoA thioesterase 7	NM_181866,NM_181865,NM_181864,NM_181862, NM_181863,NM_007274	none	
31	**BF/CBF**	complement factor B	NM_001710	none	
32	**SALPR**	relaxin/insulin-like family peptide receptor 3	NM_016568	none	
33	**KCNN1**	potassium intermediate/small conductance calcium-activated channel, subfamily N, member 1	NM_002248	CG10706	+
34	**STX10**	syntaxin 10	NM_003765	CG7736	+
35	**KCNQ1**	potassium voltage-gated channel, KQT-like subfamily, member 1	NM_181798,NM_181797,NM_000218	none	
36	**CTSF**	cathepsin F	NM_003793	CG12163	+
37	**PYC1**	PYD (pyrin domain) containing 1	NM_152901	none	
38	**AMFR**	autocrine motility factor receptor	NM_001144,NM_138958	none	
39	**ARHGAP10**	Rho GTPase activating protein 10	NM_024605	CG8948	-
40	**GPR37L1**	G protein-coupled receptor 37 like 1	NM_004767	CG14593	+
				CG30106	+
41	**MASS1**	G protein-coupled receptor 98	NM_032119	none	

42	**ACADS**	acyl-Coenzyme A dehydrogenase, C-2 to C-3 short chain	NM_000017	CG4703-PA	-
43	**CSAD**	cysteine sulfinic acid decarboxylase	NM_015989	CG7811	+
44	**HTRA3**	HtrA serine peptidase 3	NM_053044	CG8464	-
45	**GPR18**	G protein-coupled receptor 18	NM_005292	none	
46	**PGAM2**	phosphoglycerate mutase 2 (muscle)	NM_000290	CG1721	+
47	**LGR7/RXFP1**	relaxin/insulin-like family peptide receptor 1	NM_021634	CG31096 *	-
48	**OVTN**	ovochymase 2	NM_198185	none	
49	**RHBDL2**	rhomboid, veinlet-like 2 (Drosophila)	NM_017821	CG1697	+
				CG17212	+
50	**LANCL1**	LanC lantibiotic synthetase component C-like 1 (bacterial)	NM_006055	CG2061	-
51	**TSTA3**	tissue specific transplantation antigen P35B	NM_003313	CG3495	-
52	**IL17RA**	interleukin 17 receptor A	NM_014339	none	
53	**F12**	coagulation factor XII (Hageman factor)	NM_000505	none	
54	**GPR2/CCR10**	chemokine (C-C motif) receptor 10	NM_016602	none	
55	**FGFR4**	fms-related tyrosine kinase 4	NM_002020,NM_182925	CG1389	+
56	**TFPI**	tissue factor pathway inhibitor (lipoprotein-associated coagulation inhibitor)	NM_006287,NM_001032281	none	
57	**SLC4A2**	solute carrier family 4, anion exchanger, member 2 (erythrocyte membrane protein band 3-like 1)	NM_003040	CG8177	+
58	**FLJ10948**	enoyl Coenzyme A hydratase domain containing 2	NM_018281	CG8778□	+
59	**P2RY13**	purinergic receptor P2Y, G-protein coupled, 13	NM_023914,NM_176894	none	
60	**PLAU**	plasminogen activator, urokinase	NM_002658	none	
61	**PEX5**	peroxisomal biogenesis factor 5	NM_000319	CG14815	Enhancer
62	**BAIAP2**	BAI1-associated protein 2	NM_006340,NM_017450,NM_017451	none	
63	**PTPRG**	protein tyrosine phosphatase, receptor type, G	NM_002841	CG11516	-
64	**KCNQ4**	potassium voltage-gated channel, KQT-like subfamily, member 4	NM_172163,NM_004700	CG33135	+
65	**SMURF1**	SMAD specific E3 ubiquitin protein ligase 1	NM_020429,NM_181349	CG4943	-
66	**LILRB1**	leukocyte immunoglobulin-like receptor, subfamily B (with TM and ITIM domains), member 1	NM_006669	none	
67	**RET**	ret proto-oncogene	NM_020975,NM_020630	CG14396	+
68	**SDHA**	succinate dehydrogenase complex, subunit A, flavoprotein (Fp)	NM_004168	CG17246	+
69	**DHPS**	deoxyhypusine synthase	NM_001930,NM_013406,NM_013407	CG8005□	
70	**GPR124**	G protein-coupled receptor 124	NM_032777	CG15744□	+
71	**CAPN10**	calpain 10	NM_021251,NM_023088,NM_023085,NM_023083,NM_023089	none	
72	**CLIC1**	chloride intracellular channel 1	NM_001288	none	
73	**PIGK**	phosphatidylinositol glycan anchor biosynthesis, class K	NM_005482	CG4406 *	-
74	**GRIN2A**	glutamate receptor, ionotropic, N-methyl D-aspartate 2A	NM_000833	CG33513	-
75	**MMP13**	matrix metallopeptidase 13 (collagenase 3)	NM_002427	none	
76	**GPR35**	G protein-coupled receptor 35	NM_005301	none	
77	**ADRA2B**	adrenergic, alpha-2B-, receptor	NM_000682	none	
78	**DHRS4L2**	dehydrogenase/reductase (SDR family) member 4 like 2	NM_198083	CG10672	-
79	**ETFB**	electron-transfer-flavoprotein, beta polypeptide	NM_001985,NM_001014763	CG7834	+
80	**KIFC3**	kinesin family member C3	NM_005550	CG7831	+
81	**AGPAT4**	1-acylglycerol-3-phosphate O-acyltransferase 4 (lysophosphatidic acid acyltransferase, delta)	NM_020133,NM_001012734,NM_001012733	CG4753	+
82	**SLC30A1**	solute carrier family 30 (zinc transporter), member 1	NM_021194	CG17723	-
83	**VIPR1**	vasoactive intestinal peptide receptor 1	NM_004624	none	
84	**RAMP3**	receptor (G protein-coupled) activity modifying protein 3	NM_005856	none	
85	**KCNK16**	potassium channel, subfamily K, member 16	NM_032115	CG1615	-
86	**SLC24A1**	solute carrier family 24 (sodium/potassium/calcium exchanger), member 1	NM_004727	CG18660	-
				CG1090	-
87	**CACNG2**	calcium channel, voltage-dependent, gamma subunit 2	NM_006078	none	
88	**MGC15763**	oxidoreductase NAD-binding domain containing 1	NM_138381	none	
89	**ADAM8**	ADAM metallopeptidase domain 8	NM_001109	CG42252/CG9163	+
90	**SUCNR1**	succinate receptor 1	NM_033050	none	
91	**HRMT1L4**	protein arginine methyltransferase 8	NM_019854	CG6554	+
92	**CST3**	cystatin C	NM_000099	none	
93	**SLC22A2**	solute carrier family 22 (organic cation transporter), member 2	NM_153191,NM_003058	CG6331	-
94	**MPP5**	membrane protein, palmitoylated 5 (MAGUK p55 subfamily member 5)	NM_022474	CG32717	-
95	**KIF9**	kinesin family member 9	NM_182903,NM_022342,NM_182902	none	
96	**NMBR**	neuromedin B receptor	NM_002511	CG30106 (**GPR37L1)	+
97	**PNR**	trace amine associated receptor 5	NM_003967	none	
98	**IFNAR2**	interferon (alpha, beta and omega) receptor 2	NM_207584,NM_000874,NM_207585	none	
99	**HADHB**	hydroxyacyl-Coenzyme A dehydrogenase/3-ketoacyl-Coenzyme A thiolase/enoyl-Coenzyme A hydratase (trifunc	NM_000183	CG4581	+
100	**SDHB**	succinate dehydrogenase complex, subunit B, iron sulfur (Ip)	NM_003000	CG3283 *	-

101	**LTC4S**	leukotriene C4 synthase	NM_145867,NM_000897	none	
102	**TRPM2**	transient receptor potential cation channel, subfamily M, member 2	NM_001001188,NM_003307	none	
103	**SCN1B**	sodium channel, voltage-gated, type I, beta	NM_199037,NM_001037	none	
104	**EPHB3**	EPH receptor B3	NM_004443	CG1511	-
105	**ABCA2**	ATP-binding cassette, sub-family A (ABC1), member 2	NM_001606,NM_212533	none	
106	**KCNK17**	potassium channel, subfamily K, member 17	NM_031460	none	
107	**CELSR1**	cadherin, EGF LAG seven-pass G-type receptor 1 (flamingo homolog, Drosophila)	NM_014246	CG11895	-
108	**SLC19A1**	solute carrier family 19 (folate transporter), member 1	NM_003056,NM_194255	none	
109	**CTSL2**	cathepsin L2	NM_001333	CG6692	-
110	**ACE**	angiotensin I converting enzyme (peptidyl-dipeptidase A) 1	NM_152830,NM_152831,NM_000789	CG8827	-
111	**CTRC**	chymotrypsin C (caldecrin)	NM_007272	none	
112	**IL6R**	interleukin 6 receptor	NM_181359,NM_000565	none	
113	**RSC1A1**	regulatory solute carrier protein, family 1, member 1	NM_006511	none	
114	**PDE7A**	phosphodiesterase 7A	NM_002604,NM_002603	none	
115	**CRAT**	carnitine acetyltransferase	NM_004003,NM_000755,NM_144782	none	
116	**CHRNE**	cholinergic receptor, nicotinic, epsilon	NM_000080	CG11348	-
117	**SLC1A2**	solute carrier family 1 (glial high affinity glutamate transporter), member 2	NM_004171	CG3159	+
118	**NR0B1**	nuclear receptor subfamily 0, group B, member 1	NM_000475	none	
119	**C14orf20**	testis-specific serine kinase 4	NM_174944	none	
120	**USP21**	ubiquitin specific peptidase 21	NM_012475,NM_001014443	CG14619	-
121	**HRMT1L3**	protein arginine methyltransferase 3	NM_005788	CG6563	+
122	**GPT**	glutamic-pyruvate transaminase (alanine aminotransferase)	NM_005309	CG1640	-
123	**KLK8**	kallikrein-related peptidase 8	NM_144505,NM_007196,NM_144506,NM_144507	none	
124	**PPAT**	phosphoribosyl pyrophosphate amidotransferase	NM_002703	CG2867	+
				CG10078	+
125	**TRPC7**	transient receptor potential cation channel, subfamily C, member 7	NM_020389	none	
126	**FLT3**	fms-related tyrosine kinase 3	NM_004119	none	
127	**DKFZp566O084**	dehydrogenase/reductase (SDR family) member 7B	NM_015510	CG7601	-
129	**SLC10A2**	solute carrier family 10 (sodium/bile acid cotransporter family), member 2	NM_000452	none	
130	**ADORA3**	adenosine A3 receptor	NM_000677,NM_020683	none	
131	**SLC23A2**	solute carrier family 23 (nucleobase transporters), member 2	NM_203327,NM_005116	CG6293	-
132	**SLC2A2**	solute carrier family 2 (facilitated glucose transporter), member 2	NM_000340	CG1086	+
133	**FLJ39822**	solute carrier family 38, member 11	NM_173512	CG13743 ***	-
				CG17509	-
134	**KCNJ12**	similar to hkir2.2x; similar to inward rectifying K+ channel negative regulator Kir2.2v; potassium inwardly-rectifying	NM_021012	CG6747	+
135	**SLC12A7**	solute carrier family 12 (potassium/chloride transporters), member 7	NM_006598	CG5594	+
136	**GPR26**	G protein-coupled receptor 26	NM_153442	none	
137	**ASNA1**	arsA arsenite transporter, ATP-binding, homolog 1 (bacterial)	NM_004317	CG1598	-
138	**ELOVL4**	elongation of very long chain fatty acids (FEN1/Elo2, SUR4/Elo3, yeast)-like 4	NM_022726	CG32072	-
				CG11801	-
139	**SENP2**	SUMO1/sentrin/SMT3 specific peptidase 2	NM_021627	none	
140	**AVPR1A**	arginine vasopressin receptor 1A	NM_000706	CG11325	-
141	**UGT1A3**	UDP glucuronosyltransferase 1 family, polypeptide A3; UDP glucuronosyltransferase 1 family, polypeptide A5; U	NM_019093	CG8652	+
142	**MAP2K4**	mitogen-activated protein kinase kinase 4	NM_003010	CG9738	-
143	**KCNS2**	potassium voltage-gated channel, delayed-rectifier, subfamily S, member 2	NM_020697	none	
144	**CASP8**	caspase 8, apoptosis-related cysteine peptidase	NM_033356,NM_033355,NM_033357,NM_033358,NM_001228	none	
145	**KCNJ14**	potassium inwardly-rectifying channel, subfamily J, member 14	NM_170720,NM_013348	CG6747	-
146	**TNFRSF11A**	tumor necrosis factor receptor superfamily, member 11a, NFKB activator	NM_003839	none	
147	**TNFRSF5/CD40**	CD40 molecule, TNF receptor superfamily member 5	NM_152854,NM_001250	none	
148	**HSD17B4**	hydroxysteroid (17-beta) dehydrogenase 4	NM_000414	CG3415	+
149	**KLK6**	kallikrein-related peptidase 6	NM_002774,NM_001012966,NM_001012965,NM_001012964	none	
150	**CAPN5**	calpain 5	NM_004055	none	
151	**ABP1**	amiloride binding protein 1 (amine oxidase (copper-containing))	NM_001091	none	
152	**SULT1C2**	sulfotransferase family, cytosolic, 1C, member 4	NM_006588	CG5428	-
153	**OSBPL1A**	oxysterol binding protein-like 1A	NM_018030,NM_080597,NM_133268	CG3860	-
154	**ADAMTS12**	ADAM metallopeptidase with thrombospondin type 1 motif, 12	NM_030955	CG4096	+
155	**KIAA1045**		XM_048592	none	
156	**LHCGR**	luteinizing hormone/choriogonadotropin receptor	NM_000233	CG7665	+
157	**HTR1B**	5-hydroxytryptamine (serotonin) receptor 1B	NM_000863	none	
158	**CARD8**	caspase recruitment domain family, member 8	NM_014959	none	
159	**CRHR2**	corticotropin releasing hormone receptor 2	NM_001883	CG12370	-

[illegible]	**CRHR2**	[illegible]	[illegible]	CG8422 *	-
160	**GRCA**	G protein-coupled receptor 162	NM_014449,NM_019858	none	
161	**UCP1**	uncoupling protein 1 (mitochondrial, proton carrier)	NM_021833	none	
162	**SLC22A11**	solute carrier family 22 (organic anion/urate transporter), member 11	NM_018484	CG8654	+
163	**PYGM**	phosphorylase, glycogen, muscle	NM_005609	CG7254	-
164	**GALGT2**	beta-1,4-N-acetyl-galactosaminyl transferase 2	NM_153446	none	
165	**GLDC**	glycine dehydrogenase (decarboxylating)	NM_000170	CG3999	
166	**SOAT2**	sterol O-acyltransferase 2	NM_003578	CG8112	+
167	**PPARG**	peroxisome proliferator-activated receptor gamma	NM_005037,NM_015869,NM_138712,NM_138711	CG8127	-
168	**TNFRSF17**	tumor necrosis factor receptor superfamily, member 17	NM_001192	none	
169	**DPP8**	dipeptidyl-peptidase 8	NM_197960,NM_197961,NM_130434,NM_017743	CG3744	+
170	**SLC7A10**	solute carrier family 7, (neutral amino acid transporter, y+ system) member 10	NM_019849	CG3297	-
171	**SLC22A8**	solute carrier family 22 (organic anion transporter), member 8	NM_004254	none	
172	**CTRL**	chymotrypsin-like	NM_001907	none	
173	**SLCO5A1**	solute carrier organic anion transporter family, member 5A1	NM_030958	CG3811	+
174	**EPHA3**	EPH receptor A3	NM_182644,NM_005233	CG1594	-
175	**GPR54**	KISS1 receptor	NM_032551	none	
176	**SLC12A3**	solute carrier family 12 (sodium/chloride transporters), member 3	NM_000339	none	
177	**ADAM12**	ADAM metallopeptidase domain 12	NM_021641,NM_003474	none	
178	**CAPNS1**	calpain, small subunit 1	NM_001749,NM_001003962	none	
179	**RARG**	retinoic acid receptor, gamma	NM_000966	CG8127	+
180	**NDUFA6**	NADH dehydrogenase (ubiquinone) 1 alpha subcomplex, 6, 14kDa	NM_002490	CG7712	+
181	**GPR64**	G protein-coupled receptor 64	NM_005756	none	
182	**KCNK7**	potassium channel, subfamily K, member 7	NM_005714,NM_033456,NM_033455,NM_033348,NM_033347	none	
183	**PGCP**	plasma glutamate carboxypeptidase	NM_016134	none	
184	**CA12**	carbonic anhydrase XII	NM_001218,NM_206925	none	
185	**ADAM11**	ADAM metallopeptidase domain 11	NM_002390	CG42252	-
186	**USP40**	ubiquitin specific peptidase 40	NM_018218	none	
187	**LTB4R**	leukotriene B4 receptor	NM_181657	none	
188	**GABRB3**	gamma-aminobutyric acid (GABA) A receptor, beta 3	NM_000814,NM_021912	CG17336	+
189	**SLC18A2**	solute carrier family 18 (vesicular monoamine), member 2	NM_003054	CG33528	+
190	**PAK1**	p21 protein (Cdc42/Rac)-activated kinase 1	NM_002576	CG10295	+
191	**CAPN1**	Calpain 1	NM_005186	CG7563	+
192	**LRP1**	low density lipoprotein-related protein 1 (alpha-2-macroglobulin receptor)	NM_002332	CG1372	+
193	**SLC25A11**	solute carrier family 25 (mitochondrial carrier; oxoglutarate carrier), member 11	NM_003562	CG1907 CG18418 CG7514	+ + +
194	**PITRM1**	pitrilysin metallopeptidase 1	NM_014889	CG3107	+
195	**HCN4**	hyperpolarization activated cyclic nucleotide-gated potassium channel 4	NM_005477	CG8585	+
196	**GPR83**	G protein-coupled receptor 83	NM_016540	CG5811	-
197	**HTR4**	5-hydroxytryptamine (serotonin) receptor 4	NM_000870,NM_199453	none	
198	**CAPN3**	calpain 3, (p94)	NM_173089,NM_173090,NM_173088,NM_173087,NM_024344,NM_000070,NM_212465,NM_212464,NM_212467	CG7563	-
199	**GPR87**	G protein-coupled receptor 87	NM_023915	none	
200	**PKD1L2**	polycystic kidney disease 1-like 2	NM_052892,NM_182740	none	
201	**SLC1A7**	solute carrier family 1 (glutamate transporter), member 7	NM_006671	CG3747	-
202	**KCNK9**	potassium channel, subfamily K, member 9	NM_016601	CG9637 CG9361	- -
203	**MGC16169**	TBC domain-containing protein kinase-like	NM_033115	CG4041	+
204	**SOAT1**	sterol O-acyltransferase 1	NM_003101	CG8112	-
205	**GPR8**	neuropeptides B/W receptor 2	NM_005286	none	
206	**M160**	CD163 molecule-like 1	NM_174941	none	
207	**PVRL2**	poliovirus receptor-related 2 (herpesvirus entry mediator B)	NM_002856	none	
208	**GPR150**	G protein-coupled receptor 150	NM_199243	none	
209	**PTPRM**	protein tyrosine phosphatase, receptor type, M	NM_002845	CG10975	+
210	**EDNRB**	endothelin receptor type B	NM_003991,NM_000115	none	
211	**MGC23280**	dehydrogenase/reductase (SDR family) member 13	NM_144683	none	
212	**NR3C2**	nuclear receptor subfamily 3, group C, member 2	NM_000901	none	
213	**HAP1**	huntingtin-associated protein 1	NM_003949,NM_177977	none	
214	**TRAR5**	trace amine associated receptor 8	NM_053278	none	
215	**IL22RA1**	interleukin 22 receptor, alpha 1	NM_021258	none	

216	**GPR75**	G protein-coupled receptor 75	NM_006794	none	
217	**B3GNT5**	UDP-GlcNAc:betaGal beta-1,3-N-acetylglucosaminyltransferase 5	NM_032047	CG4934	-
218	**DRD4**	dopamine receptor D4	NM_000797	none	
219	**ACY1**	aminoacylase 1	NM_000666	CG6465	-
220	**EBI2**	G protein-coupled receptor 183	NM_004951	none	
221	**VNN3**	vanin 3	NM_078625,NM_018399,NM_001024460	none	
222	**FZD10**	frizzled homolog 10 (Drosophila)	NM_007197	CG17697	-
				CG4626	-
223	**LRP3**	low density lipoprotein receptor-related protein 3	NM_002333	none	
224	**FUT10**	fucosyltransferase 10 (alpha (1,3) fucosyltransferase)	NM_032664	CG4435	-
225	**GPR41**	free fatty acid receptor 3	NM_005304	none	
226	**SLC12A5**	solute carrier family 12 (potassium-chloride transporter), member 5	NM_020708	CG5594	+
227	**FAAH**	fatty acid amide hydrolase	NM_001441	CG30502	-
228	**ADAM33**	ADAM metallopeptidase domain 33	NM_025220,NM_153202	CG42252	-
229	**HTR5A**	5-hydroxytryptamine (serotonin) receptor 5A	NM_024012	CG16720	+
				CG15113 (**HTR1B)	+
230	**GPR151**	G protein-coupled receptor 151	NM_194251	none	
231	**HTR3A**	5-hydroxytryptamine (serotonin) receptor 3A	NM_000869,NM_213621	CG11822	+
232	**GPR25**	G protein-coupled receptor 25	NM_005298	none	
233	**SCN11A**	sodium channel, voltage-gated, type XI, alpha subunit	NM_014139	CG9907	+
234	**FGFR4**	fibroblast growth factor receptor 4	NM_022963,NM_002011,NM_213647	CG1389	+
235	**PSMB9**	proteasome (prosome, macropain) subunit, beta type, 9 (large multifunctional peptidase 2)	NM_148954,NM_002800	CG8392	-
236	**TBC1D8**		NM_007063	CG7324 *	
237	**VLDLR**	very low density lipoprotein receptor	NM_003383,NM_001018056	CG31094	+
				CG31092	+
238	**RAB40A**	RAB40A, member RAS oncogene family	NM_080879	CG1900	-
239	**CLCA4**	chloride channel accessory 4	NM_012128	none	
240	**OSGEPL1**	O-sialoglycoprotein endopeptidase-like 1	NM_022353	CG14231	+
241	**SLC27A3**	solute carrier family 27 (fatty acid transporter), member 3	NM_024330	CG30194 (**SLC27A4)	+
242	**TACR1**	tachykinin receptor 1	NM_015727,NM_001058	CG7887	-
				CG6515	-
243	**TRPM6**	transient receptor potential cation channel, subfamily M, member 6	NM_017662	CG34123	+
244	**MMP17**	matrix metallopeptidase 17 (membrane-inserted)	NM_016155	CG1794	+
245	**GPR157**	G protein-coupled receptor 157	NM_024980	none	
246	**SLC22A3**	solute carrier family 22 (extraneuronal monoamine transporter), member 3	NM_021977	none	
247	**UBE2D1**	ubiquitin-conjugating enzyme E2D 1 (UBC4/5 homolog, yeast)	NM_003338	CG7425	-
248	**IL2RB**	interleukin 2 receptor, beta	NM_000878	none	
249	**FMO3**	flavin containing monooxygenase 3	NM_006894,NM_001002294	none	
250	**TRPM8**	transient receptor potential cation channel, subfamily M, member 8	NM_024080	none	
251	**SLC25A3**	solute carrier family 25 (mitochondrial carrier; phosphate carrier), member 3	NM_002635,NM_005888 ,NM_213612,NM_213611	CG4994	-
				CG9090	-
252	**USP34**	ubiquitin specific peptidase 34	NM_014709	CG5794	-
253	**ELA2A**	chymotrypsin-like elastase family, member 2A	NM_033440	none	
254	**SPPL2A**	signal peptide peptidase-like 2A	NM_032802	none	
255	**PARK7**	Parkinson disease (autosomal recessive, early onset) 7	NM_007262	CG1349	+
				CG6646	-
256	**SEPHS1**	selenophosphate synthetase 1; similar to selenophosphate synthetase 1	NM_012247	CG8553	+
				CG5025	+
257	**ACVR1B**	activin A receptor, type IB	NM_020328,NM_020327,NM_004302	CG8224	+

* No RNAi lines available

** Also homologue

*** RNAi line with off target effect

Supplementary Data Set 2. List of RNAi *Drosophila* lines that rescued Q48-eye degeneration and their effect on GFP levels

Table shows the list of *Drosophila* orthologs that were confirmed to rescue Q48-eye degeneration, employing GD- or KK-RNAi lines depending on availability. For KK lines, the p-value was calculated by scoring individuals for the presence or absence of black necrotic spots, and comparing genotypes using Fisher's exact test in both female and male RNAi expressing flies. In order to account for multiple testing, results that showed a p<0.005 in at least one sex were considered significant. Weak, medium or strong rescue of Q48-eye pigmentation was used as a criterion for assessing suppression of degeneration by the GD RNAi lines. Positive RNAi lines were crossed with transgenic flies that expressed EGFP under control of GMR-GAL4 and GFP levels were assessed by western blotting and indicated when significant.
Columns E-F: BS= presence of black necrotic-like spots; columns E and F show p-values obtained with the Fisher's exact test.

	Mammalian gene	*Drosophila Ortholog*	*Symbol*	*KK lines*	*KK BS p-value*		*Eye pigmentation rescue GD lines*	*GFP levels*
					Female	*Male*		
1	ACACA	CG11198	ACC	KK108631	8,19E-06	2,75E-03	GD8105 no effect	***not tested***
2	KCNN1	CG10706	SK	KK103985	5,96E-04	6,06E-03	GD28155 weak	no changes
3	STX10	CG7736	Syx6	KK104795	3,04E-04	3,16E-04	GD1579 no effect	no changes
4	CSAD	CG7811	b	KK105436	3,04E-04	1,09E-03	GD2890 no effect	no changes
5	KCNQ4	CG33135	KCNQ	KK106655	6,38E-07	1,19E-02	GD8754 lethal RNAi toxic	no changes
6	ETFB	CG7834	CG7834	KK110434	1,48E-02	2,15E-05	GD36661 weak	no changes
7	KIFC3	CG7831	ncd	KK110355	4,83E-05	1,38E-07	GD22570 no effect	no changes
8	AGPAT4	CG4753	CG4753	KK109865	1,21E-03	1,09E-04	GD1731 no effect	no changes
9, 10, 11	ADAM8/33/11	CG42252	mmd	KK103449	7,81E-04	5,31E-03	GD45927 no effect	*significant reduction*
12	HRMT1L4	CG6554	Art1	KK110391	1,97E-05	2,33E-07	GD40388 weak	no changes
13	MPP5	CG32717	sdt	KK100685	5,83E-05	3,70E-01	GD2984 medium	no changes
14	HADHB	CG4581	Thiolase	KK105500	2,01E-11	1,58E-08		no changes
15	SLC1A2	CG3159	Eaat2	KK104371	6,51E-05	4,55E-03		no changes
16	HRMT1L3	CG6563	Art3	KK109448	4,83E-05	1,36E-03		no changes
17	PPAT	CG2867	Prat				GD20926 weak	no changes
		CG10078	Prat2	KK108948	7,81E-04	4,40E-02	GD48823 no effect	no changes
18	SLC2A2	CG1086	Glut1	KK101365	1,47E-06	4,29E-01	GD13326 weak	no changes
19	SLC12A7	CG5594	kcc	KK101742	2,78E-02	1,79E-03	GD10278 weak	*not tested*
20	UGT1A3	CG8652	Ugt37c1				GD46514 medium	no changes
21	HSD17B4	CG3415	Mfe2	KK108880	4,12E-03	2,06E-02	GD34613 no effect	no changes
22	ADAMTS12	CG4096	CG4096	KK108353	5,45E-03	4,55E-03		no changes
23	LHCGR	CG7665	Lgr1	KK104877	1,20E-04	1,96E-06	GD13566 no effect	no changes
24	SLC22A11	CG8654	CG8654	KK100112	4,83E-05	1,65E-09	GD4715 no effect	no changes
25	DPP8	CG3744	CG3744				GD34696	no changes
26	SLCO5A1	CG3811	Oatp30B	KK110237	8,74E-05	4,55E-03	GD22983 no effect	no changes
27	RARG	CG8127	Eip75B	KK108399	3,04E-04	7,96E-05	GD44851 enhancer/RNAi toxic	no changes
28	NDUFA6	CG7712	CG7712	KK100616	2,52E-05	2,29E-04	GD35923 strong	no changes
29	GABRB3	CG17336	Lcch3	KK109606	2,80E-07	1,19E-02	GD37408 no effect	no changes
30	SLC18A2	CG33528	Vmat	KK104072	5,14E-05	7,52E-04	GD4856 no effect	no changes
31	PAK1	CG10295	Pak	KK108937	1,77E-03	1,96E-01	GD12553 weak	no changes
32	CAPN1	CG7563	CalpA	KK101294	2,80E-07	7,25E-08	GD35261 no effect	no changes
33	LRP1	CG1372	yl	KK109716	1,98E-05	2,42E-02	GD36345 medium	no changes
34	SLC25A11	CG1907	CG1907	KK103359	3,10E-03	3,50E-03	GD1341 medium	no changes
		CG18418	CG18418	KK102109	3,04E-04	4,21E-02	GD9008 no effect	no changes
		CG7514	CG7514	KK103023	1,97E-05	1,61E-06	GD37233 no effect	no changes
35	PITRM1	CG3107	CG3107	KK103826	1,47E-06	7,52E-04	GD40196 no effect	no changes
36	HCN4	CG8585	Ih	KK110274	4,83E-05	6,13E-08		no changes
37	MGC16169	CG4041	CG4041	KK108887	8,60E-06	3,50E-03		no changes
38	PTPRM	CG10975	Ptp69D	KK104761	1,98E-05	8,77E-04	GD4789 no effect	no changes
39	SLC12A5	CG5594	kcc	KK101742	2,78E-02	1,79E-03	GD10278 weak	no changes
40	HTR5A	CG16720	5-HT1A	KK106094	1,97E-05	4,55E-03		no changes
40,41	HTR1B/HTR5A	CG15113	5-HT1B	KK109929	1,70E-16	3,90E-07	GD46485 medium	no changes
42	HTR3A	CG11822	nAChRβ3	KK101868	4,83E-05	1,92E-01		no changes
43	SCN11A	CG9907	para	KK104775	1,20E-04	7,96E-05	GD6131 no effect	no changes
44	FGFR4/FLT4	CG1389	tor	KK101154	5,86E-06	4,40E-02	GD4298 weak	no changes
45	VLDLR	CG31094	LpR1	KK106364	7,75E-10	5,32E-05	GD14756 no effect	no changes

Supplementary Data Set 3. Heat shock proteins and chaperones PCR array.

Fold changes in mRNA of 84 heat shock proteins and chaperones were analyzed by quantitative PCR in cells expressing HTT(Q74) and treated with 25 µM SEN177 for 24 h relative to DMSO-treated cells. Fold-change values greater than one indicates a positive- or an up-regulation, and the fold-regulation is equal to the fold-change. Fold-change values less than one indicate a negative or down-regulation, and the fold-regulation is the negative inverse of the fold-change. Fold-changes greater than 1.25 are indicated in blue; fold-change values less than 0.75 are indicated in red.

Refseq	Symbol	Description	Gene name	Fold Change (SEN177 compared to DMSO)	Comments
NM_020247	ADCK3	AarF domain containing kinase 3	ARCA2/CABC1/COQ10D4/COQ8/SCAR9	0,9155	OKAY
NM_007348	ATF6	Activating transcription factor 6	ATF6A	0,8924	OKAY
NM_004323	BAG1	BCL2-associated athanogene	BAG-1/HAP/RAP46	1,4241	OKAY
NM_004282	BAG2	BCL2-associated athanogene 2	BAG-2/dJ417I1.2	1,0861	OKAY
NM_004281	BAG3	BCL2-associated athanogene 3	BAG-3/BIS/CAIR-1/MFM6	0,999	OKAY
NM_004874	BAG4	BCL2-associated athanogene 4	BAG-4/SODD	0,6602	OKAY
NM_004873	BAG5	BCL2-associated athanogene 5	BAG-5	0,8111	OKAY
NM_005125	CCS	Copper chaperone for superoxide dismutase	-	1,2383	OKAY
NM_006431	CCT2	Chaperonin containing TCP1, subunit 2 (beta)	99D8.1/CCT-beta/CCTB/HEL-S-100n/PRO1633/TCP-1-beta	0,8909	OKAY
NM_005998	CCT3	Chaperonin containing TCP1, subunit 3 (gamma)	CCT-gamma/CCTG/PIG48/TCP-1-gamma/TRIC5	1,0192	OKAY
NM_006430	CCT4	Chaperonin containing TCP1, subunit 4 (delta)	CCT-DELTA/Cctd/SRB	0,8621	OKAY
NM_012073	CCT5	Chaperonin containing TCP1, subunit 5 (epsilon)	CCT-epsilon/CCTE/HEL-S-69/TCP-1-epsilon	0,8809	OKAY
NM_001762	CCT6A	Chaperonin containing TCP1, subunit 6A (zeta 1)	CCT-zeta/CCT-zeta-1/CCT6/Cctz/HTR3/MoDP-2/TCP-1-zeta/TCP20/TCPZ/TTCP20	0,9147	OKAY
NM_006584	CCT6B	Chaperonin containing TCP1, subunit 6B (zeta 2)	CCT-zeta-2/CCTZ-2/Cctz2/TCP-1-zeta-2/TSA303	0,9504	OKAY
NM_006429	CCT7	Chaperonin containing TCP1, subunit 7 (eta)	CCTETA/CCTH/NIP7-1/TCP1ETA	0,9388	OKAY
NM_000394	CRYAA	Crystallin, alpha A	CRYA1/CTRCT9/HSPB4	0,9372	C
NM_001885	CRYAB	Crystallin, alpha B	CMD1II/CRYA2/CTPP2/CTRCT16/HEL-S-101/HSPB5/MFM2	2,5924	OKAY
NM_001539	DNAJA1	DnaJ (Hsp40) homolog, subfamily A, member 1	DJ-2/DjA1/HDJ2/HSDJ/HSJ2/HSPF4/NEDD7/hDJ-2	1,0184	OKAY
NM_005880	DNAJA2	DnaJ (Hsp40) homolog, subfamily A, member 2	CPR3/DJ3/DJA2/DNAJ/DNJ3/HIRIP4/PRO3015/RDJ2	0,9699	OKAY
NM_005147	DNAJA3	DnaJ (Hsp40) homolog, subfamily A, member 3	HCA57/TID1/hTID-1	0,8901	OKAY
NM_018602	DNAJA4	DnaJ (Hsp40) homolog, subfamily A, member 4	MST104/MSTP104/PRO1472	1,376	B
NM_006145	DNAJB1	DnaJ (Hsp40) homolog, subfamily B, member 1	HSPF1/Hdj1/Hsp40/RSPH16B/Sis1	0,9089	OKAY
NM_016306	DNAJB11	DnaJ (Hsp40) homolog, subfamily B, member 11	ABBP-2/ABBP2/DJ9/Dj-9/EDJ/ERdj3/ERj3/ERj3p/PRO1080/UNQ537/hDj-9	0,936	OKAY
NM_017626	DNAJB12	DnaJ (Hsp40) homolog, subfamily B, member 12	DJ10	1,0729	OKAY
NM_153614	DNAJB13	DnaJ (Hsp40) homolog, subfamily B, member 13	RSPH16A/TSARG5/TSARG6	0,9143	OKAY
NM_001031723	DNAJB14	DnaJ (Hsp40) homolog, subfamily B, member 14	EGNR9427/PRO34683	1,0162	OKAY
NM_006736	DNAJB2	DnaJ (Hsp40) homolog, subfamily B, member 2	DSMA5/HSJ-1/HSJ1/HSPF3	0,8643	OKAY
NM_012266	DNAJB5	DnaJ (Hsp40) homolog, subfamily B, member 5	Hsc40	0,9873	OKAY
NM_005494	DNAJB6	DnaJ (Hsp40) homolog, subfamily B, member 6	DJ4/DnaJ/HHDJ1/HSJ-2/HSJ2/LGMD1E/MRJ/MSJ-1	0,7307	OKAY
NM_145174	DNAJB7	DnaJ (Hsp40) homolog, subfamily B, member 7	DJ5/HSC3	1,1617	B
NM_153330	DNAJB8	DnaJ (Hsp40) homolog, subfamily B, member 8	DJ6	0,9372	C
NM_012328	DNAJB9	DnaJ (Hsp40) homolog, subfamily B, member 9	ERdj4/MDG-1/MDG1/MST049/MSTP049	0,5872	OKAY
NM_022365	DNAJC1	DnaJ (Hsp40) homolog, subfamily C, member 1	DNAJL1/ERdj1/HTJ1/MTJ1	0,9288	OKAY
NM_018981	DNAJC10	DnaJ (Hsp40) homolog, subfamily C, member 10	ERdj5/JPDI/MTHr/PDIA19	0,9562	OKAY
NM_018198	DNAJC11	DnaJ (Hsp40) homolog, subfamily C, member 11	dJ126A5.1	0,9371	OKAY
NM_201262	DNAJC12	DnaJ (Hsp40) homolog, subfamily C, member 12	JDP1	1,0116	OKAY
NM_015268	DNAJC13	DnaJ (Hsp40) homolog, subfamily C, member 13	RME8	1,0081	OKAY
NM_032364	DNAJC14	DnaJ (Hsp40) homolog, subfamily C, member 14	DNAJ/DRIP78/HDJ3/LIP6	1,0847	OKAY
NM_013238	DNAJC15	DnaJ (Hsp40) homolog, subfamily C, member 15	DNAJD1/HSD18/MCJ	0,9673	OKAY
NM_015291	DNAJC16	DnaJ (Hsp40) homolog, subfamily C, member 16	-	0,9971	OKAY
NM_018163	DNAJC17	DnaJ (Hsp40) homolog, subfamily C, member 17	-	1,1312	OKAY
NM_152686	DNAJC18	DnaJ (Hsp40) homolog, subfamily C, member 18	-	0,862	OKAY
NM_194283	DNAJC21	DnaJ (Hsp40) homolog, subfamily C, member 21	DNAJA5/GS3/JJJ1	1,0204	OKAY
NM_006260	DNAJC3	DnaJ (Hsp40) homolog, subfamily C, member 3	ERdj6/HP58/P58/P58IPK/PRKRI	0,9051	OKAY
NM_005528	DNAJC4	DnaJ (Hsp40) homolog, subfamily C, member 4	DANJC4/HSPF2/MCG18	1,253	OKAY
NM_025219	DNAJC5	DnaJ (Hsp40) homolog, subfamily C, member 5	CLN4/CLN4B/CSP/DNAJC5A/NCL	1,3822	OKAY
NM_033105	DNAJC5B	DnaJ (Hsp40) homolog, subfamily C, member 5 beta	CSP-beta	0,7327	B
NM_173650	DNAJC5G	DnaJ (Hsp40) homolog, subfamily C, member 5 gamma	CSP-gamma	0,9372	C
NM_014787	DNAJC6	DnaJ (Hsp40) homolog, subfamily C, member 6	DJC6/PARK19	0,7604	OKAY
NM_003315	DNAJC7	DnaJ (Hsp40) homolog, subfamily C, member 7	DJ11/DJC7/TPR2/TTC2	0,9956	OKAY
NM_014280	DNAJC8	DnaJ (Hsp40) homolog, subfamily C, member 8	HSPC331/SPF31	0,9706	OKAY
NM_015190	DNAJC9	DnaJ (Hsp40) homolog, subfamily C, member 9	HDJC9/JDD1/SB73	0,9068	OKAY
NM_005526	HSF1	Heat shock transcription factor 1	HSTF1	0,9946	OKAY
NM_004506	HSF2	Heat shock transcription factor 2	HSF 2/HSTF 2	0,9175	OKAY
NM_001538	HSF4	Heat shock transcription factor 4	CTM/CTRCT5	1,1293	OKAY

NM_001017963	HSP90AA1	Heat shock protein 90kDa alpha (cytosolic), class A member 1	EL52/HSP86/HSP89A/HSP90A/HSP90N/HSPC1/HSPCA/HSPCAL1/HSPCAL4/HSPN/Hsp89/Hsp90/LAP2	0,9373	OKAY
NM_007355	HSP90AB1	Heat shock protein 90kDa alpha (cytosolic), class B member 1	D6S182/HSP84/HSP90B/HSPC2/HSPCB	0,9321	OKAY
NM_003299	HSP90B1	Heat shock protein 90kDa beta (Grp94), member 1	ECGP/GP96/GRP94/HEL-S-125m/HEL35/TRA1	0,9207	OKAY
NM_016299	HSPA14	Heat shock 70kDa protein 14	HSP70-4/HSP70L1	1,0878	OKAY
NM_005345	HSPA1A	Heat shock 70kDa protein 1A	HEL-S-103/HSP70-1/HSP70-1A/HSP70I/HSP72/HSPA1	1,0103	OKAY
NM_005346	HSPA1B	Heat shock 70kDa protein 1B	HSP70-1B/HSP70-2	0,8173	OKAY
NM_005527	HSPA1L	Heat shock 70kDa protein 1-like	HSP70-1L/HSP70-HOM/HSP70T/hum70t	1,0183	OKAY
NM_021979	HSPA2	Heat shock 70kDa protein 2	HSP70-2/HSP70-3	1,0782	OKAY
NM_002154	HSPA4	Heat shock 70kDa protein 4	APG-2/HS24/P52/HSPH2/RY/hsp70/hsp70RY	0,931	OKAY
NM_014278	HSPA4L	Heat shock 70kDa protein 4-like	APG-1/HSPH3/Osp94	0,8327	OKAY
NM_005347	HSPA5	Heat shock 70kDa protein 5 (glucose-regulated protein, 78kDa)	BIP/GRP78/HEL-S-89n/MIF2	1,0561	OKAY
NM_002155	HSPA6	Heat shock 70kDa protein 6 (HSP70B')	-	0,9372	C
NM_006597	HSPA8	Heat shock 70kDa protein 8	HEL-33/HEL-S-72p/HSC54/HSC70/HSC71/HSP71/HSP73/HSPA10/LAP1/NIP71	1,0581	OKAY
NM_004134	HSPA9	Heat shock 70kDa protein 9 (mortalin)	CSA/GRP-75/GRP75/HSPA9B/MOT/MOT2/MTHSP75/PBP74	0,8929	OKAY
NM_001540	HSPB1	Heat shock 27kDa protein 1	CMT2F/HEL-S-102/HMN2B/HS.76067/HSP27/HSP28/Hsp25/SRP27	1,1449	OKAY
NM_001541	HSPB2	Heat shock 27kDa protein 2	HSP27/Hs.78846/LOH11CR1K/MKBP	0,7428	B
NM_006308	HSPB3	Heat shock 27kDa protein 3	DHMN2C/HMN2C/HSPL27	1,3923	OKAY
NM_144617	HSPB6	Heat shock protein, alpha-crystallin-related, B6	HEL55/Hsp20	1,3377	B
NM_014424	HSPB7	Heat shock 27kDa protein family, member 7 (cardiovascular)	cvHSP	1,4979	B
NM_014365	HSPB8	Heat shock 22kDa protein 8	CMT2L/DHMN2/E2IG1/H11/HMN2/HMN2A/HSP22	0,8032	OKAY
NM_002156	HSPD1	Heat shock 60kDa protein 1 (chaperonin)	CPN60/GROEL/HLD4/HSP-60/HSP60/HSP65/HuCHA60/SPG13	0,9396	OKAY
NM_002157	HSPE1	Heat shock 10kDa protein 1 (chaperonin 10)	CPN10/EPF/GROES/HSP10	1,0345	OKAY
NM_006644	HSPH1	Heat shock 105kDa/110kDa protein 1	HSP105/HSP105A/HSP105B/NY-CO-25	0,8431	OKAY
NM_002622	PFDN1	Prefoldin subunit 1	PDF/PFD1	1,0932	OKAY
NM_012394	PFDN2	Prefoldin subunit 2	PFD2	0,8477	OKAY
NM_001235	SERPINH1	Serpin peptidase inhibitor, clade H (heat shock protein 47), member 1, (collagen binding protein 1)	AsTP3/CBP1/CBP2/HSP47/OI10/PPROM/RA-A47/SERPINH2/gp46	1,1666	OKAY
NM_022464	SIL1	SIL1 homolog, endoplasmic reticulum chaperone (S. cerevisiae)	BAP/MSS/ULG5	1,1833	OKAY
NM_030752	TCP1	T-complex 1	CCT-alpha/CCT1/CCTa/D6S230E/TCP-1-alpha	0,9971	OKAY
NM_000113	TOR1A	Torsin family 1, member A (torsin A)	DQ2/DYT1	0,8676	OKAY
NM_001101	ACTB	Actin, beta	BRWS1/PS1TP5BP1	1,0037	OKAY
NM_004048	B2M	Beta-2-microglobulin	-	1,0289	OKAY
NM_002046	GAPDH	Glyceraldehyde-3-phosphate dehydrogenase	G3PD/GAPD	0,9706	OKAY
NM_000194	HPRT1	Hypoxanthine phosphoribosyltransferase 1	HGPRT/HPRT	1,0929	OKAY
NM_001002	RPLP0	Ribosomal protein, large, P0	L10E/LP0/P0/PRLP0/RPP0	1,1432	OKAY
SA_00105	HGDC	Human Genomic DNA Contamination	HIGX1A	0,9372	C

Columns A, B, C and D indicate the Refseq, symbol, description and gene name respectively of the chaperones and heat shock proteins analysed in the PCR array.

Fold changes in mRNA levels in SEN177 treated HeLa cells relative to DMSO is shown in column E. Fold-change values greater than one indicate a positive- or an up-regulation, and the fold-regulation is equal to the fold-change. Fold-change values less than one indicate a negative or down-regulation, and the fold-regulation is the negative inverse of the fold-change. Fold-changes greater than 1.25 are indicated in blue; fold-change values less than 0.75 are indicated in red.

Column F indicates the gene's expression levels:*OKAY*, this gene's average threshold cycle is reasonably detected; *B*, this gene's average threshold cycle is relatively high (> 30), meaning that its relative expression level is low, in both control and test samples; C: This gene's average threshold cycle is either not determined or greater than the defined cut-off value (35), in both samples meaning that its expression was undetected, making this fold-change result erroneous and un-interpretable.